Petrologie sedimentárních hornin

G421P13, ZS 2/1, 3-4.roč.

Karel Martínek

Ústav geologie a paleontologie

sylabus

Přednáška (3 h bloky)

1. Siliciklastické sedimenty
   - granulometrická analýza, provenience a geotektonická pozice → modální složení, těžké minerály
   - sedimentační prostředí viz kurz Sedimentární geologie (2.roč.)
   - diageneze: kompakce, porozita, autigeneze, typy tmelů, diagenetická prostředí
2. Karbonáty I.
   - mineralogie, specifické struktury, typy zrn (Folk 1962), strukturní klasifikace (Dunham 1962) a přehled sedimentačních prostředí
3. Karbonáty II.
   - dolomitizace, dedolomitizace, změny porozity, raná & pozdní diageneze, typy tmelů, diagenetická prostředí

4. Evapority, silicity, ferolity
5. Organická hmota, kaustobiolity, úvod do ropné geologie, glaukonit, fosfáty
6. Paleopůdy, geochemie sedimentů
   - humidní, semiaridní, aridní; kalkrusty, silkrusty, dolokrusty
   - stabilní izotopy, stopové prvky, chemostratigrafie, změny paleoprostředí; katodová luminiscence; další metody a přístupy – případové studie

praktika

- 3 h terénní cvičení – dokumentace karbonátového/siliciklastického profilu
- 6 h mikroskopické praktikum vzorků ze studovaného profilu

Semestrální práce – 9 h

---

požadavky k zápočtu: ústní prezentace odborného textu, terénní cvičení + semestrální práce

zkouška: test - znalostní kviz + esej

---

základní učebnice kurzu:

- **M.E.Tucker: Sedimentary petrology. 3rd ed. Blackwell, 2001, 2003.**

1. Siliciklastika

primární struktury a složení

- zrnitost a granulometrie, vytřídění, šikmost - kvantitativní metody, analýza obrazu, směry distribuce sedimentů v pánvi
- klasifikace – viz 1.roč.; arenit, orto- , parakonglomerát
- sedimentární struktury – viz. Základy petrologie sedim.hor. 1.roč. a Sedimentární geologie 2.roč.

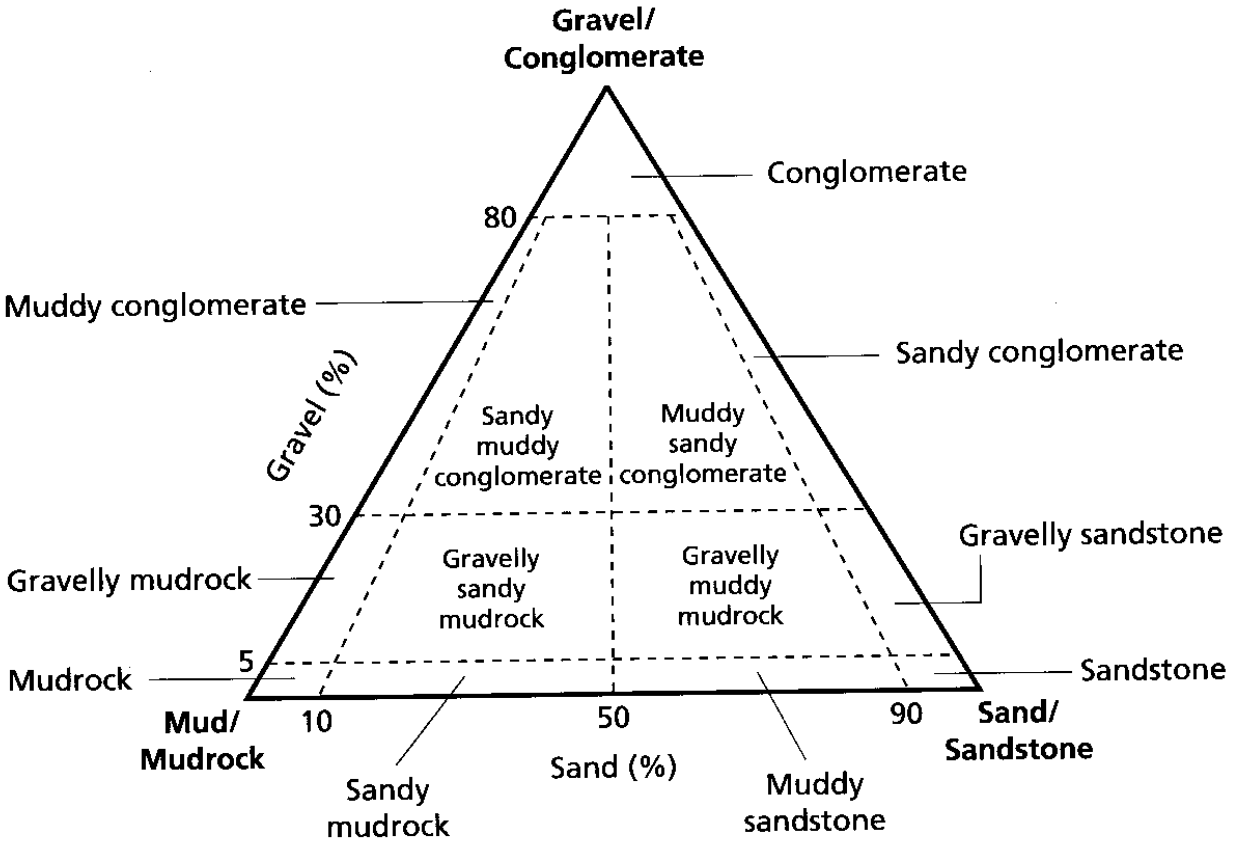

Fig. 2.1 Scheme for classifying sand–gravel–mud mixtures and the terms for sediment and rock (after Udden–Wentworth and Blair & McPherson, 1999).

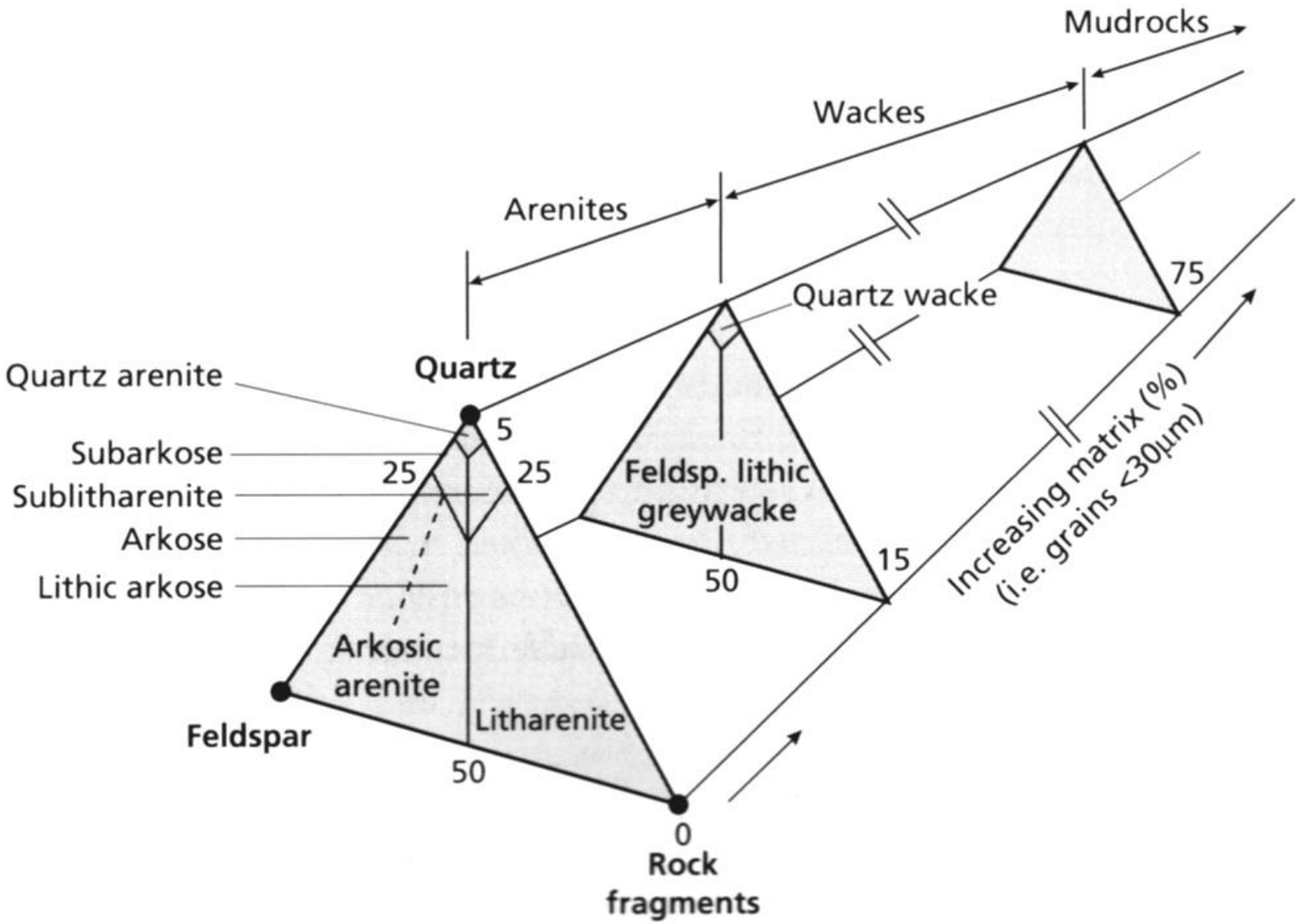
Mudrocks
Wackes
Arenites
Quartz wacke
75
Quartz arenite
Quartz
5
Subarkose
25
25
Sublitharenite
Arkose
Lithic arkose
Feldsp. lithic greywacke
50
15
Increasing matrix (%) (i.e. grains <30μm)
Arkosic arenite
Litharenite
Feldspar
50
0
Rock fragments

Granulometrie

- Sítová (nezpevněný materiál)
- Laserová (nezpevněný materiál)
- Optická (analýza obrazu)

Laserová granulometrie (nezpevněný materiál)

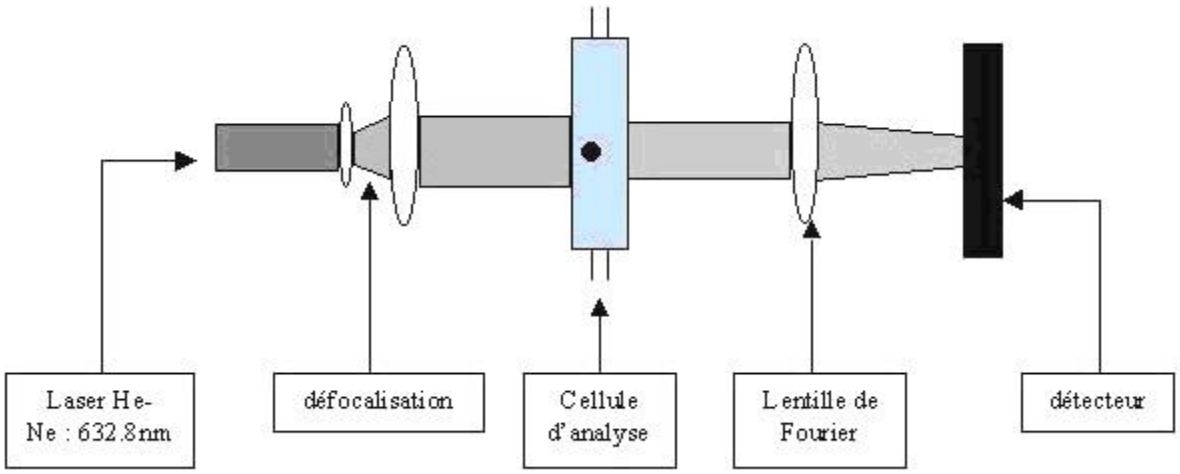

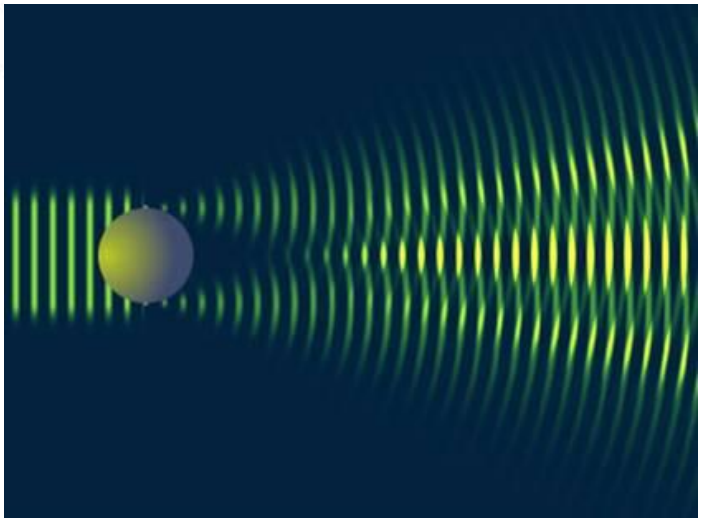

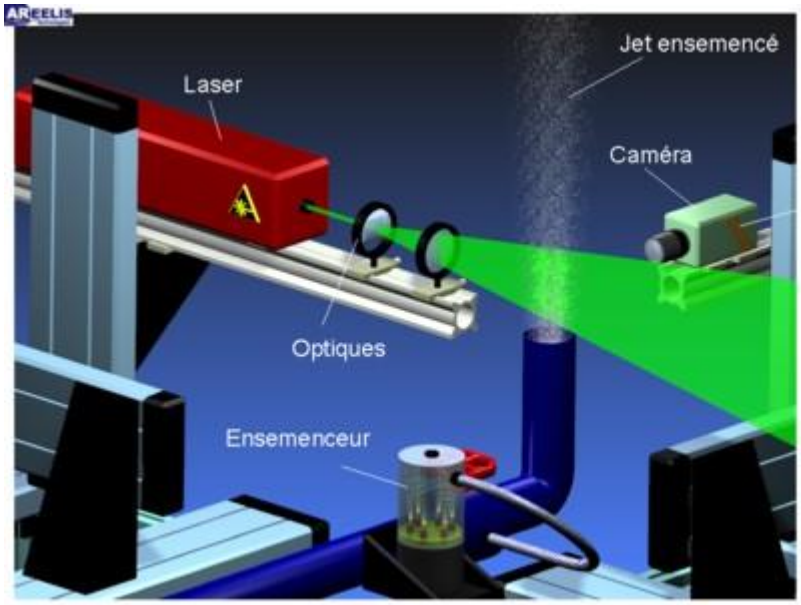

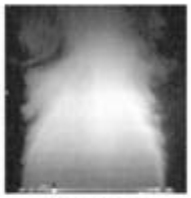

Image du jet dans un plan

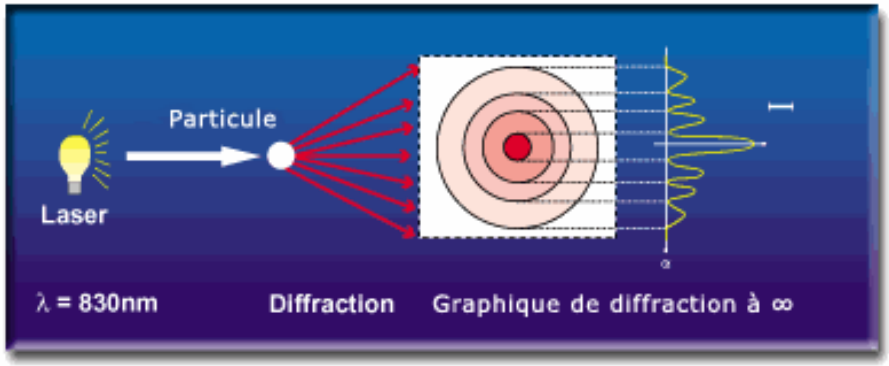

Class	Freq.	Freq. %	Cum. freq.
4–5	40	8	100
3–4	220	44	92
2–3	160	32	48
1–2	60	12	16
0–1	20	4	4

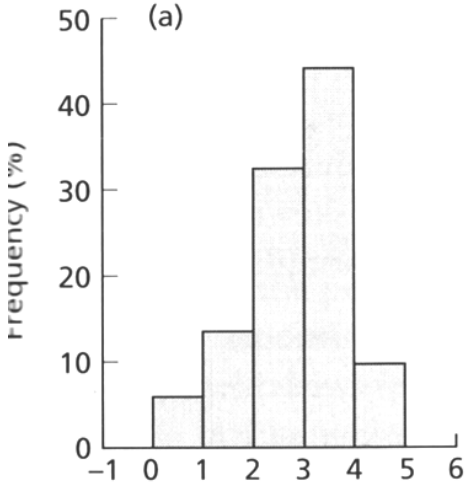

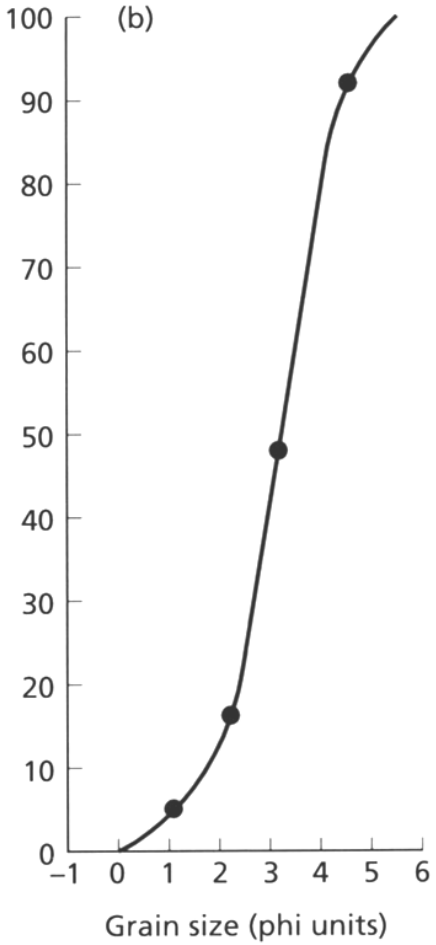

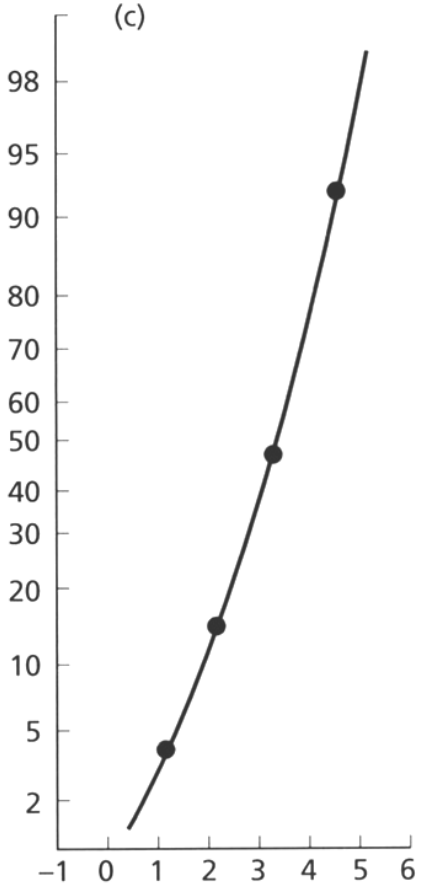

Grain size parameters
derived graphically,
Folk and Ward formulae

median	3.05ϕ
mean	2.95ϕ
sorting	0.92 (moderately sorted)
skewness	–0.21 (coarse skew)
kurtosis	0.96

$\Phi = - \log_2 D$

D[mm]:	Φ:
1	0,25
0,5	1
0,25	2
0,0625	4

Optická granulometrie (analýza obrazu)

Step 1: Taking a photo- A sample of the material you would like to measure

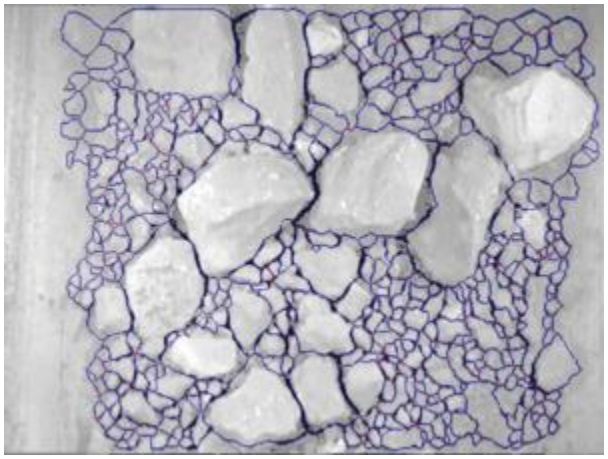

Step 2: Edge Detection- By completing an edge detection process, the software can determine the various sizes of material in the photo

Step 3: Virtual Sieve- The length to width ratio is measured in this step of the process. The individual particle sizes are measured instantly

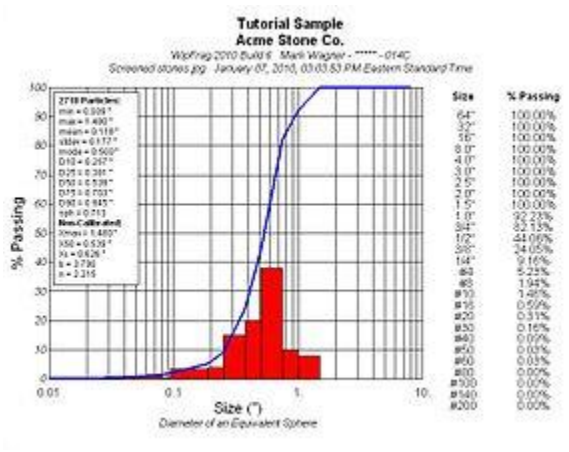

Step 4: Graphical Output- In this step, statistical data and size distribution is plotted on an easy-to-read form for operators.

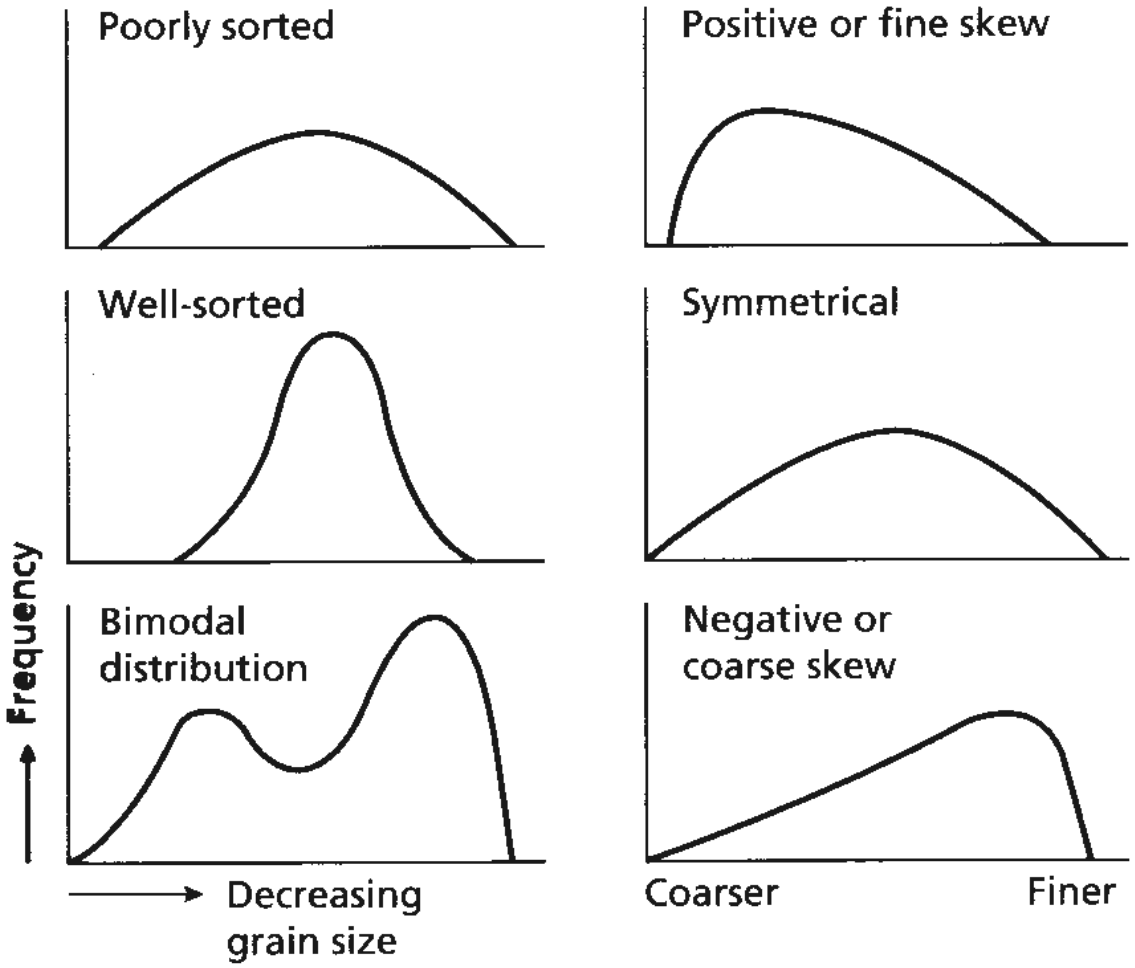

Fig. 2.2 Smoothed frequency distribution curves showing types of sorting and skewness.

Table 2.2 Formulae for the calculation of grain-size parameters from a graphic presentation of the data in a cumulative frequency plot. With the Trask formulae, the percentile measure Pn is the grain size in millimetres at the nth percentage frequency, and with the Folk & Ward formulae, the percentile measure ϕ_n is the grain size in phi units at the nth percentage frequency

Parameter	Trask formula	Folk & Ward formula
Median	$Md = P_{50}$	$Md = \phi_{50}$
Mean	$M = \frac{P_{25} + P_{75}}{2}$	$M = \frac{\phi_{16} + \phi_{50} + \phi_{84}}{3}$
Sorting	$So = \frac{P_{75}}{P_{25}}$	$\sigma\phi = \frac{\phi_{84} - \phi_{16}}{4} + \frac{\phi_{95} - \phi_5}{6.6}$
Skewness	$Sk = \frac{P_{25}P_{75}}{Md^2}$	$Sk = \frac{\phi_{16} + \phi_{84} - 2\phi_{50}}{2(\phi_{84} - \phi_{16})} + \frac{\phi_5 + \phi_{95} - 2\phi_{50}}{2(\phi_{95} - \phi_5)}$

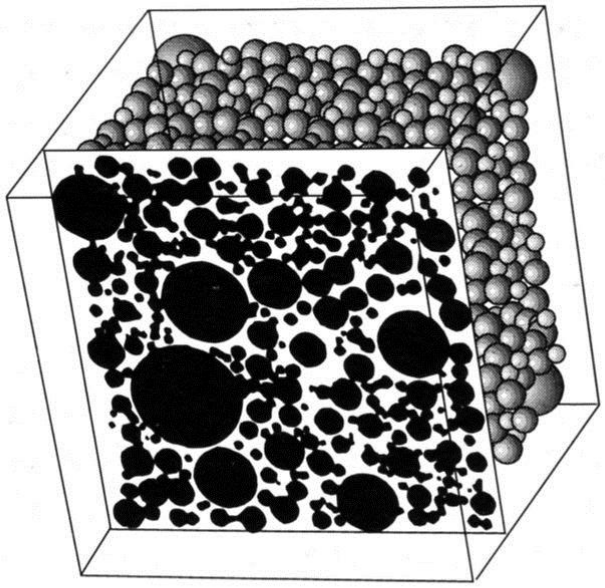

3-D dataset

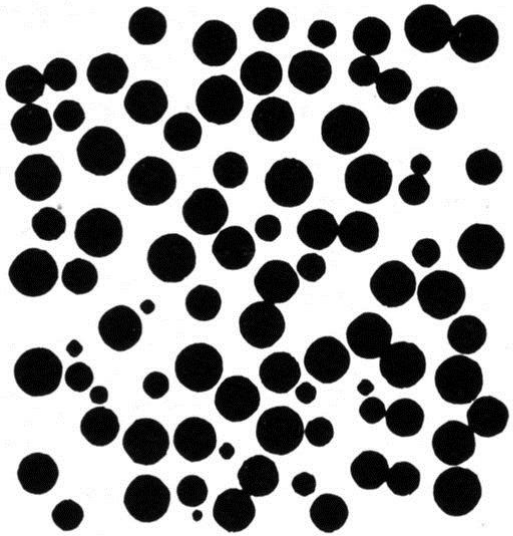

Very well sorted $\phi = 0.0$

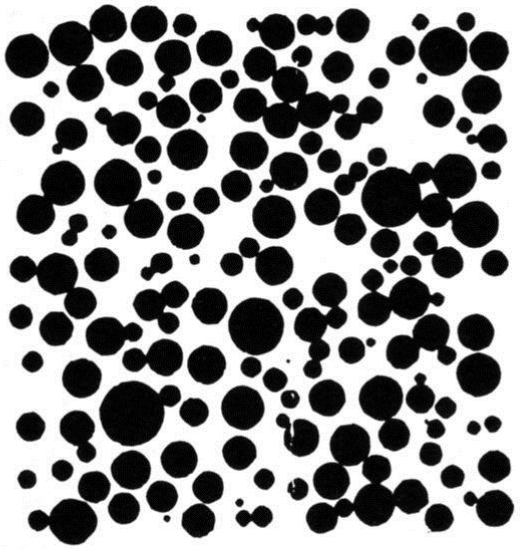

Well sorted $\phi = 0.36$

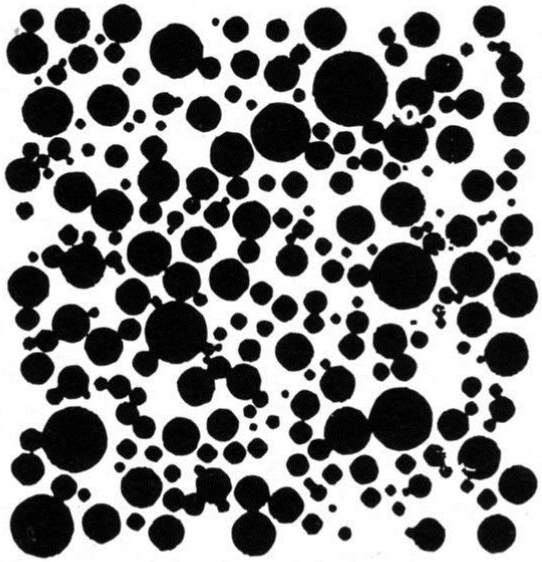

Moderately well sorted $\phi = 0.67$

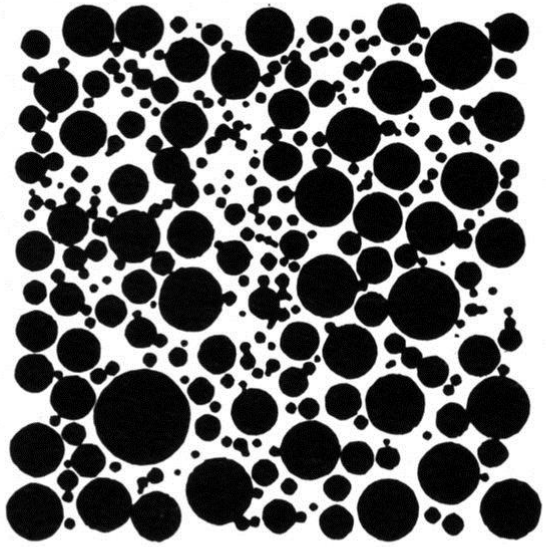

Moderately sorted $\phi = 0.74$

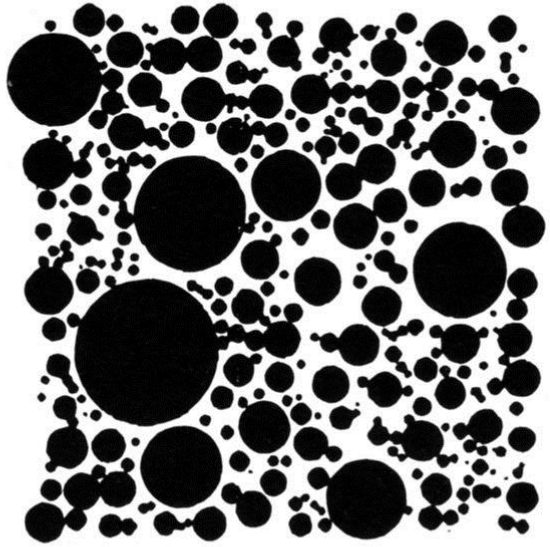

Poorly sorted $\phi = 1.15$

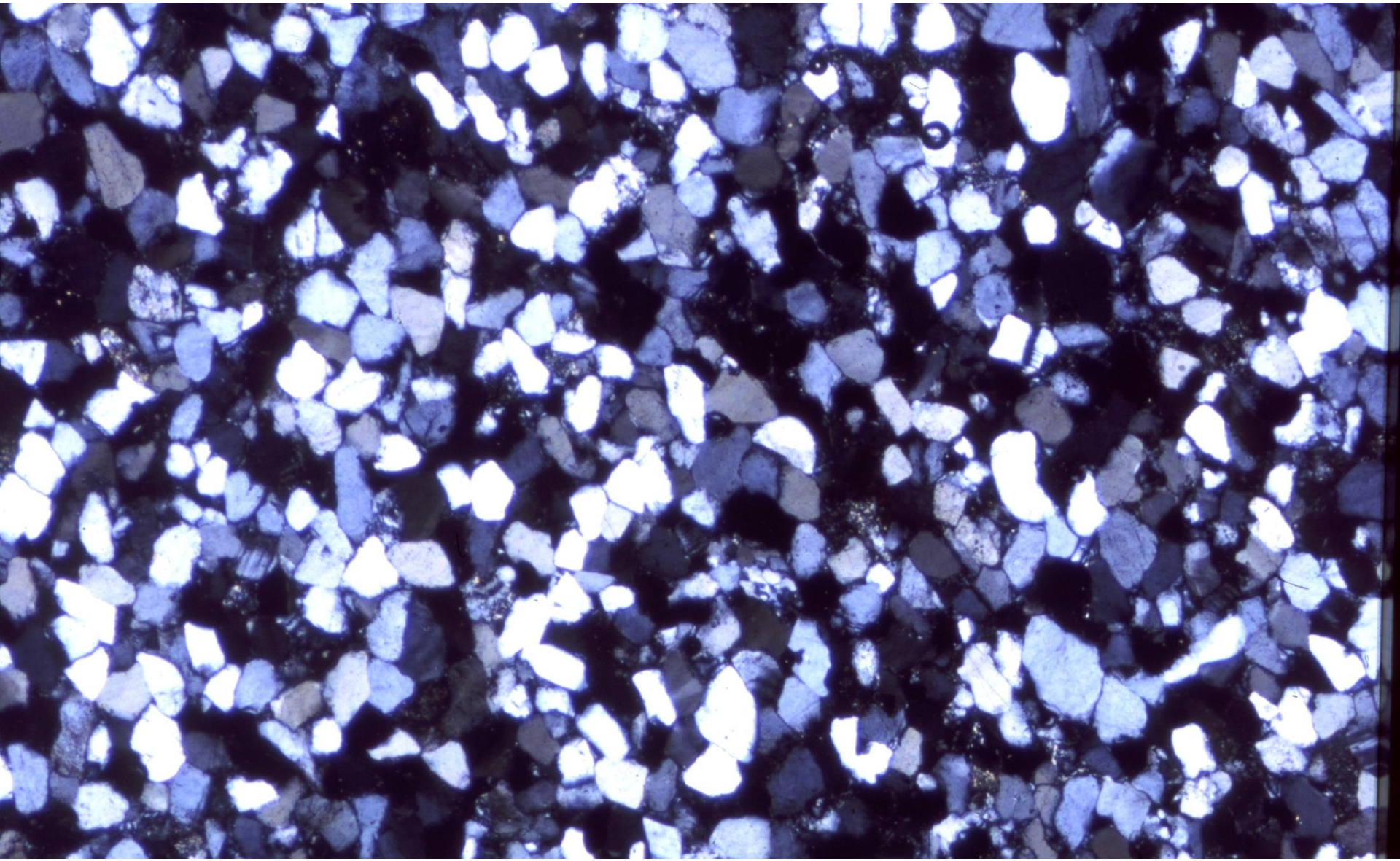

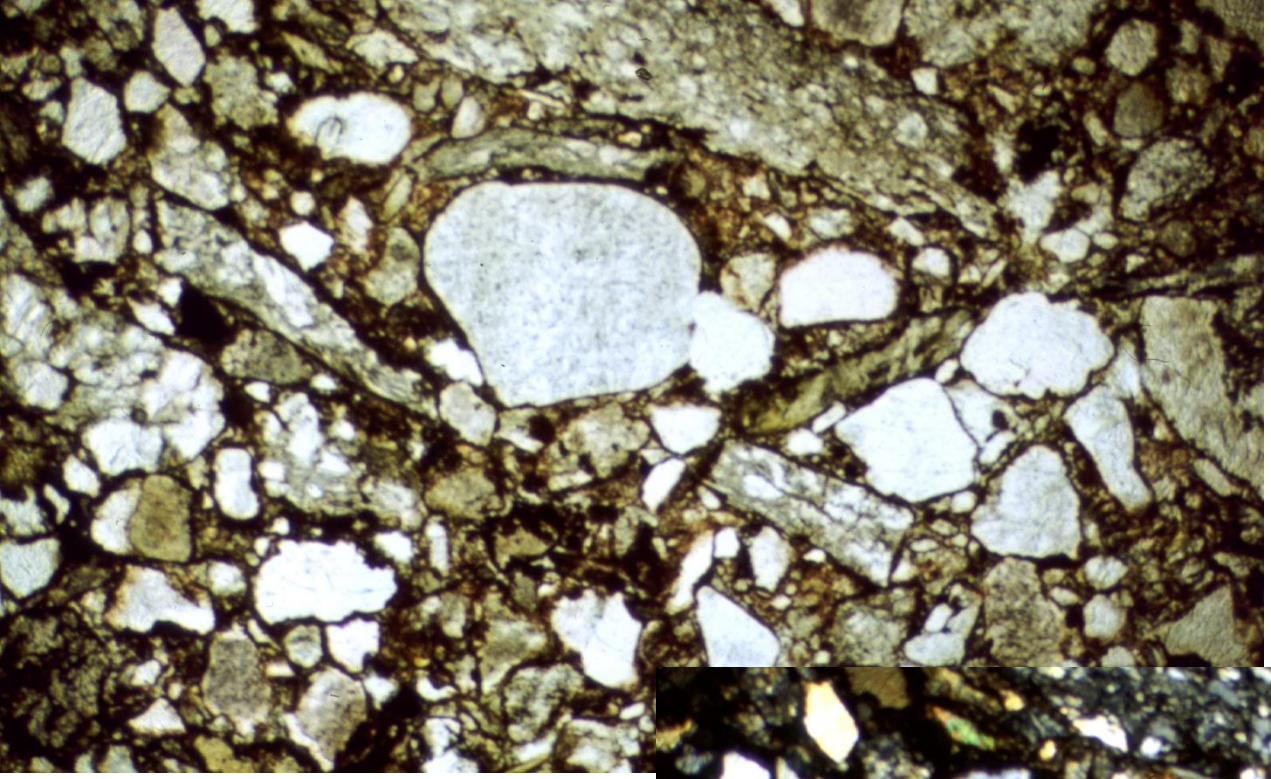

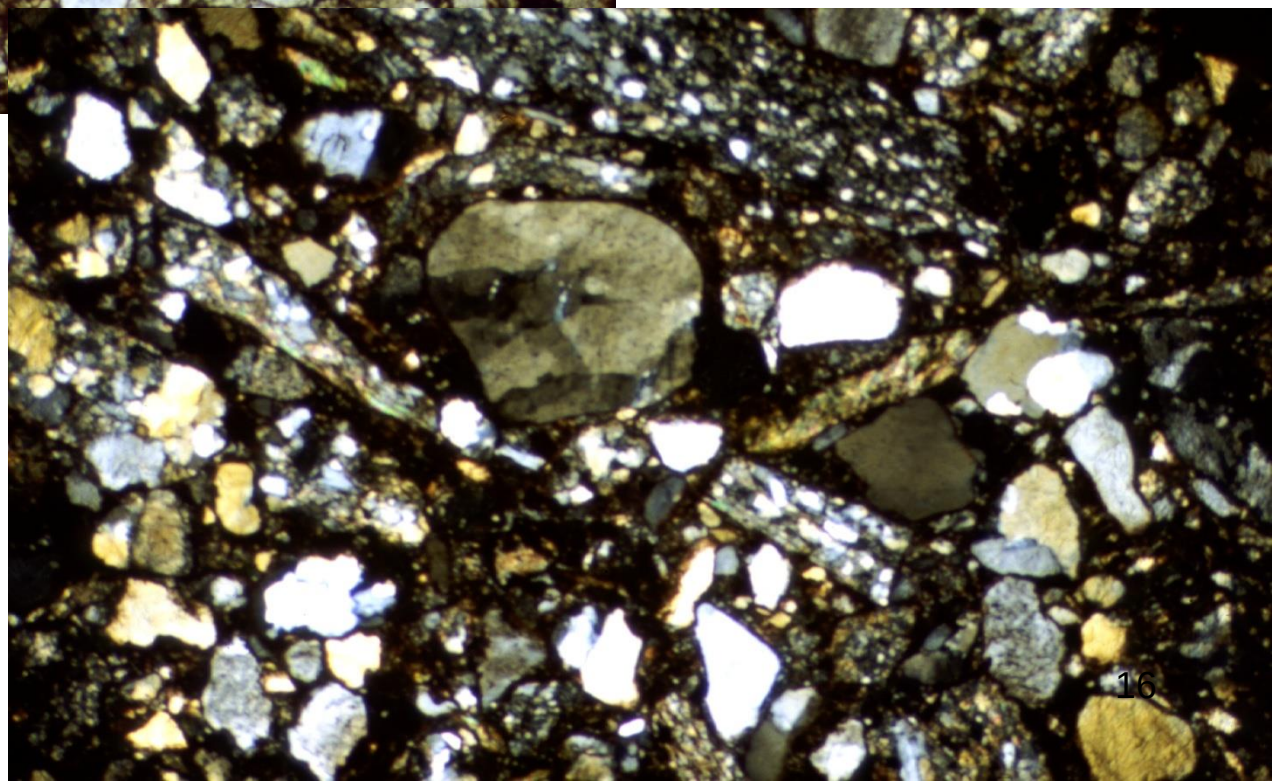

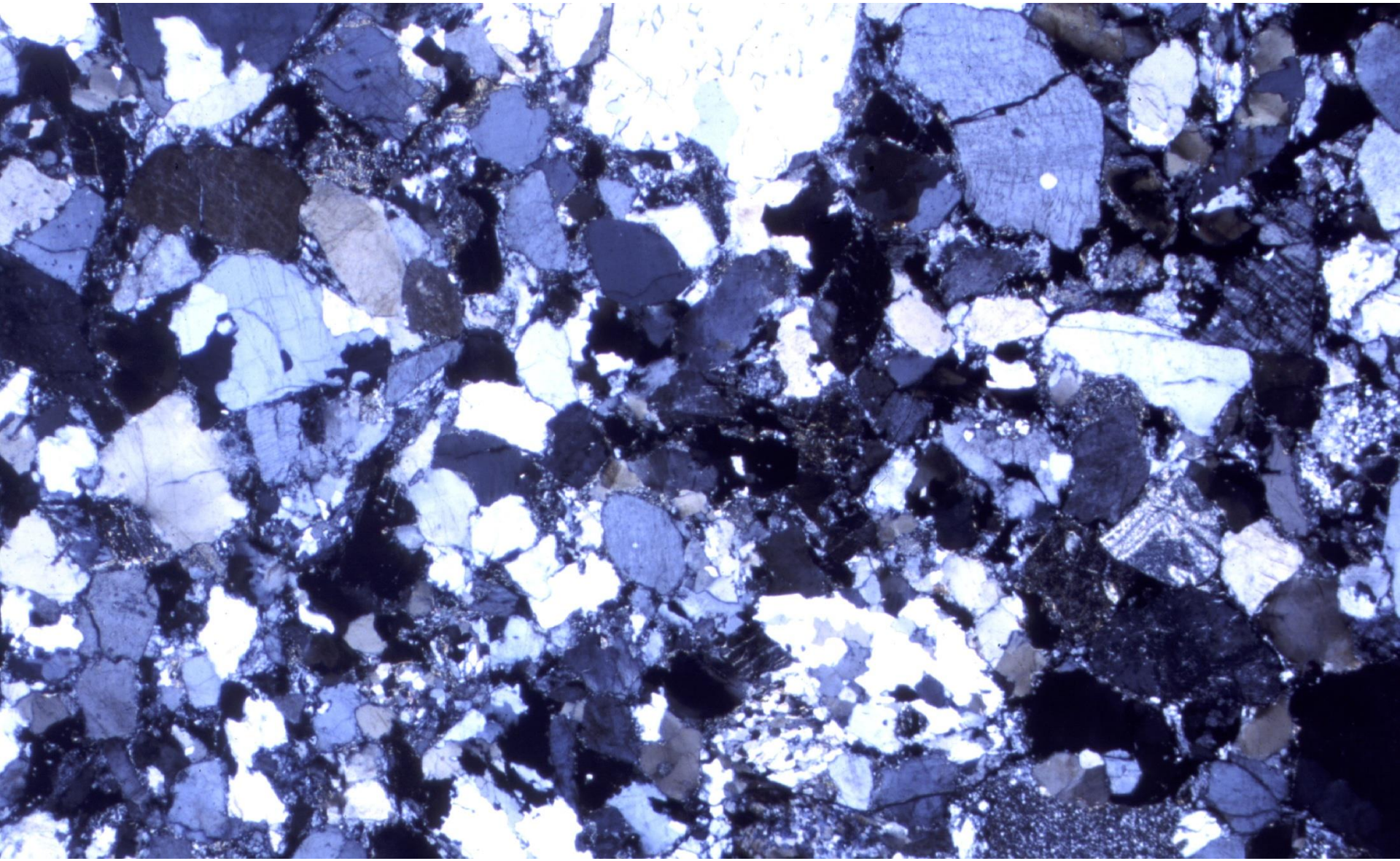

sféricita

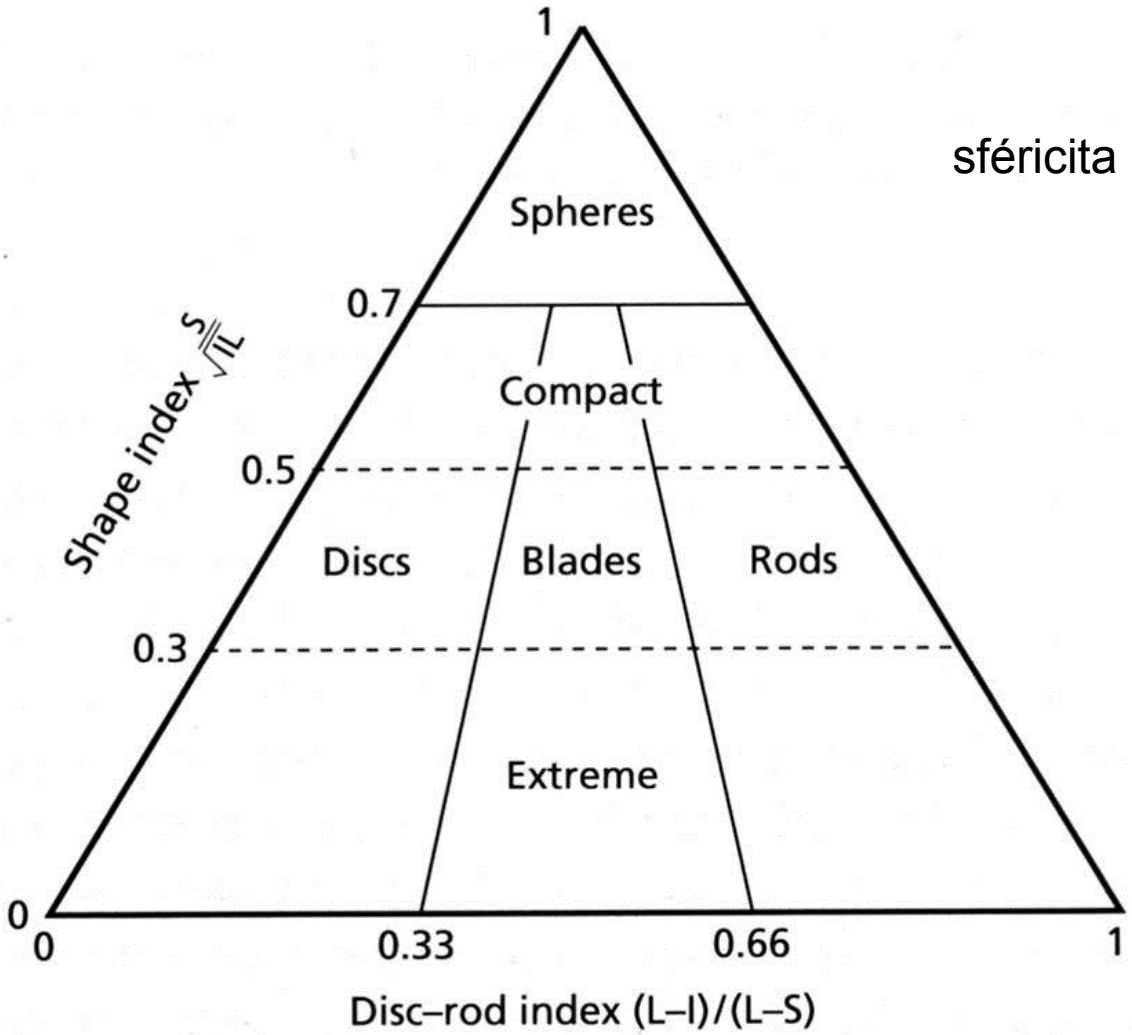

Fig. 2.5 The four classes of grain shape: spheres, discs, rods and blades, based on the shape index (a measure of the sphericity) and the disc–rod index. L, I and S represent the long, intermediate short axes of the grains, respectively (after Illenberger, 1991).

zaoblení

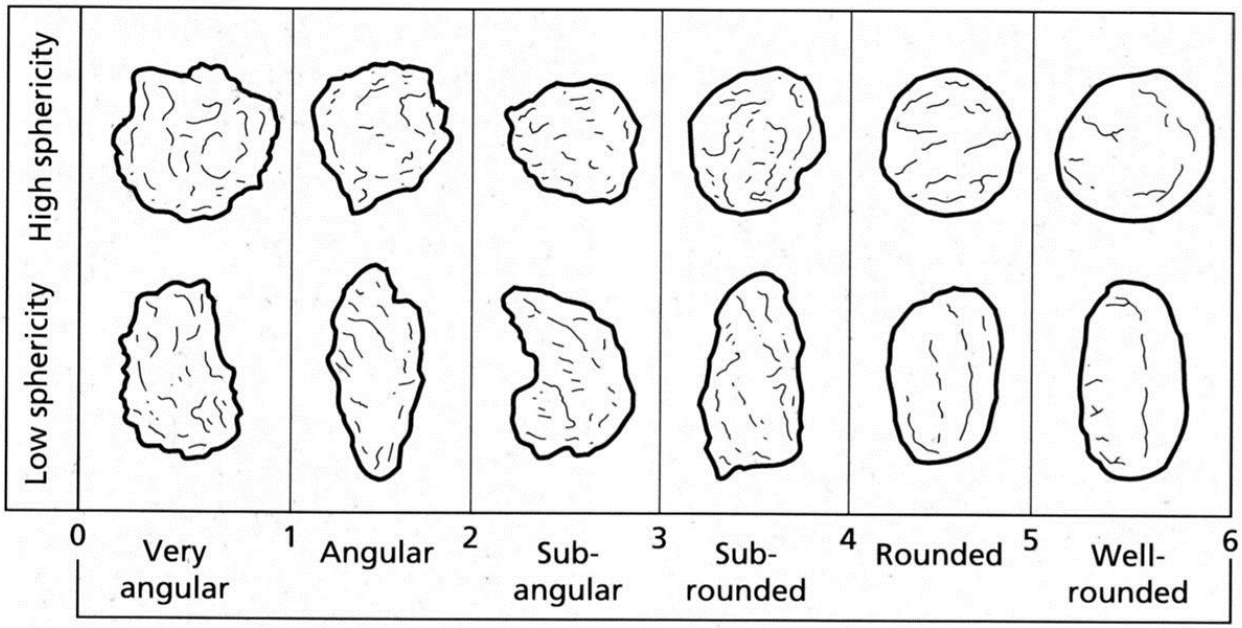

Fig. 2.6 Categories of roundness for sediment grains. For each category a grain of low and high sphericity is shown. After Pettijohn *et al.* (1987).

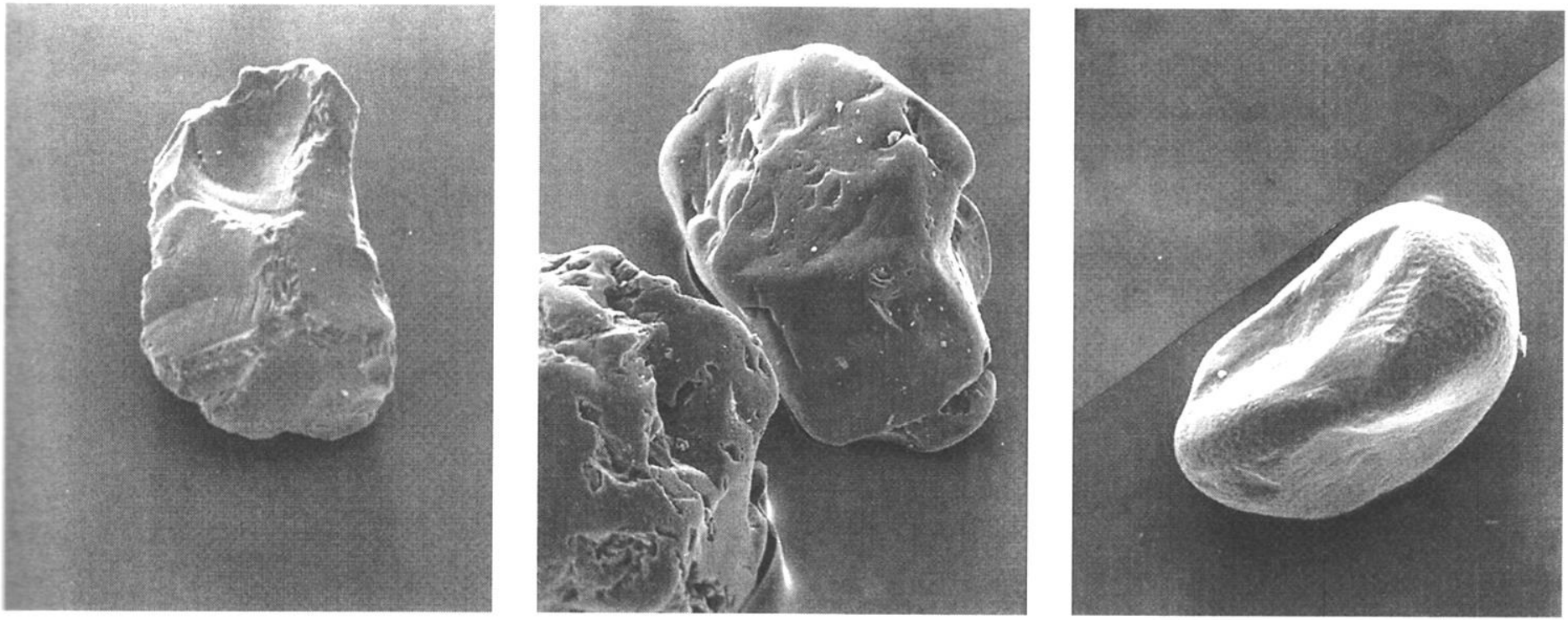

Fig. 2.7 Scanning electron micrographs of quartz sand grains from three modern environments. (a) Grain from glacial outwash deposit, Ottawa, Canada, showing conchoidal fractures and angular shape. (b) Grain from high-energy beach, Sierra Leone, West Africa, showing rounded shape and smooth surface with small v-shaped percussion marks. (c) Grain from desert sand sea, Saudi Arabia, showing frosted, pock-marked surface (as a result of upturned plates, which are visible at higher magnifications) and conchoidal fractures resulting from mechanical chipping.

Mikrostruktury (angl. texture)

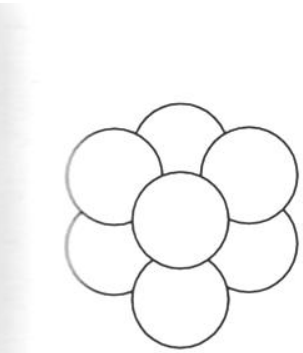

(a) Cubic packing (48% porosity)

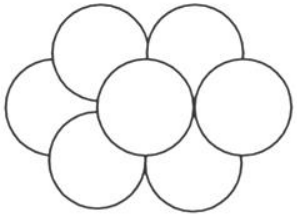

(b) Rhombohedral packing (26% porosity)

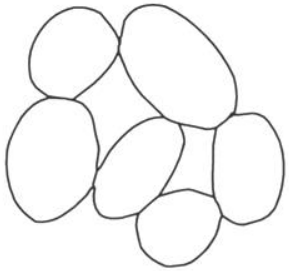

(c) Point contacts

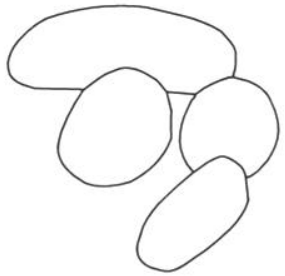

(d) Concavo-convex contacts

(e) Sutured contacts

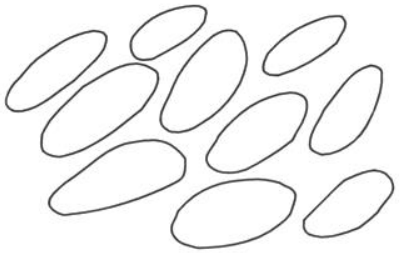

(f) Preferred orientation of grains

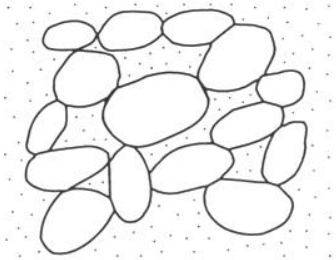

(g) Grain-supported fabric

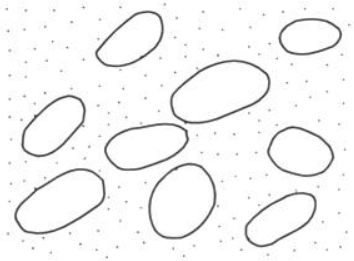

(h) Matrix-supported fabric

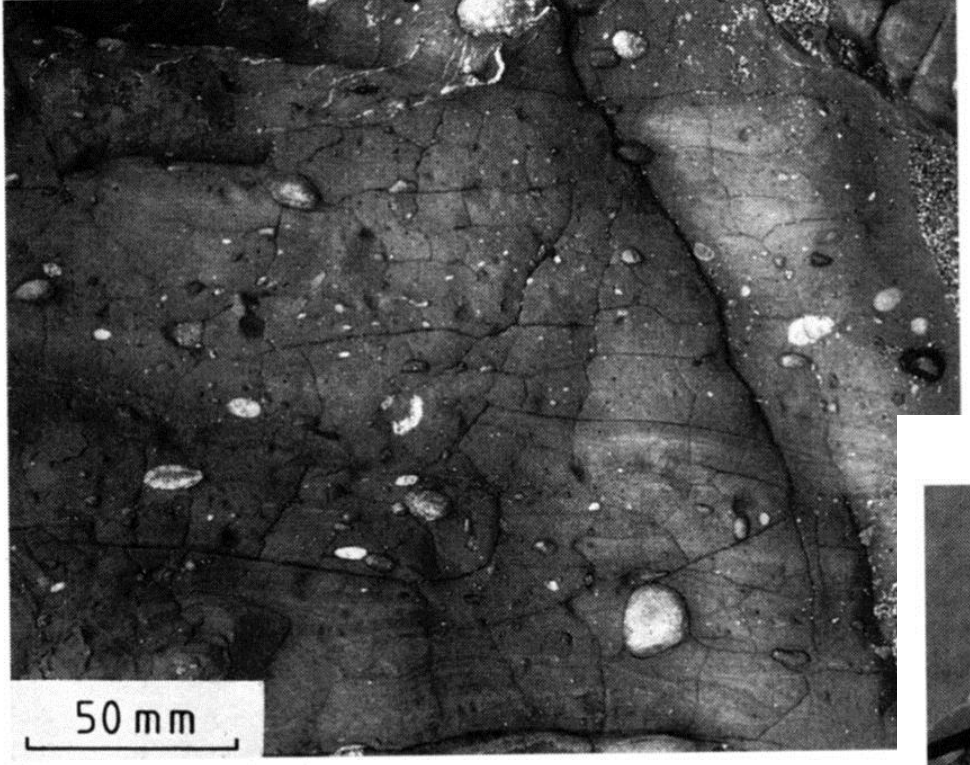

Fig. 2.9 Matrix-support fabric: pebbles 'float' in matrix. Noti also subtle synsedimentary folds. Tertiary deep-water pebbly mudstone of debris-flow origin. California, USA.

Fig. 2.10 Clast-support fabric; pebbles, mainly quartzite, are in contact and were deposited on a fan delta. Late Precambrian, Southern Norway.

analýza provenience

modální složení - klima, geotektonická pozice, erozní historie zdrojových oblastí; asociace těžkých minerálů vs. akcesorie zdrojových hornin: různá citlivost jednotlivých TM na klima/transport;

pokročilé metody:

- detailní mineralogie/chemismus TM (granáty, turmalíny, pyroxeny)
- geochronologie zirkonů, fission-track analýzy apatitu - tektonosedimentární vývoj
- provenience jílovců - stopové prvky/geochronologie

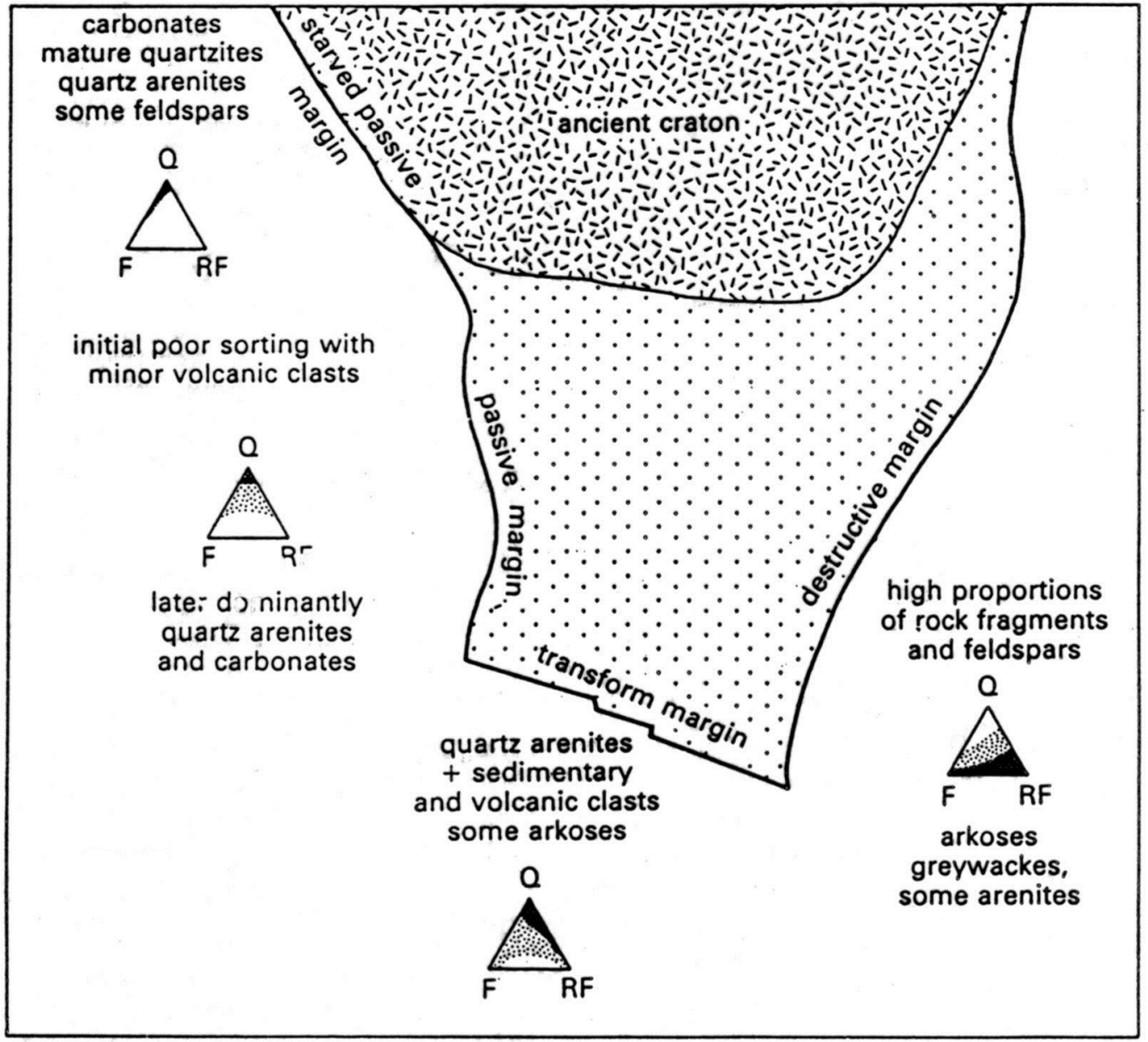

Fig. 5.10. Average modal compositions of groups of sandstones from different tectonic environments. This technique is only valid where many different sandstone modal compositions are available and cannot be used for single sandstone samples (modified from Folk, 1974b). Component details are documented in Table 5.5.

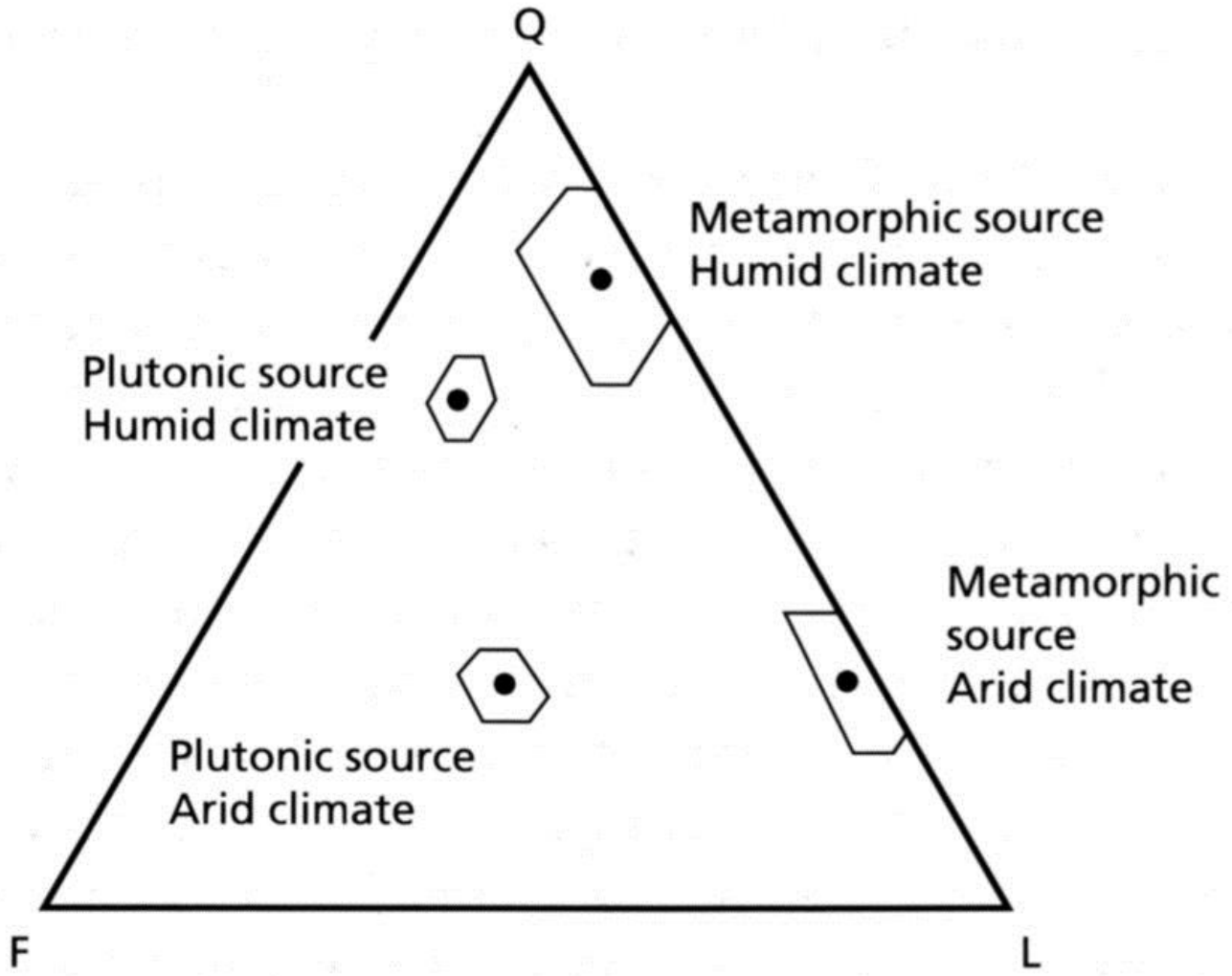

Fig. 2.46 Average compositions of medium sand-size fraction of first-cycle stream sediment derived from plutonic igneous and metamorphic sources under different climatic conditions. Q, quartz; F, feldspar; L, lithics.

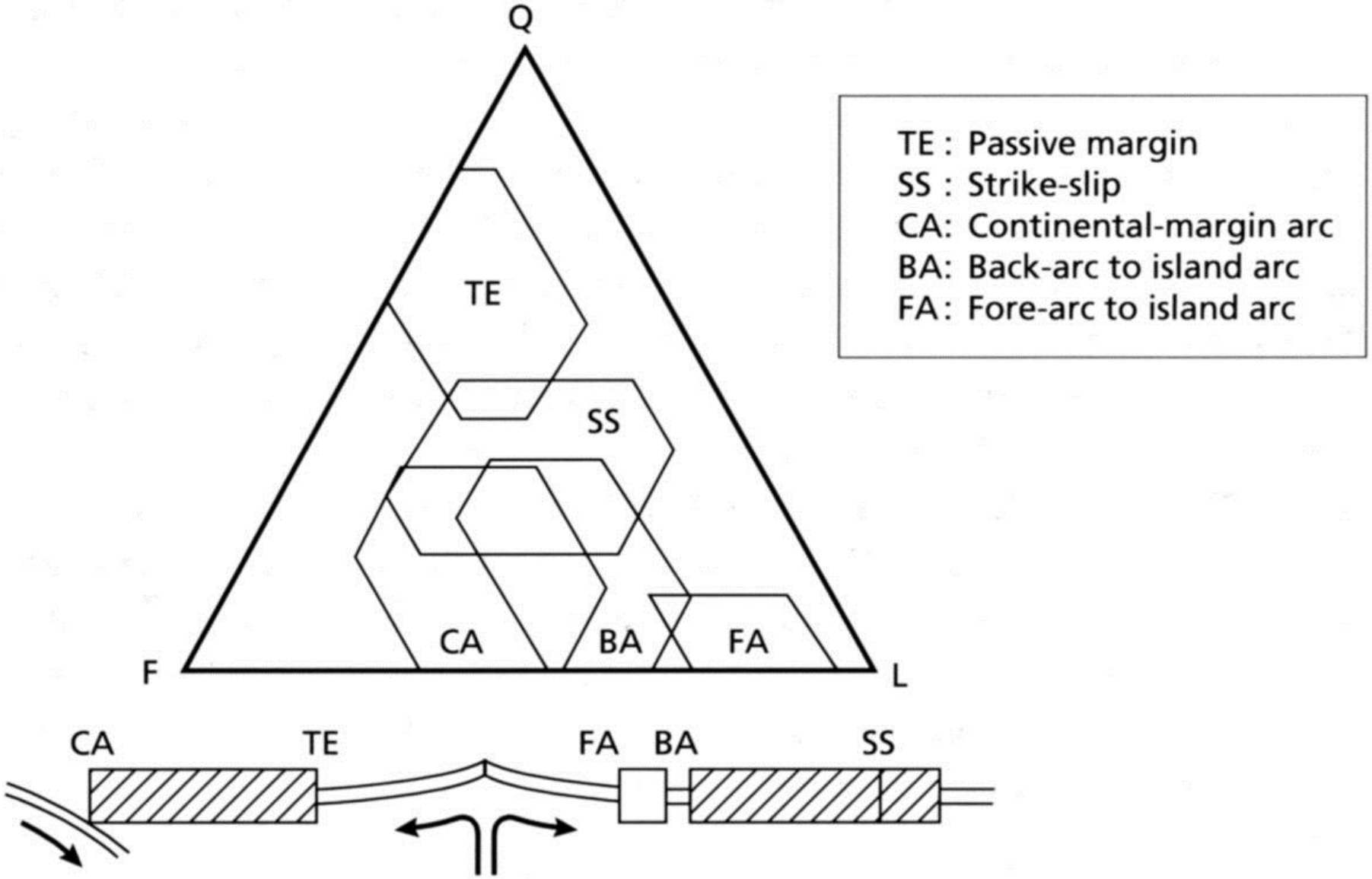
Q
TE
SS
CA
BA
FA
F
L
TE : Passive margin
SS : Strike-slip
CA: Continental-margin arc
BA: Back-arc to island arc
FA: Fore-arc to island arc
CA
TE
FA
BA
SS

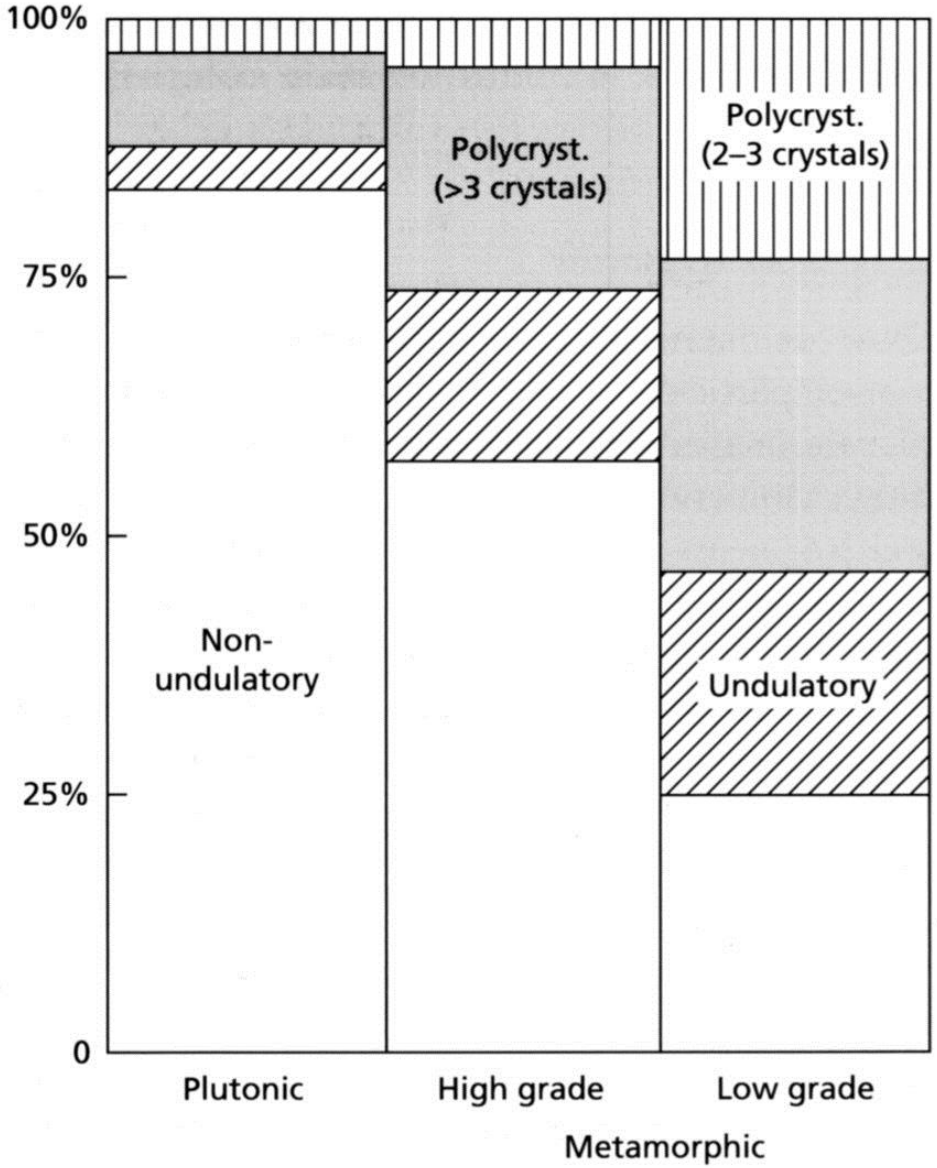

Fig. 2.48 Relative abundance of detrital monocrystalline and polycrystalline quartz grains in Holocene sands derived from known plutonic and metamorphic sources. After Basu *et al.* (1975).

total

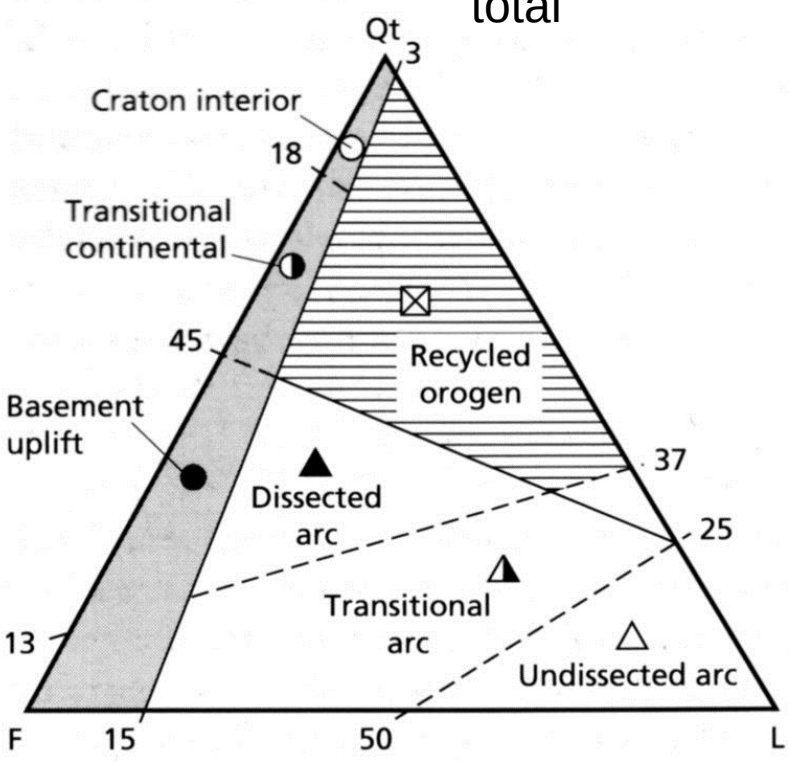

monocrystalline

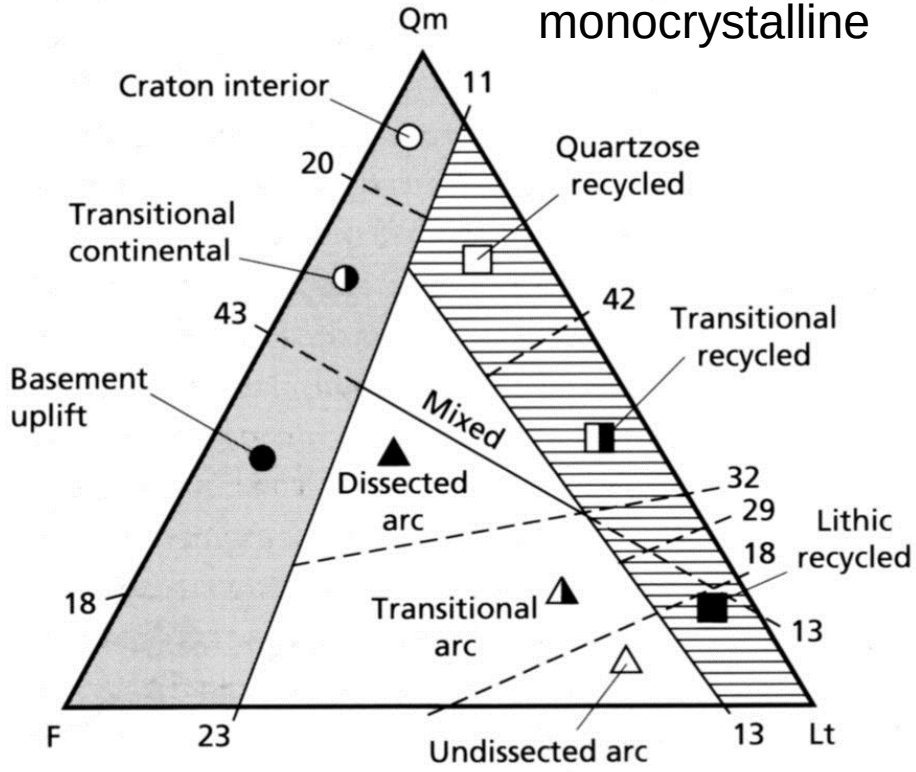

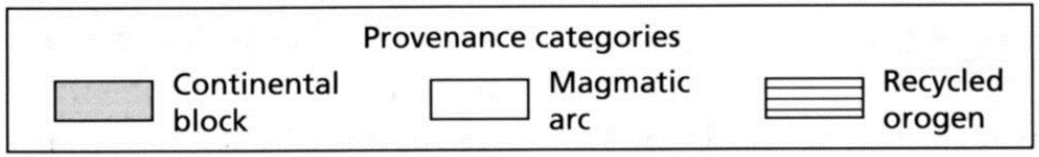

L+Qpolycryst.

erozní historie

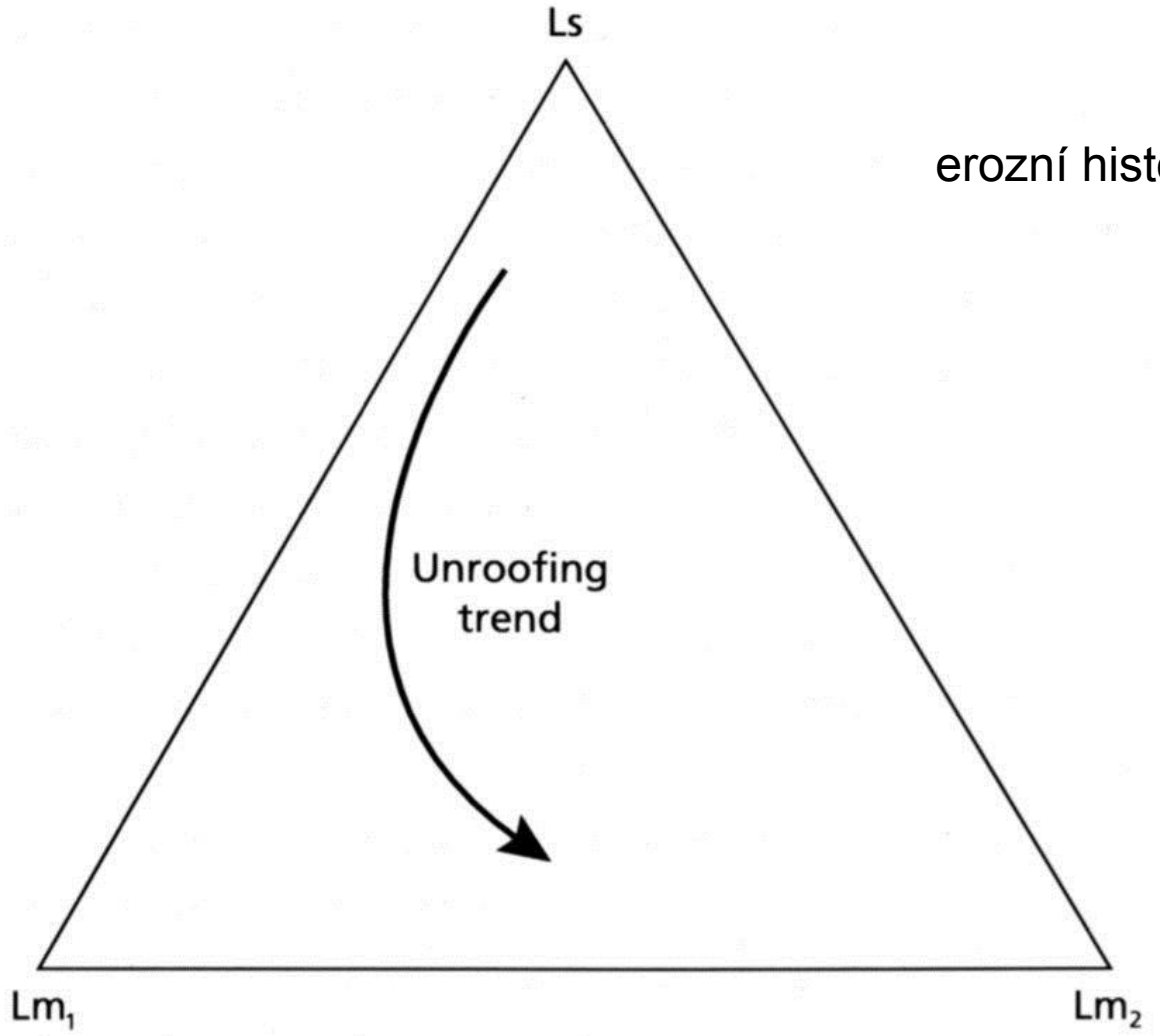

Fig. 2.47 The trend in lithic grains (Ls, sedimentary; Lm_1, low-grade metamorphic; Lm_2, medium-grade metamorphic) in sandstones derived from the unroofing of a sedimentary–metasedimentary complex of an arc–continent collision belt.

těžké minerály

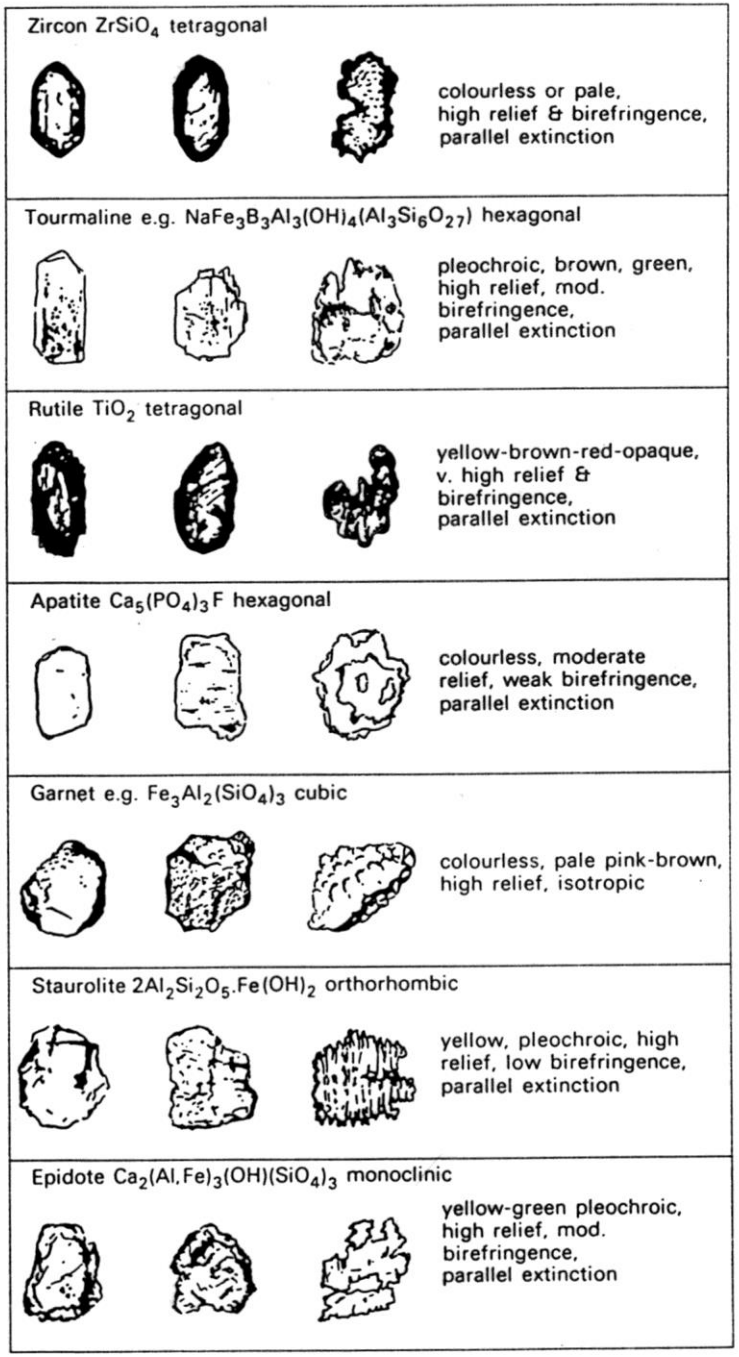

Fig. 2.55 Sketches of the seven most common heavy minerals (with the degree of weathering and or dissolution increasing to the right) together with their optical properties. After Füchtbauer (1974).

Table 4-2
Common Accessory Minerals in Sandstones and Types of Crystalline Rocks in Which They Usually Originate

Igneous rocks	Metamorphic rocks	Indeterminate[a]
Aegerine	Actinolite	Enstatite
Augite	Andalusite	Hornblende
Chromite	Chloritoid	Hypersthene
Ilmenite	Cordierite	Magnetite
Olivine	Diopside	Sphene
Topaz	Epidote	Tourmaline
	Garnet	Zircon
	Glaucophane	
	Kyanite	
	Jadeite	
	Rutile	
	Sillimanite	
	Staurolite	
	Tremolite	
	Wollastonite	

[a] Common in both igneous and metamorphic rocks.

Table 8-2. *Heavy mineral associations and provenance (modified from Feo-Codecido, 1956, p. 997)*

Association	*Source*
Apatite, biotite, brookite, hornblende, monazite, muscovite, rutile, titanite, tourmaline (pink variety), zircon	Acid igneous rocks
Cassiterite, dumortierite, fluorite, garnet, monazite, muscovite, topaz, tourmaline (blue variety), wolframite, xenotime	Granite pegmatites
Augite, chromite, diopside, hypersthene, ilmenite, magnetite, olivine, picotite, pleonaste	Basic igneous rocks
Andalusite, chondrodite, corundum, garnet, phlogopite, staurolite, topaz, vesuvianite, wollastonite, zoisite	Contact metamorphic rocks
Andalusite, chloritoid, epidote, garnet, glaucophane, kyanite, sillimanite, staurolite, titanite, zoisite-clinozoisite	Dynamothermal metamorphic rocks
Barite, iron ores, leucoxene, rutile, tourmaline (rounded grains), zircon (rounded grains)	Reworked sediments

Table 8-3. *Stability of some detrital heavy minerals*

Ultrastable	Rutile, zircon, tourmaline, anatase
Stable	Apatite, garnet (iron-poor), staurolite, monazite, biotite, ilmenite, magnetite
Moderately stable	Epidote, kyanite, garnet (iron-rich), sillimanite, sphene, zoisite
Unstable	Hornblende, actinolite, augite, diopside, hypersthene, andalusite
Very unstable	Olivine

faktory ovlivňující složení asociace těžkých minerálů v klastickém sedimentu:

- složení zdrojových hornin
- zvětrávání zdrojových hornin
- transport v sedimentačním prostředí, zvětrávání, hydraulické třídění
- zvětrávání na aluviální plošině, pedogeneze – raně diagenetické procesy
- kompakce a alterace během pohřbení – pozdější diageneze
- recyklace (sedimentární, magmatická, metamorfní)

(Morton a Hallsworth 1999, ad.)

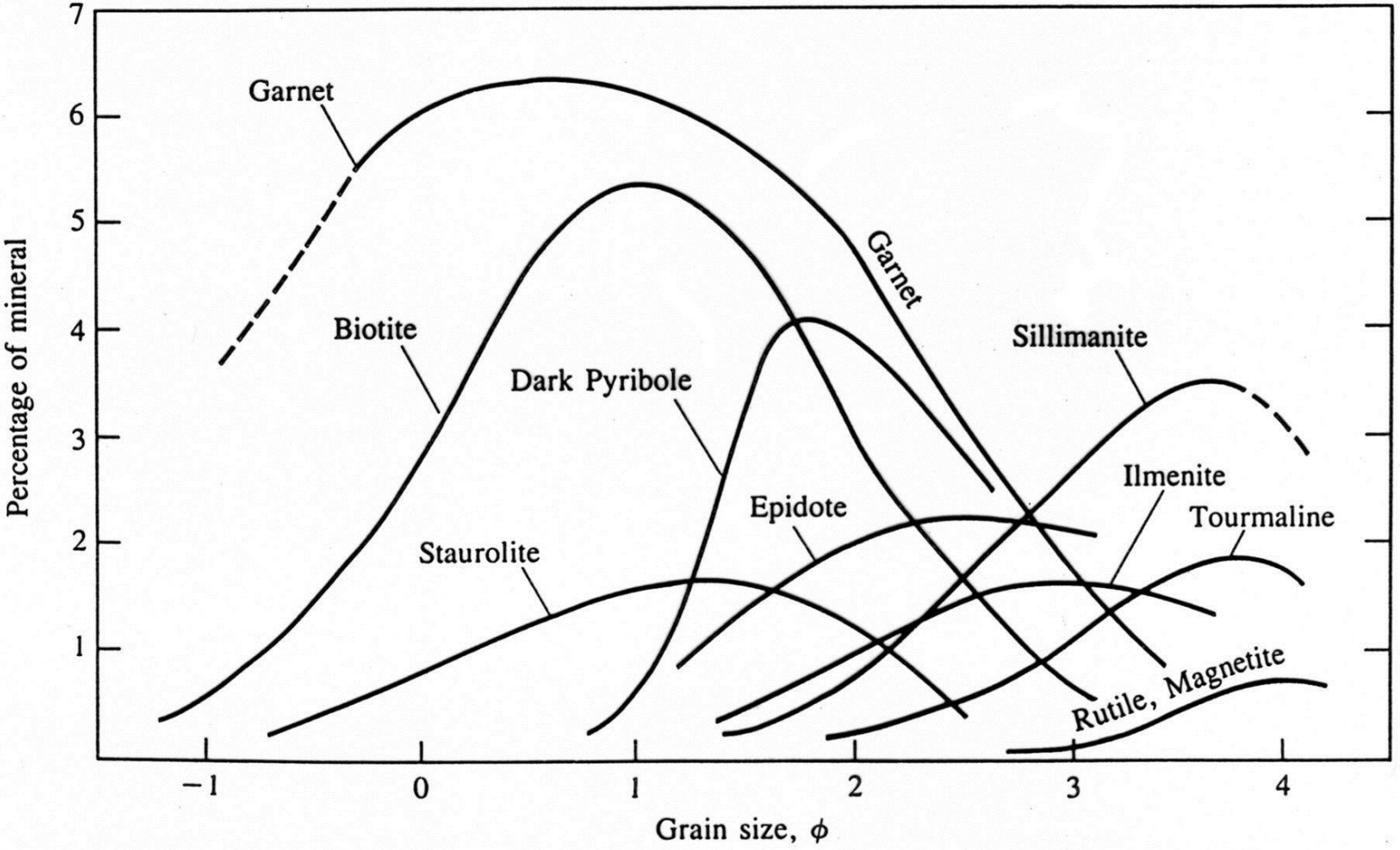

Figure 4-15
Size distributions of heavy minerals in the Kitt Brook delta (Pleistocene), Connecticut. The distributions are the combined effect of the sizes of these minerals in the source terrane and the sorting processes during transport and deposition. [E. R. Force and B. D. Stone, 1990, *U.S. Geol. Surv. Bull., 1874,* 19.]

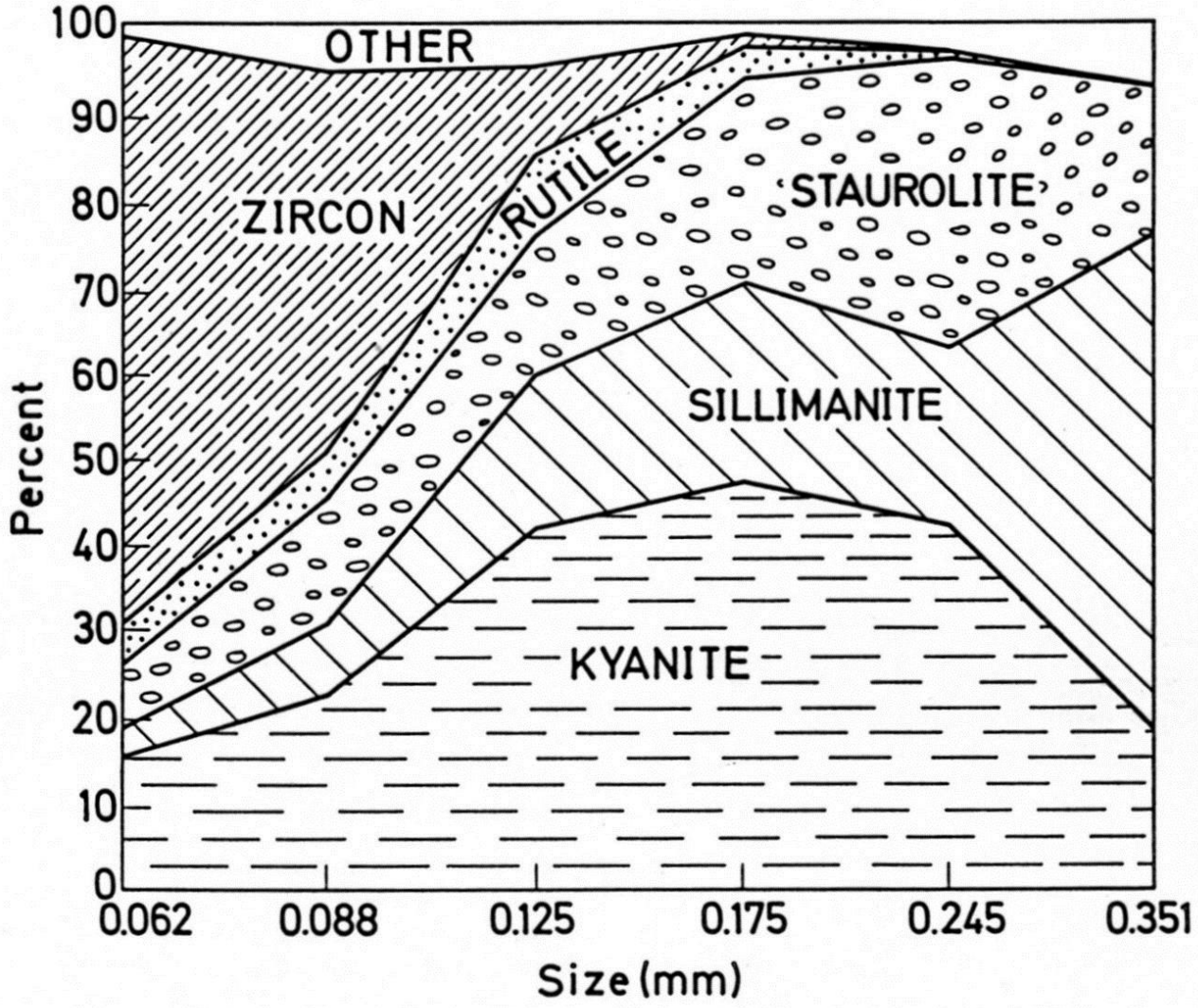

Fig. 8-7. Diagram showing relations between grain size and heavy mineral frequencies. Lafayette sand, western Kentucky (redrawn from Potter, 1955, Fig. 3)

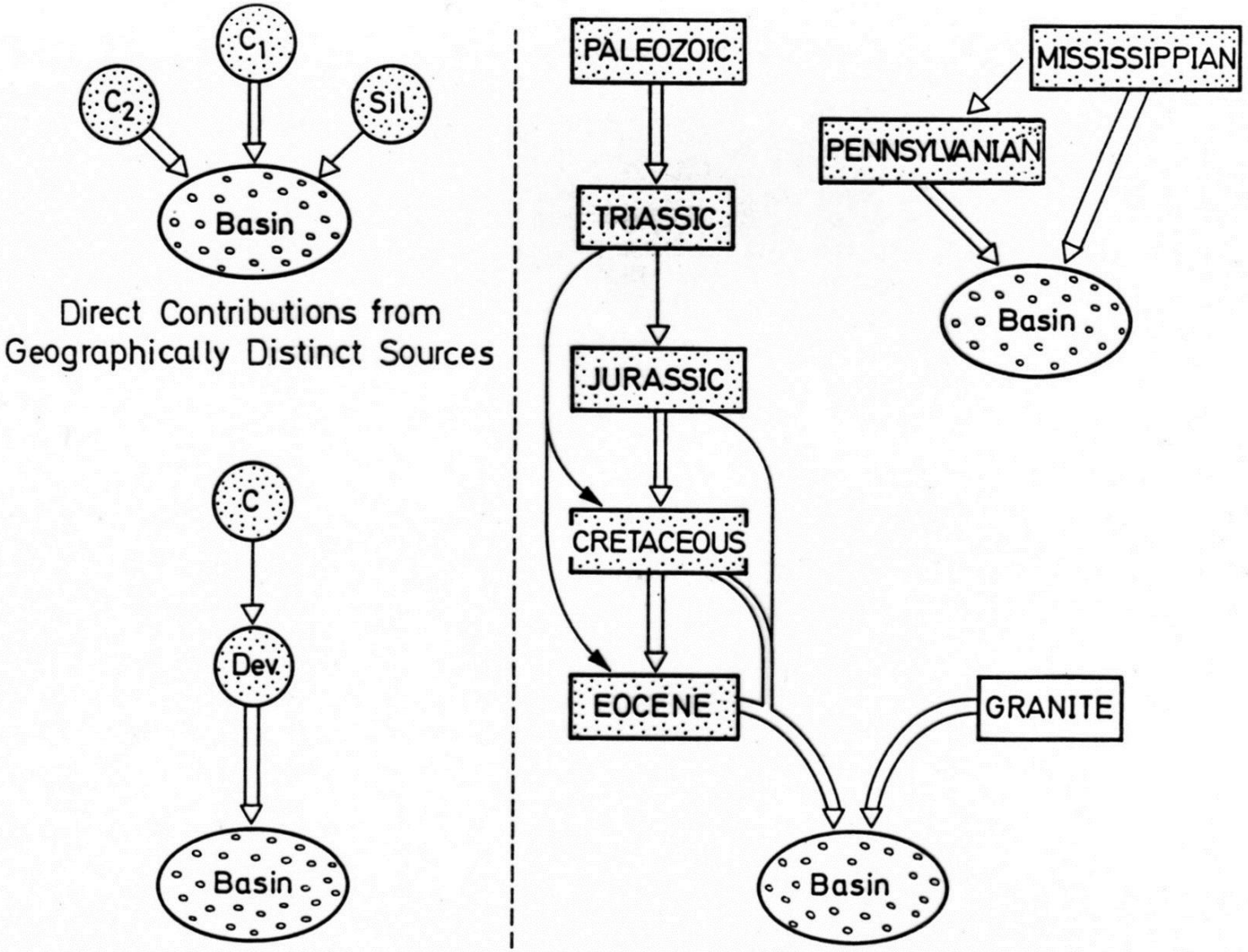

Fig. 8-8. Some common paths of mineral evolution

složení turmalínu

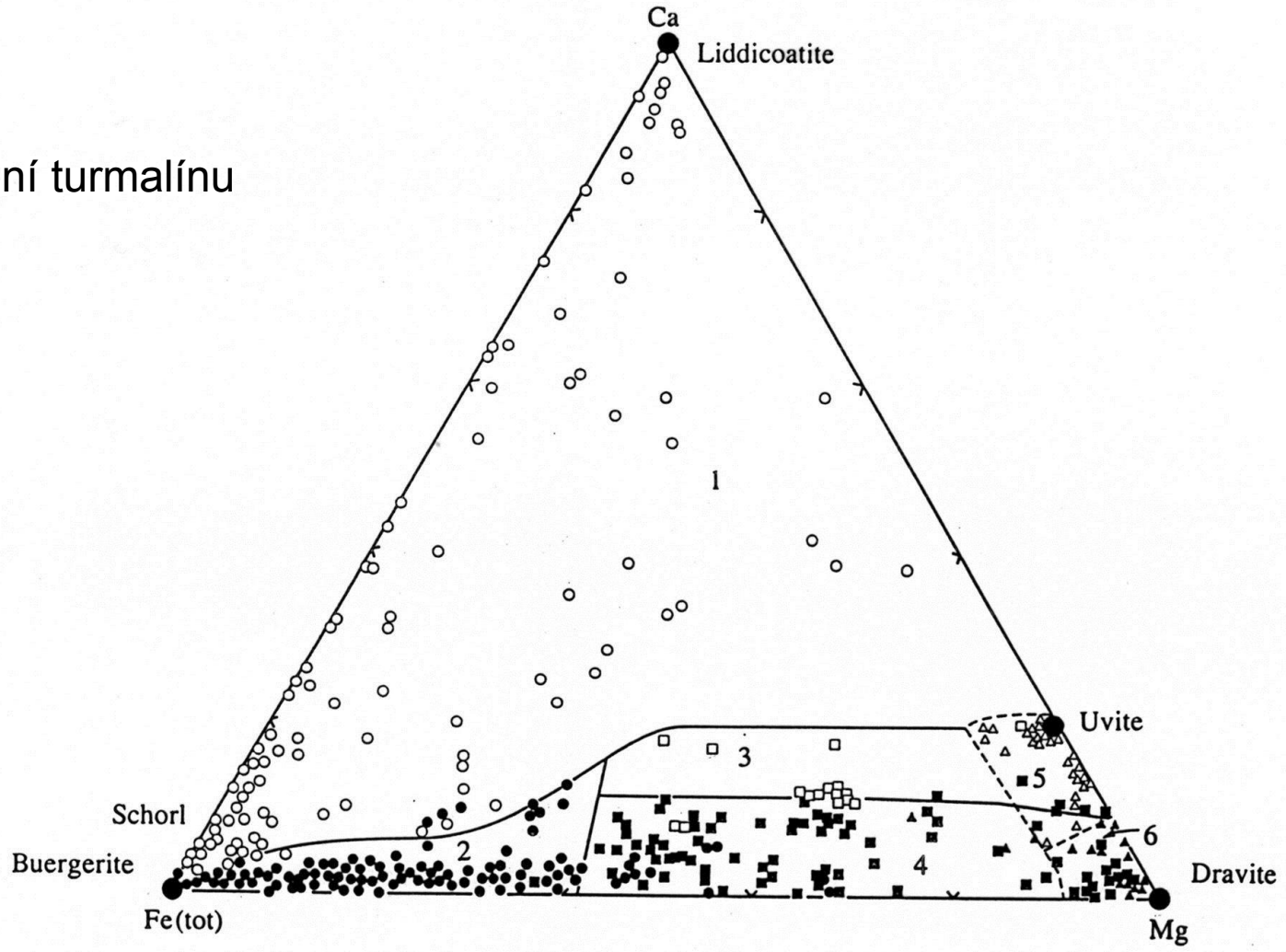

Figure 4-16
Ca–Fe–Mg molecular proportions for tourmaline from various types of crystalline rocks. Several of the common end-members are plotted for reference. The fields are (1) Li-rich granitoid pegmatites and aplites; (2) Li-poor granitoids and associated pegmatites and aplites; (3) Ca-rich metapelites, metasandstones, and calcsilicate rocks; (4) Ca-poor metapelites, metasandstones, and quartz-tourmaline rocks; (5) metacarbonates; and (6) meta-ultramafics. [D. J. Henry and C. V. Guidotti, 1985, *Amer. Miner., 70,* 4.]

složení granátu

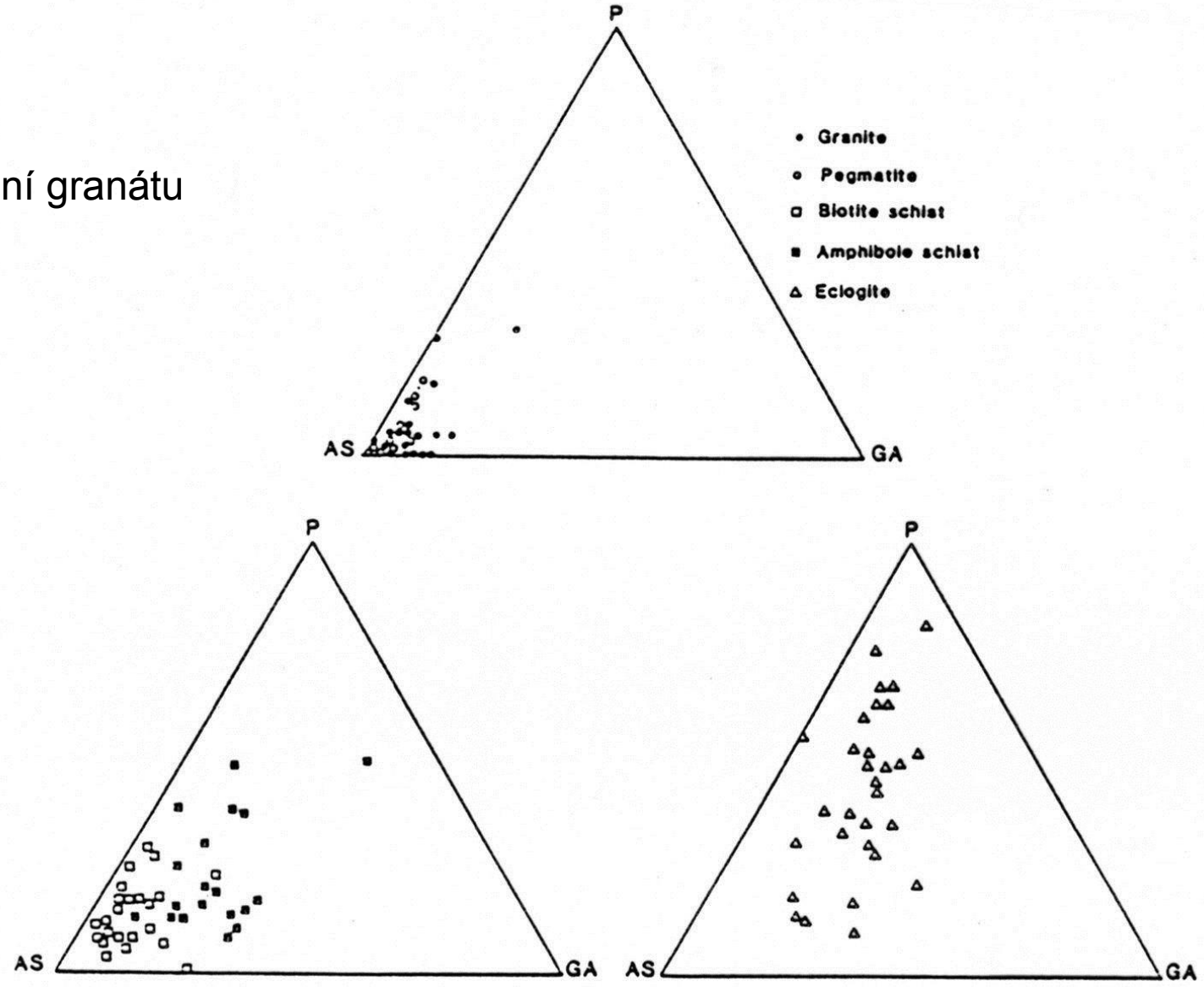

Fig. 11. Variation in composition of garnets from different source lithologies, from Wright (1938). AS, almandine + spessartine; P, pyrope; GA, grossular + andradite.

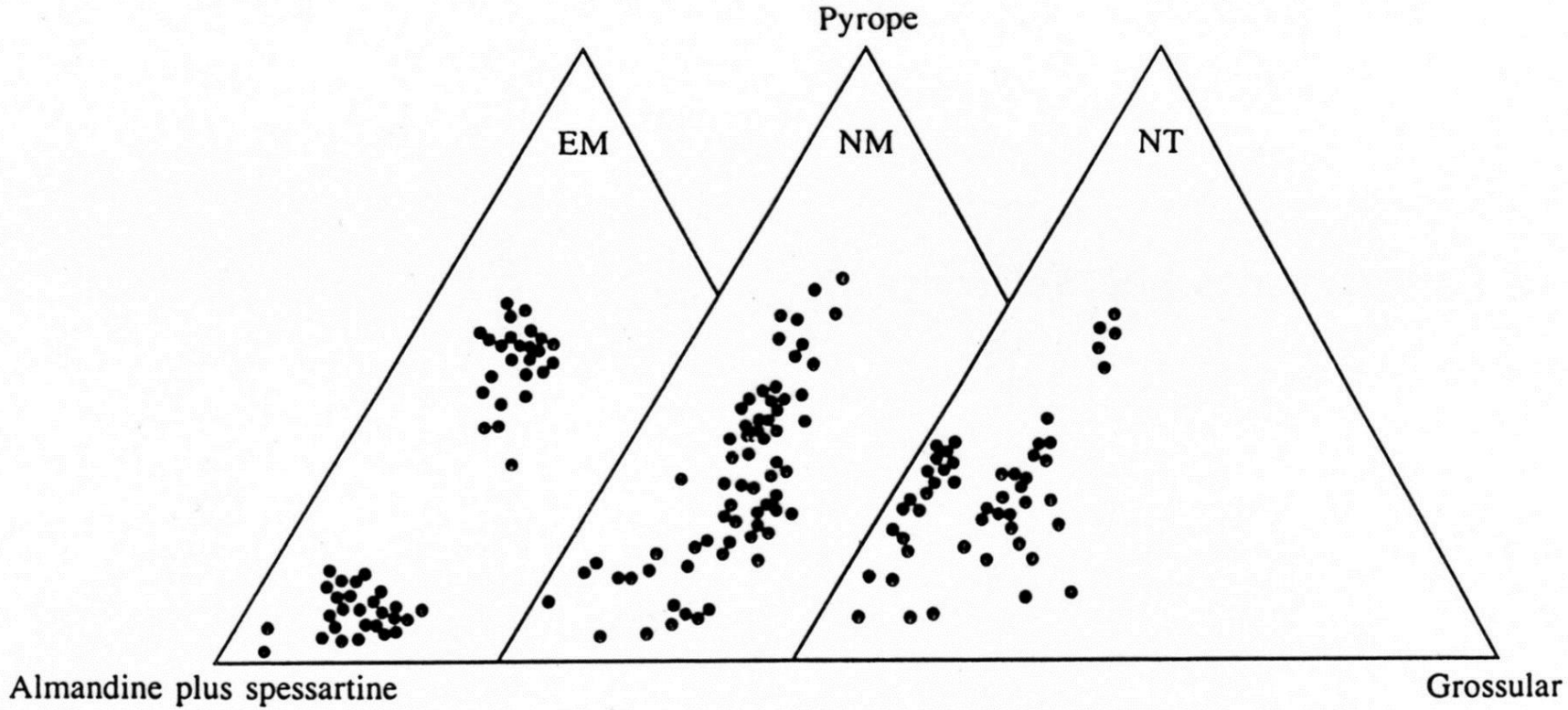

Figure 4-17
Comparison of electron microprobe analyses of garnet grains. Sample EM is from Etive Formation, Murchison Field; NM, from Ness Formation, Murchison Field, NT, from Ness Formation, Tern Field, which is about 50 km from Murchison. The Ness Formation immediately overlies the Etive Formation. [Modified from Morton, 1985a, p. 556.]

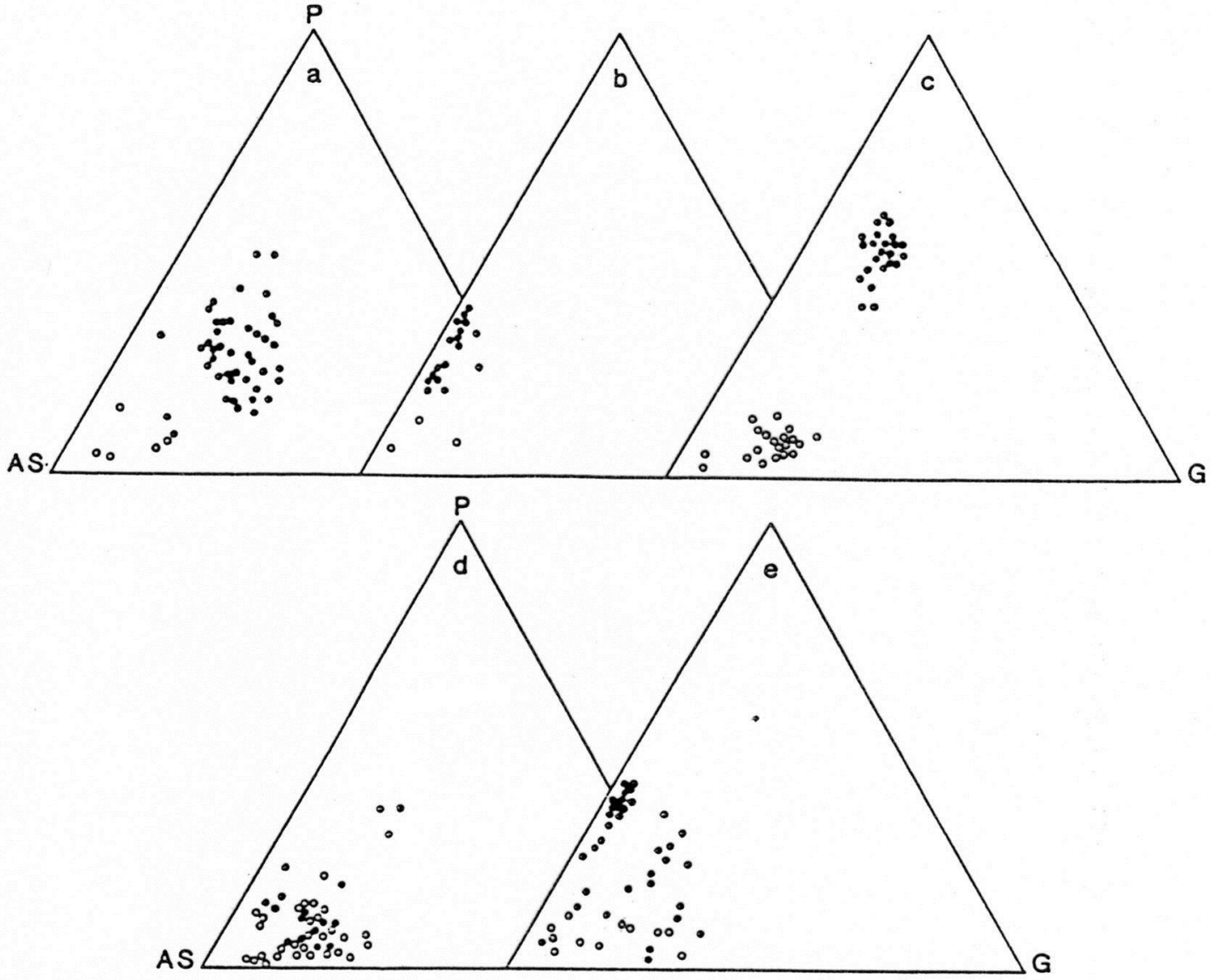

Fig. 10. Illustration of the variety of compositions shown by detrital garnets of North Sea sediments. (a) Oseberg Formation (Middle Jurassic), Oseberg Field (from Hurst & Morton 1988). (b) Broom Formation (Middle Jurassic), Murchison Field (from Morton 1985*b*). (c) Etive Formation (Middle Jurassic), Murchison Field (from Morton 1985*b*). (d) Ness Formation (Middle Jurassic), Oseberg Field (from Hurst & Morton 1988). (e) Forties formation (Palaeocene), Forties Field (from Morton 1987*b*). AS, almandine + spessartine; P, pyrope; g, grossular. Open circles have spessartine > 5%, closed circles have spessartine < 5%.

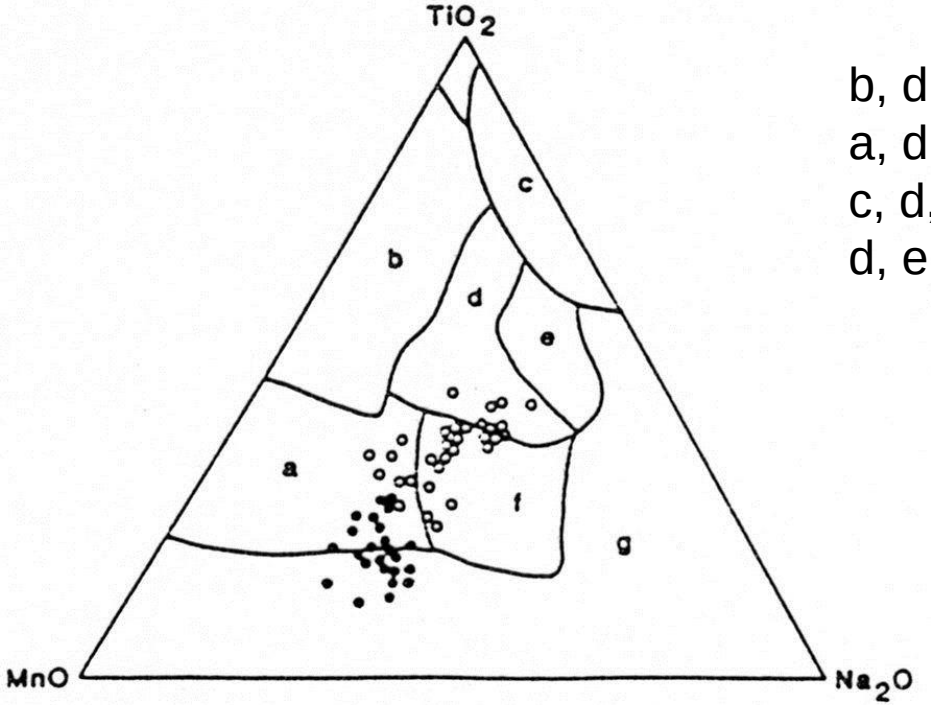

Fig. 4. Discrimination of provenance of detrital pyroxenes from two formations belonging to a Palaeozoic clastic sequence in eastern Australia, using the plot described by Nisbet & Pearce (1977). Ocean floor basalts plot in fields b and d. Volcanic arc basalts plot in fields a, d, e and f. Within-plate alkalic basalts plot in fields c, d, f and g. Within-plate tholeiites plot in fields d and e.

b, d – oc. basalt
a, d, e, f – volc. arc basalt
c, d, f, g – within-plate alkali basalts
d, e – within-plate tholeiites

složení pyroxenu

vulkanosedimentární historie

authigenic minerals : abundant
allogenic minerals : stable to ultrastable
proportion of allogenic heavy minerals : small (locally nil)

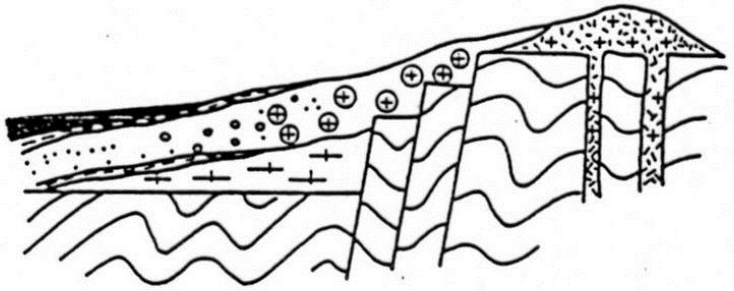

pyroclastic fan
(e.g. Stockheim)

authigenic minerals : common
allogenic minerals : labile to ultrastable
proportion of allogenic heavy minerals : large

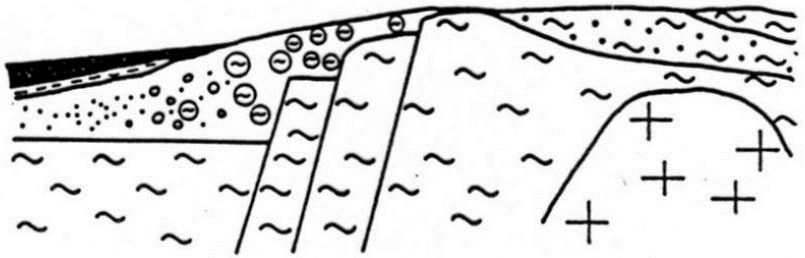

mixed fan
alluvial > pyroclastic
(e.g. Erbendorf)

authigenic minerals : common
allogenic minerals : labile to ultrastable
proportion of allogenic heavy minerals : large

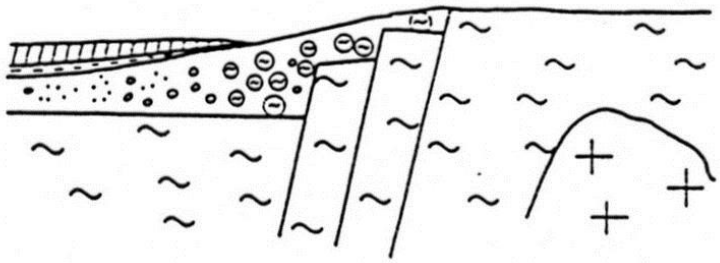

alluvial fan with subordinate tuffaceous intercalations (e.g. Weiden)

authigenic minerals : rare
allogenic minerals : labile to ultrastable
proportion of allogenic heavy minerals : large

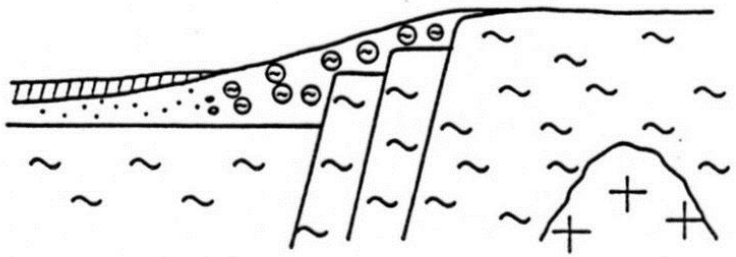

alluvial fan (e.g. Schmidgaden)

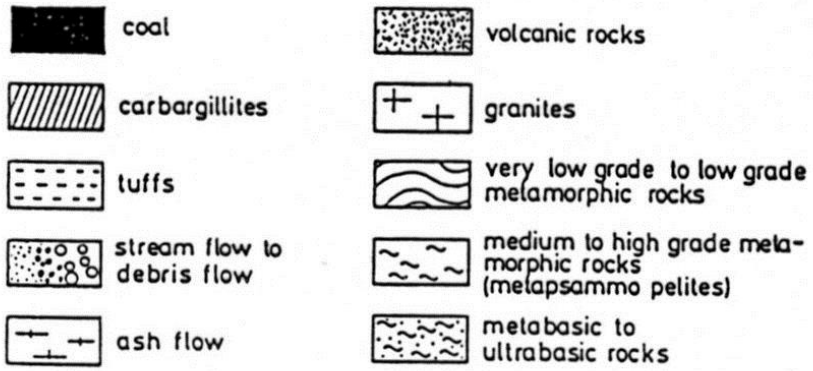

Fig. 5. Cartoon to illustrate the various types of fans as well as the sort and amount of heavy minerals present in these clastic and volcaniclastic rocks.

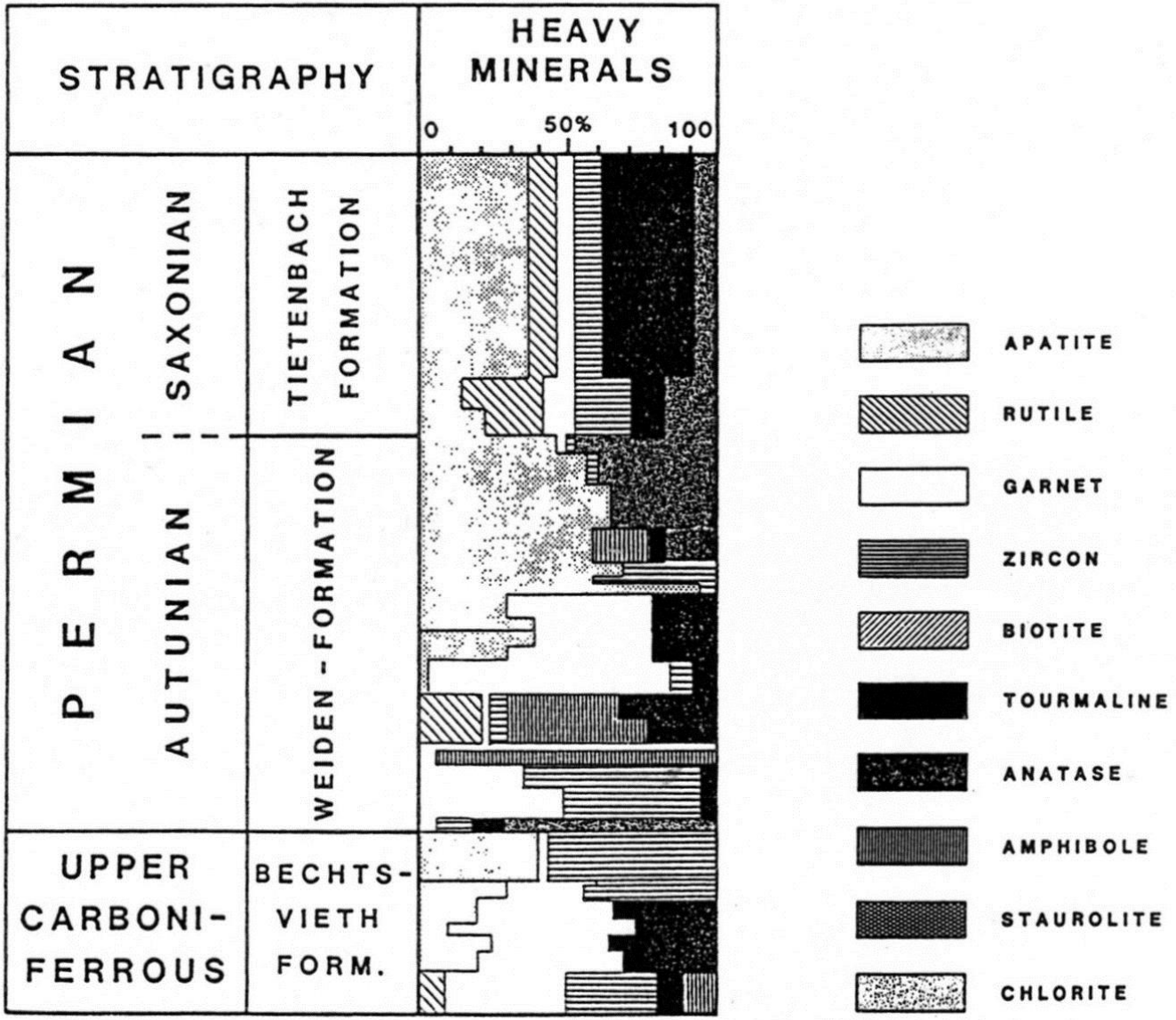

Fig. 6. The heavy mineral log of Erbendorf basin (mixed fan type II) taken as representative for the stratigraphically-controlled

magmaticky
recyklovaný
turmalín

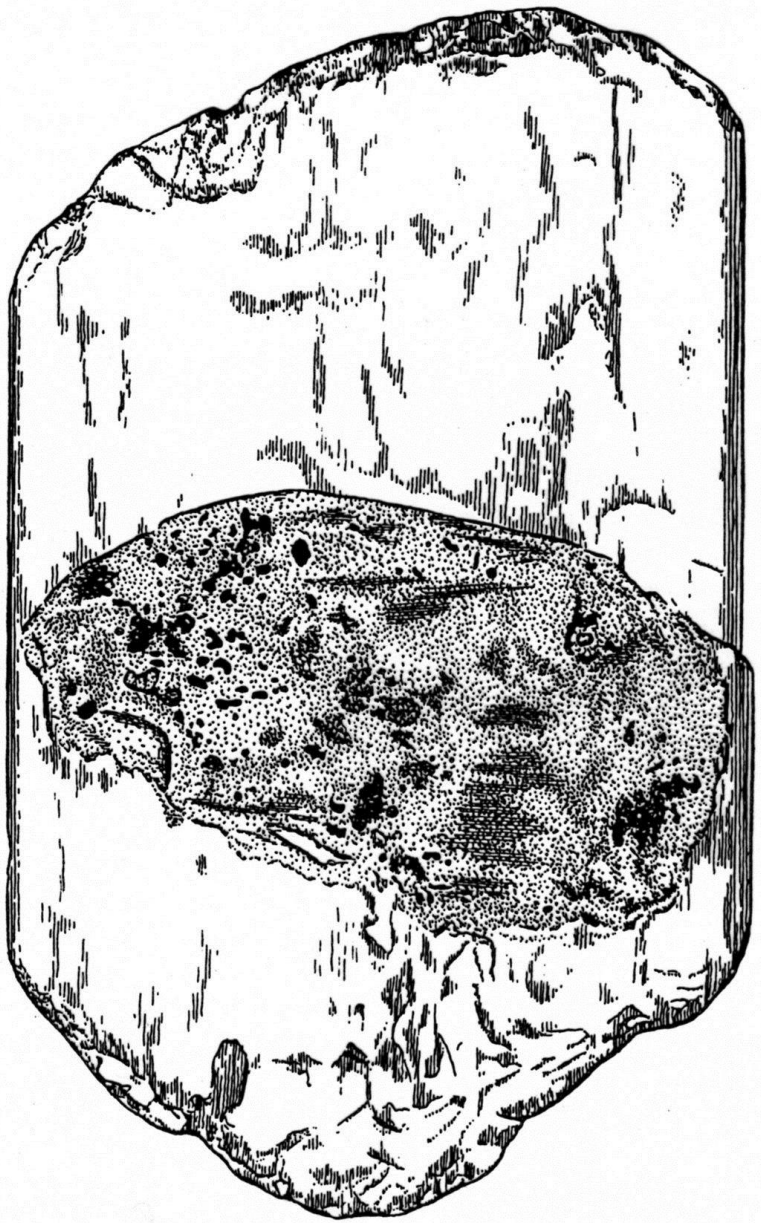

Fig. 8-3. Abraded tourmaline overgrowth on abraded detrital core, Cretaceous McNairy Sand, Henry County, Tennessee, U.S.A. (Redrawn from Potter and Pryor, 1961, Plate 2)

datování - geochronologie

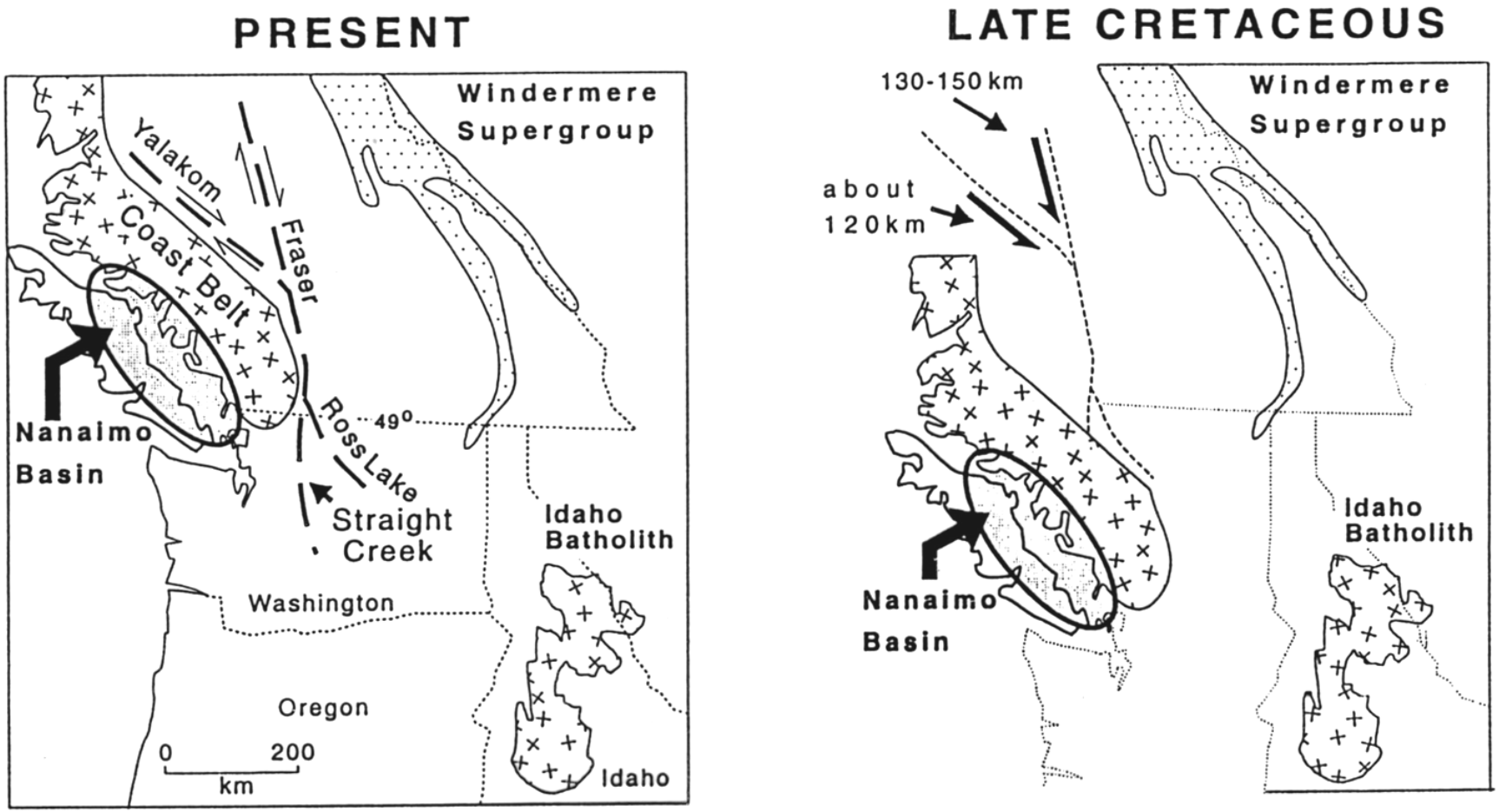

FIG. 5.—Schematic diagrams showing position of Nanaimo Basin and Coast Belt at present (left) and approximate position during latest Cretaceous (right) with about 250 of dextral strike-slip movement restored on Fraser-Straight Creek and Yalakom-Ross Lake fault systems. This minimum estimate of offset does not include offset on the several other early Tertiary strike-slip faults in northwest Washington and southern B. C. or any estimate of the amount of early Tertiary extension.

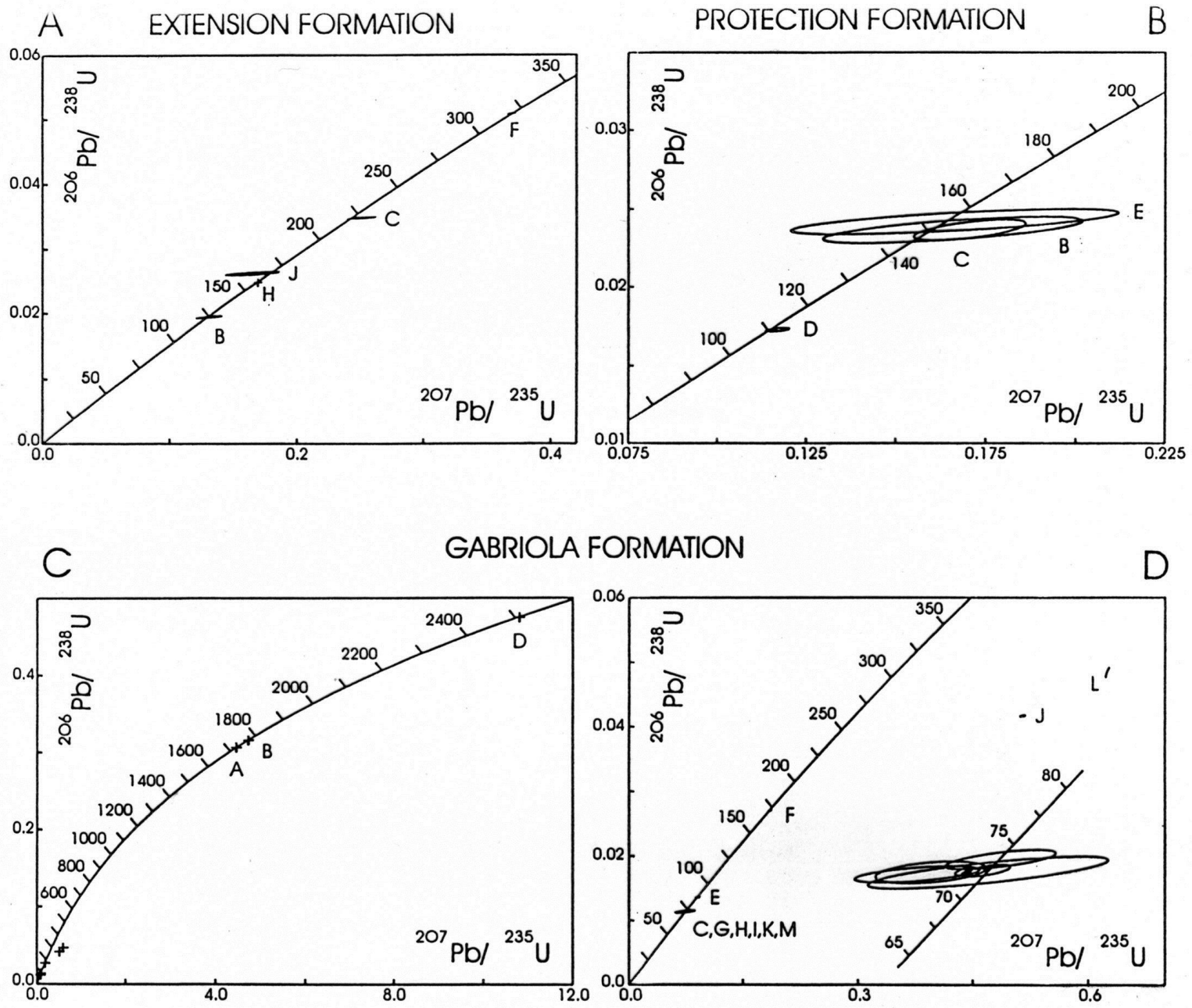

FIG. 4.—U-Pb Concordia plots showing detrital zircon data. (A) Extension Formation; (B) Protection Formation; (C) Gabriola Formation (all data); (D) Gabriola Formation, expanded scale plot of post Pre-Cambrian data.

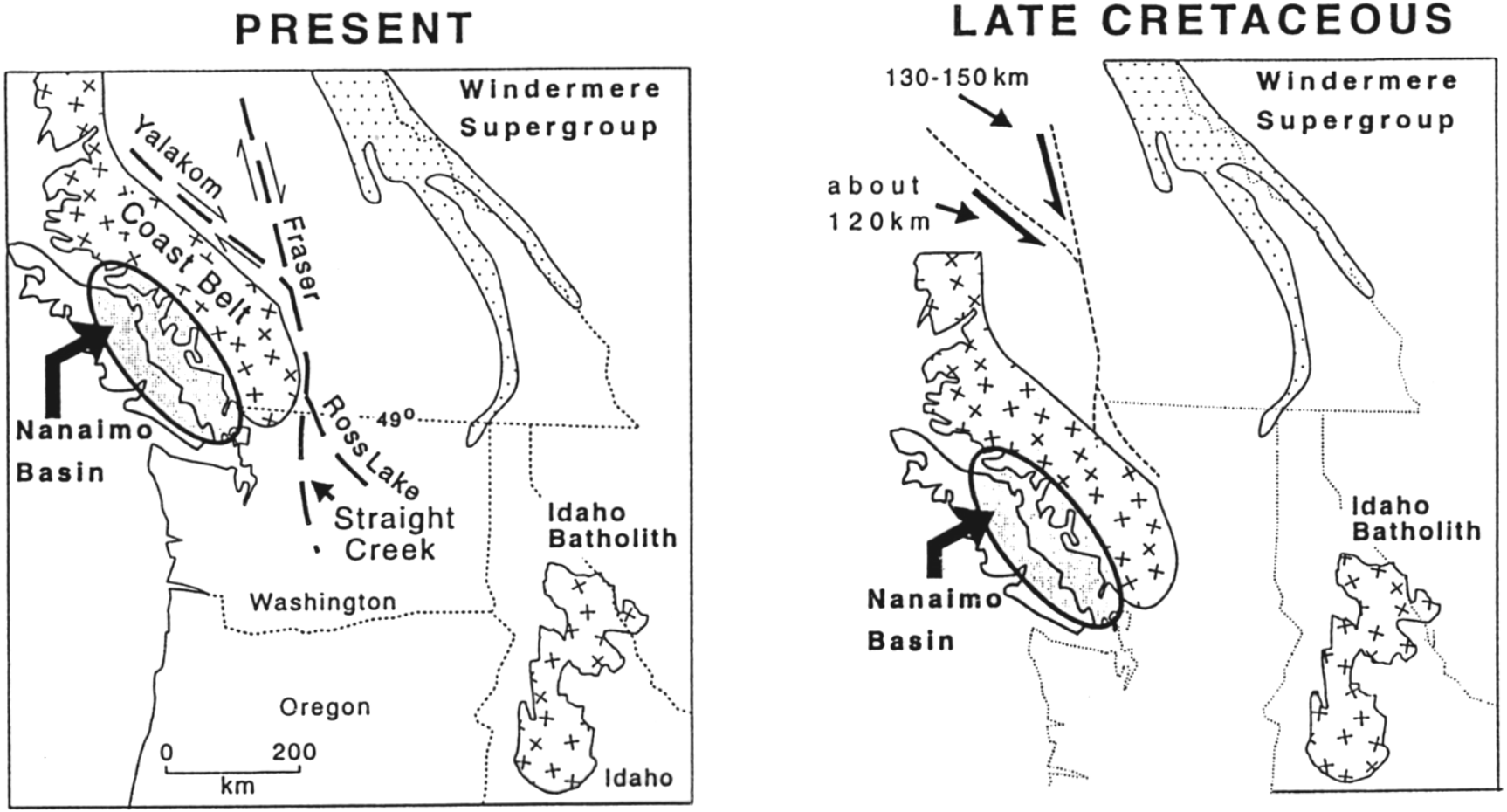

FIG. 5.—Schematic diagrams showing position of Nanaimo Basin and Coast Belt at present (left) and approximate position during latest Cretaceous (right) with about 250 of dextral strike-slip movement restored on Fraser-Straight Creek and Yalakom-Ross Lake fault systems. This minimum estimate of offset does not include offset on the several other early Tertiary strike-slip faults in northwest Washington and southern B. C. or any estimate of the amount of early Tertiary extension.

diageneze

- geotermální gradient, termální modely
- porozita, permeabilita
- tlakové rozpouštění, sekundární porozita
- kompakce
- tmely - křemité (syntaxiální nárůsty, ..), karbonátové, autigenní živce (nárůsty), jíl.minerály a zeolity, hematit, baryt
- diagenetická prostředí
- stupeň proměny a krystalinity jílových minerálů

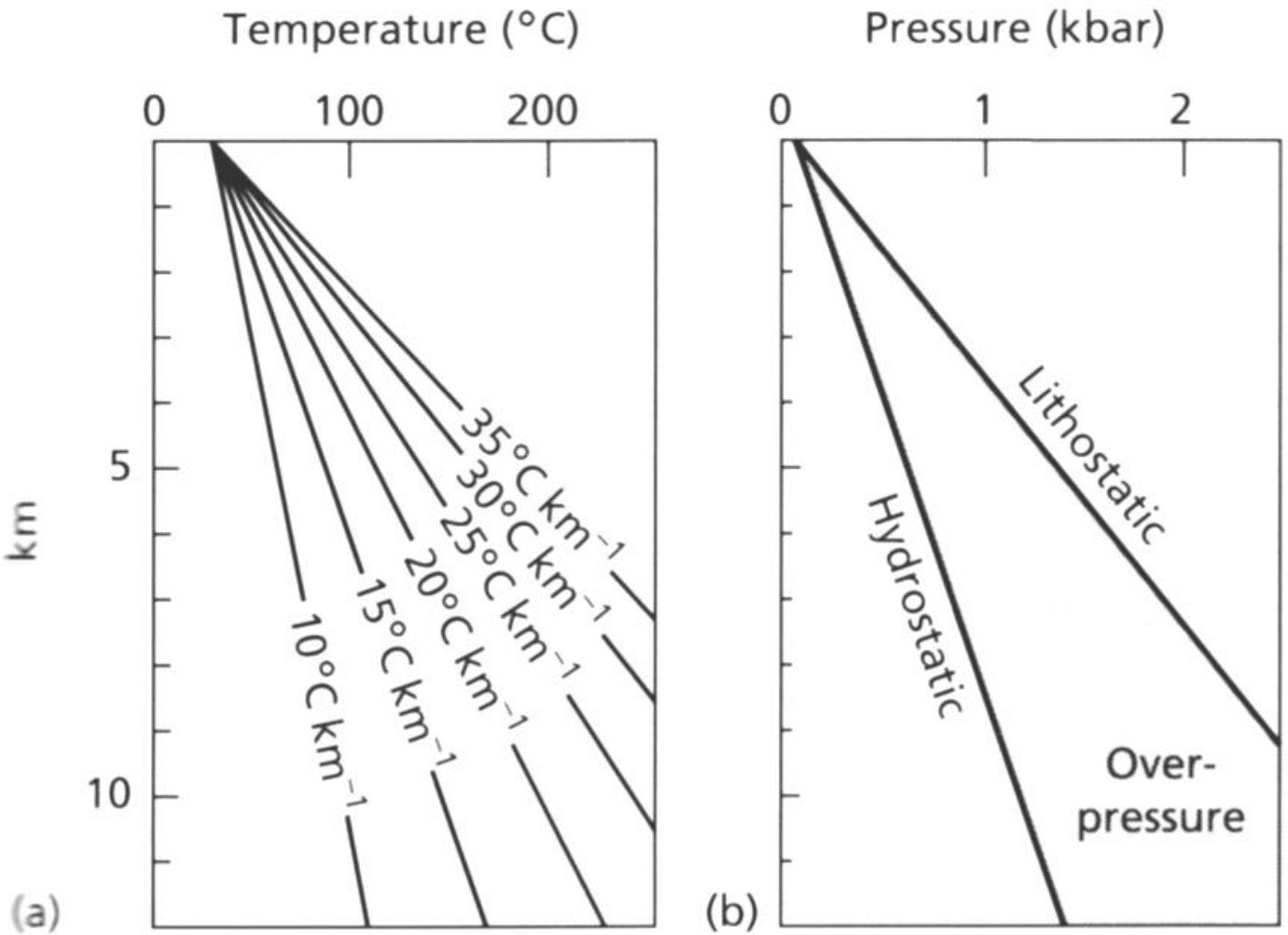

Fig. 2.53 (a) Increase in temperature with increasing depth for different geothermal gradients. (b) Increase in hydrostatic and lithostatic (overburden) pressure with increasing depth.

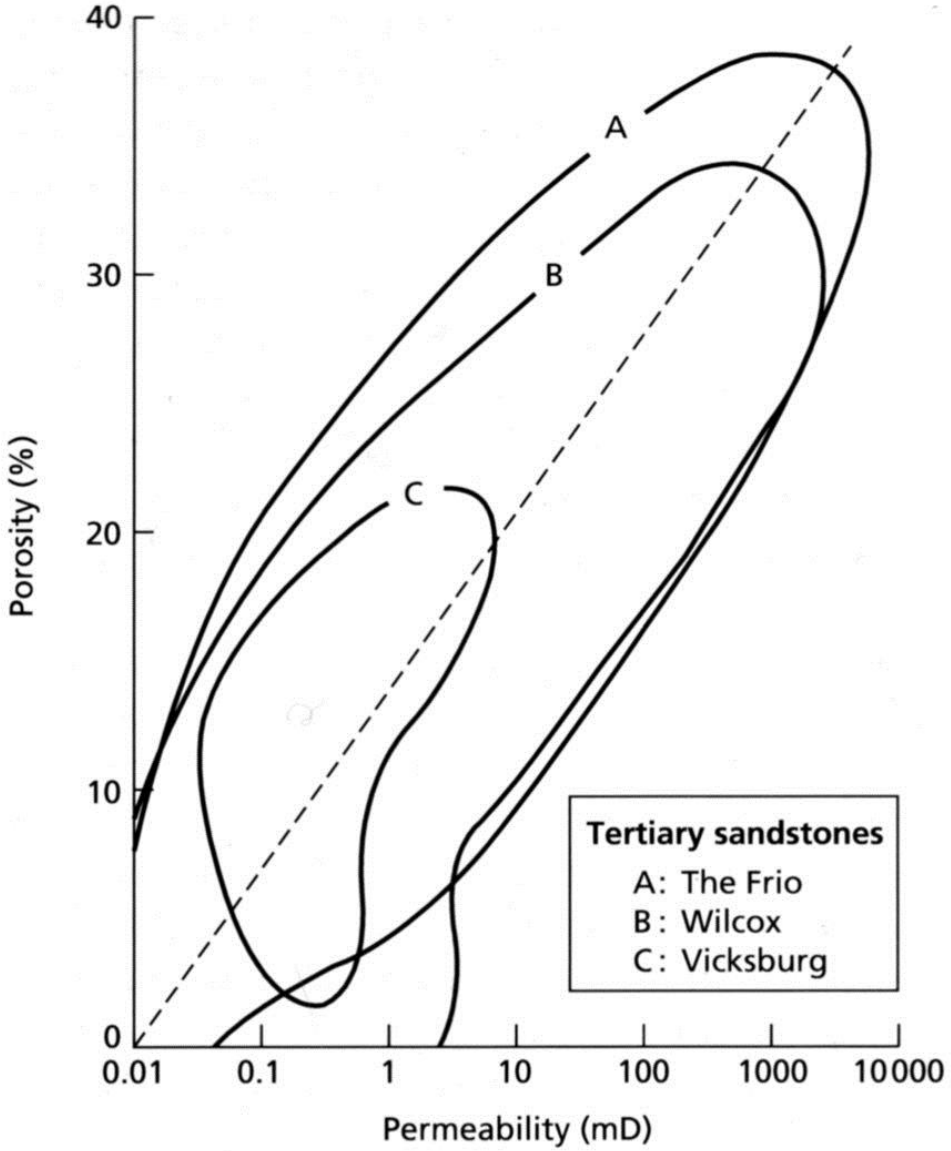

Fig. 2.59 Porosity–permeability plot for three Tertiary sandstones of the Gulf Coast subsurface, the Frio (a), Wilcox (b) and Vicksburg (c), showing the general increase in permeability with increasing porosity. After Loucks *et al*. (1984).

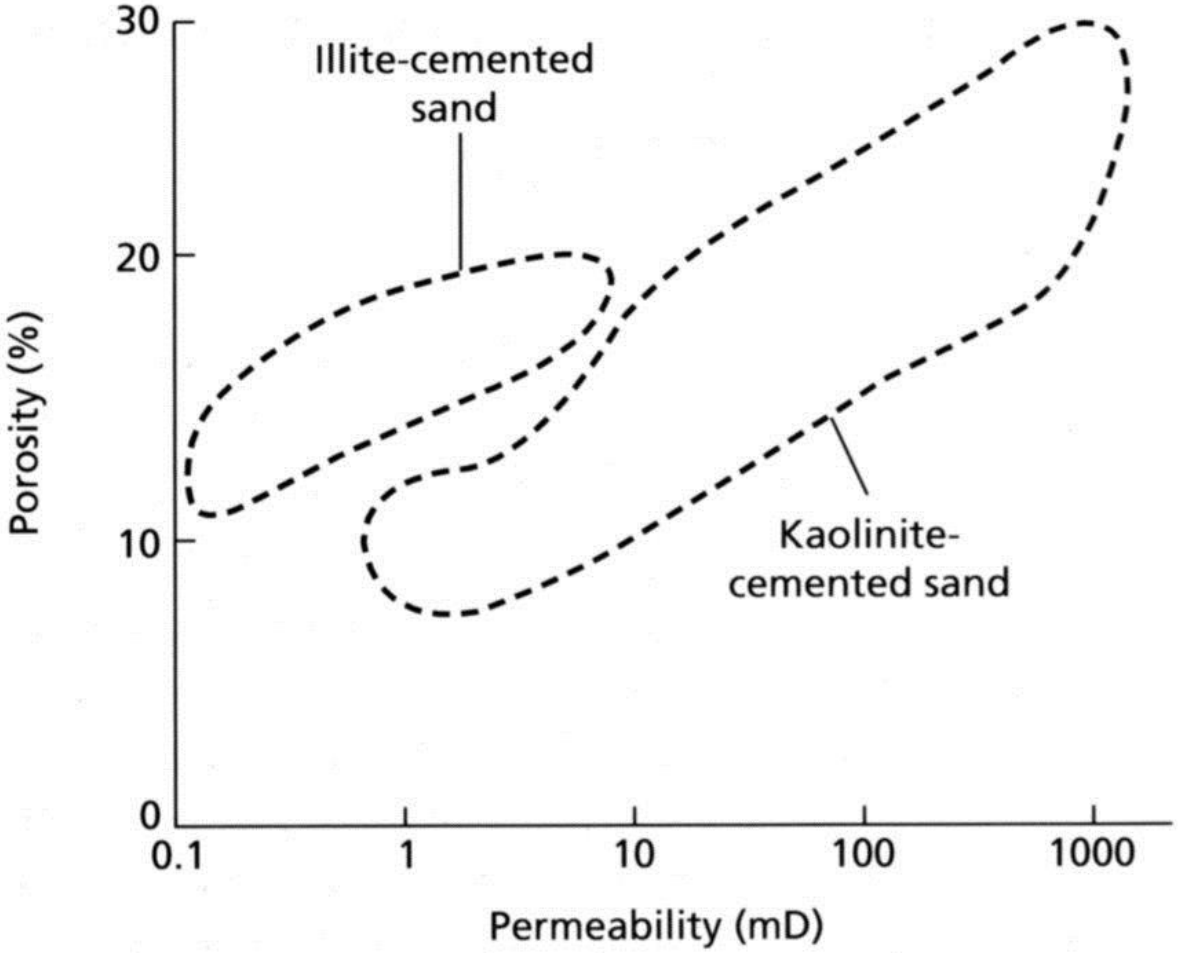

Fig. 2.56 Porosity–permeability plot for kaolinite- and illite-cemented aeolian sandstones in the Permian Rotliegendes. Southern North Sea. After Stalder (1973).

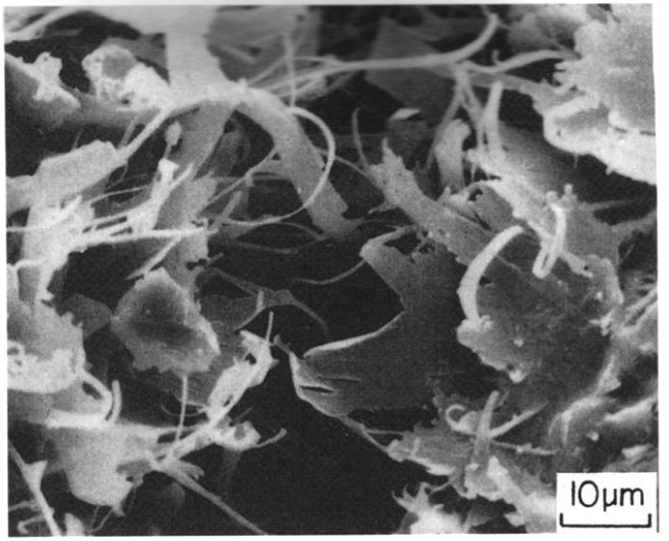

Fig. 2.54 Scanning electron micrograph of authigenic illite in the form of radially arranged flakes and whiskers growing into pore space between two sand grains (left and right of picture). Rotliegend desert sandstone, Lower Permian. Northern Germany.

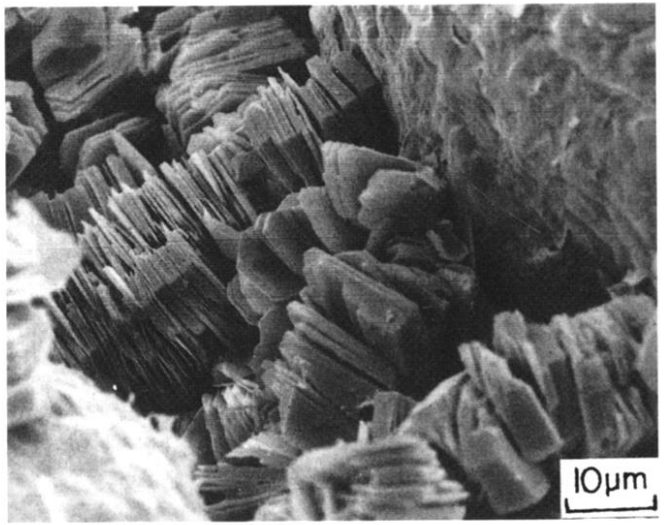

Fig. 2.55 Scanning electron micrograph of authigenic kaolinite, consisting of stacked pseudohexagonal platy crystals, between rounded sand grains. Rotliegend desert sandstone. Lower Permian. Northern Germany.

pohřbená arkóza ⟶ kvarcit

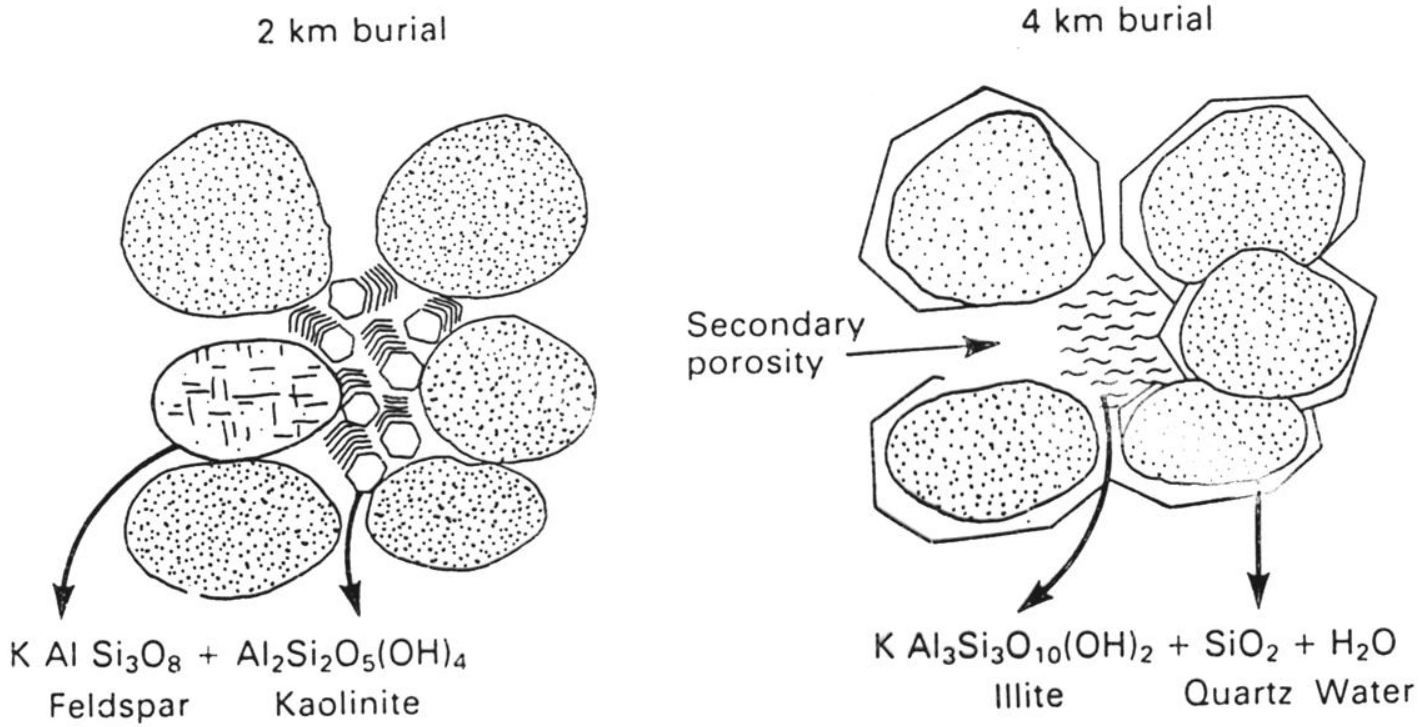

Fig. 5.28. Chemical reactions between feldspar and kaolinite are triggered by continued burial to produce illite, quartz overgrowth cements plus secondary porosity (from Bjørlykke, 1983).

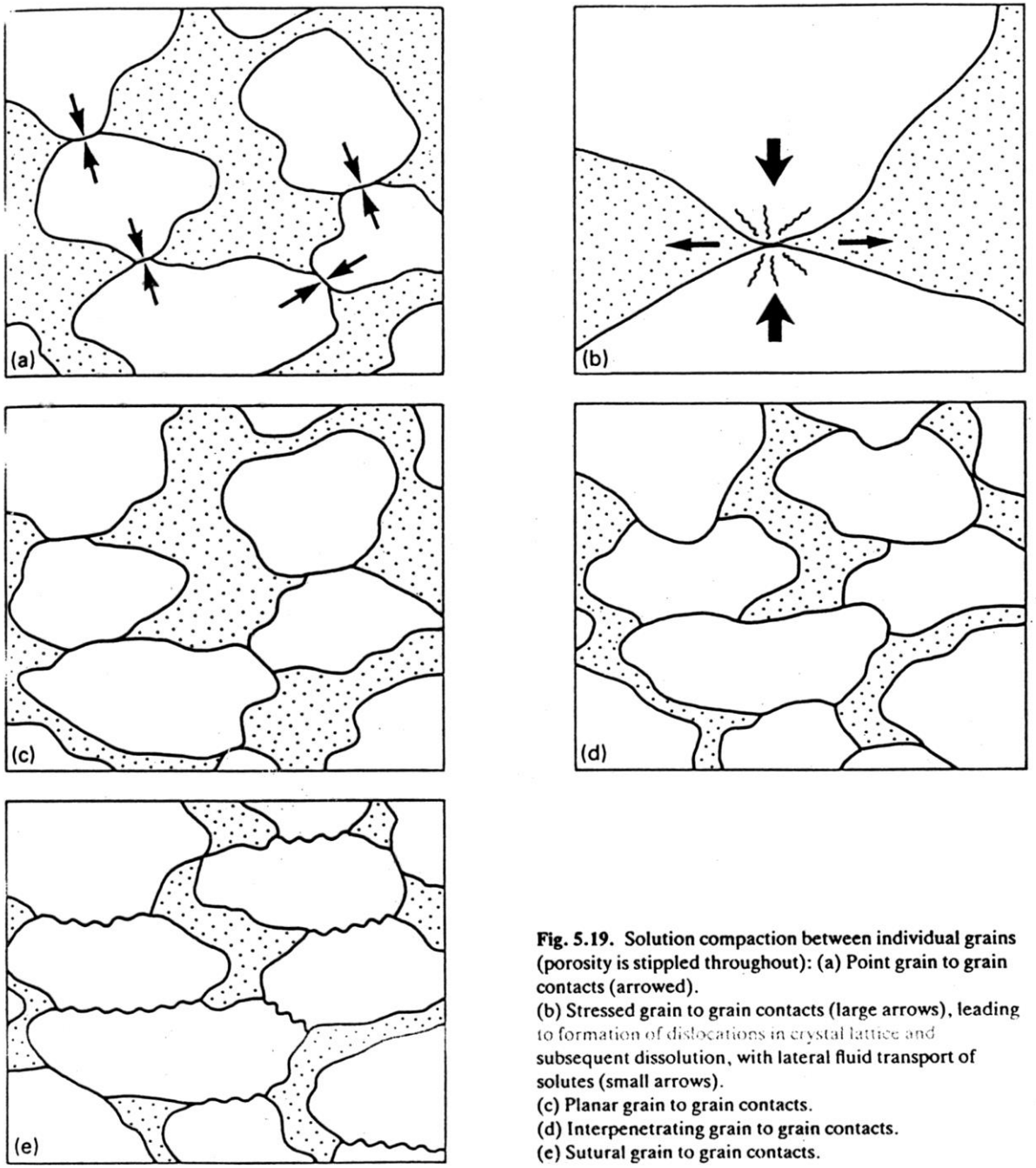

Fig. 5.19. Solution compaction between individual grains (porosity is stippled throughout): (a) Point grain to grain contacts (arrowed).
(b) Stressed grain to grain contacts (large arrows), leading to formation of dislocations in crystal lattice and subsequent dissolution, with lateral fluid transport of solutes (small arrows).
(c) Planar grain to grain contacts.
(d) Interpenetrating grain to grain contacts.
(e) Sutural grain to grain contacts.

tlakové rozpouštění

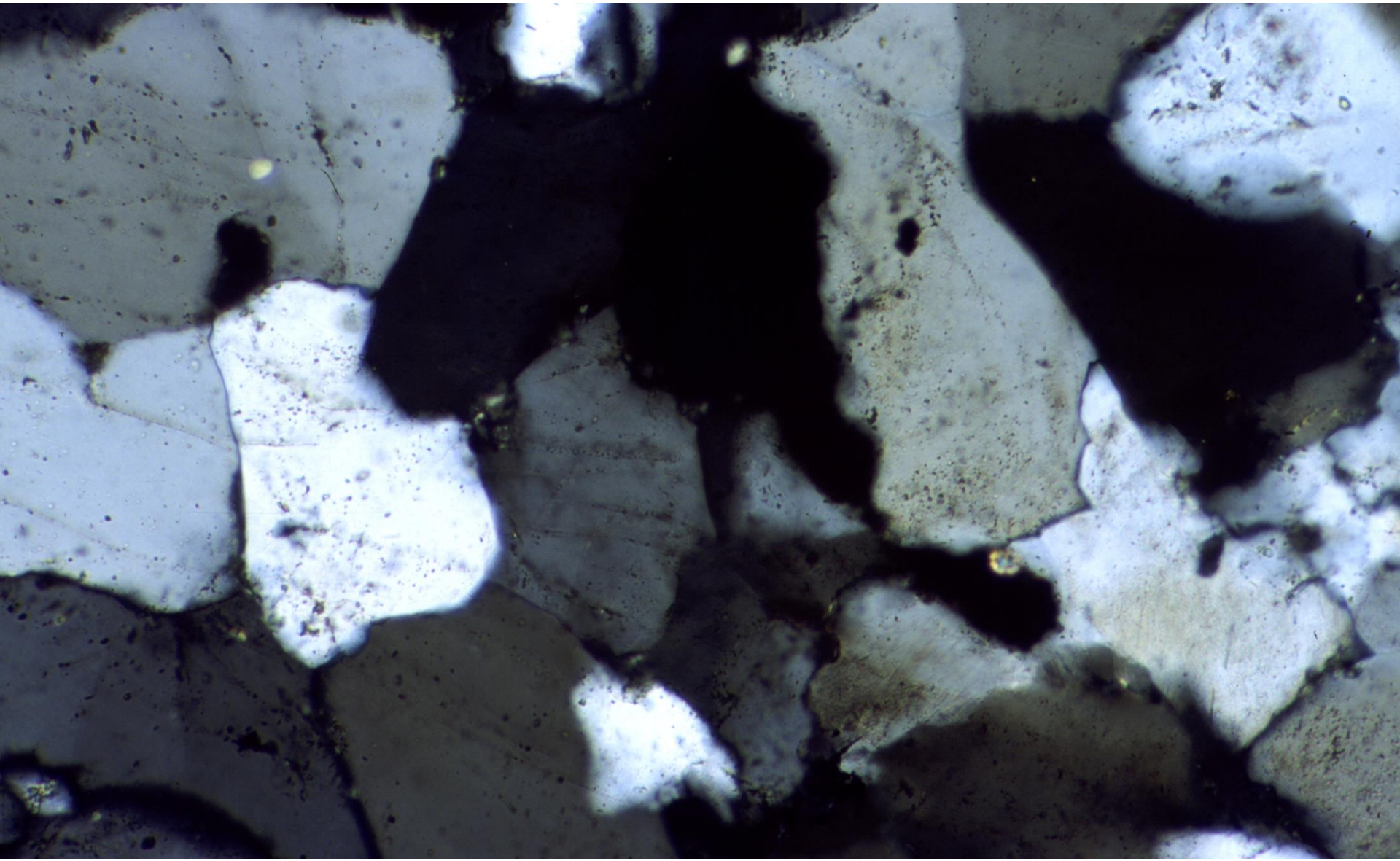

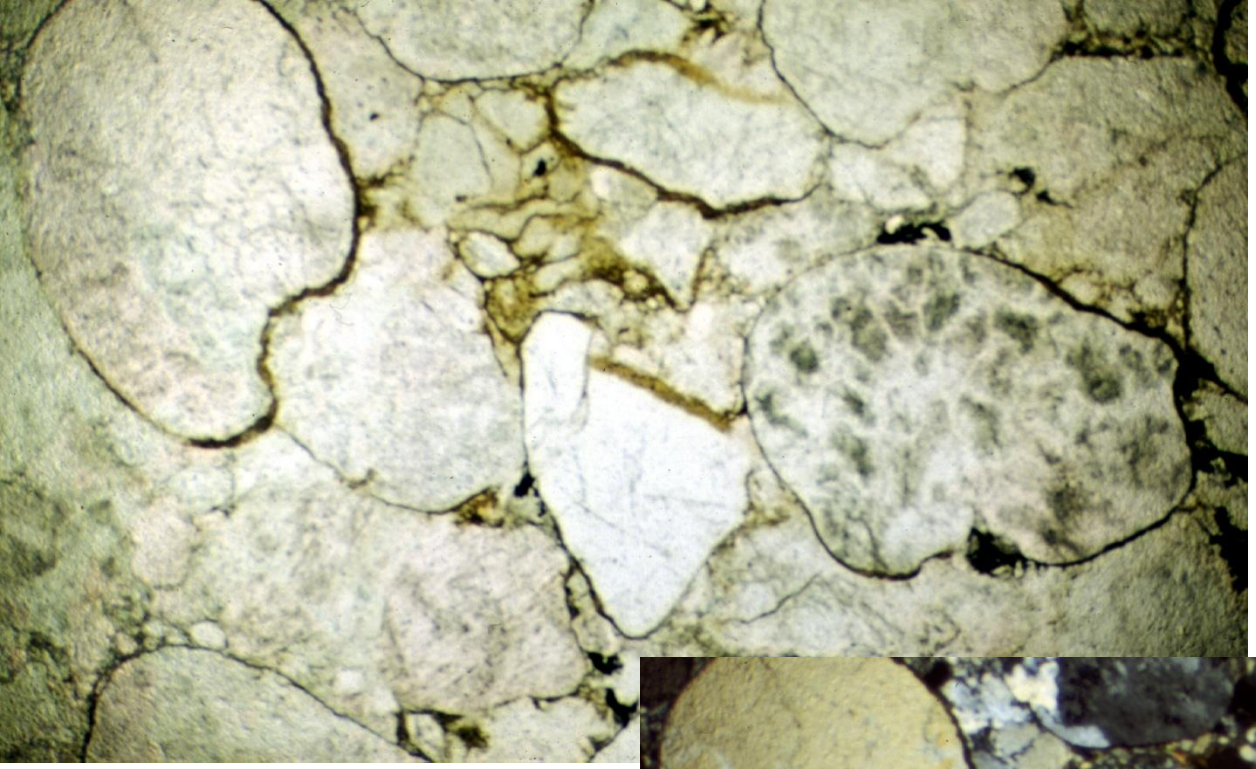

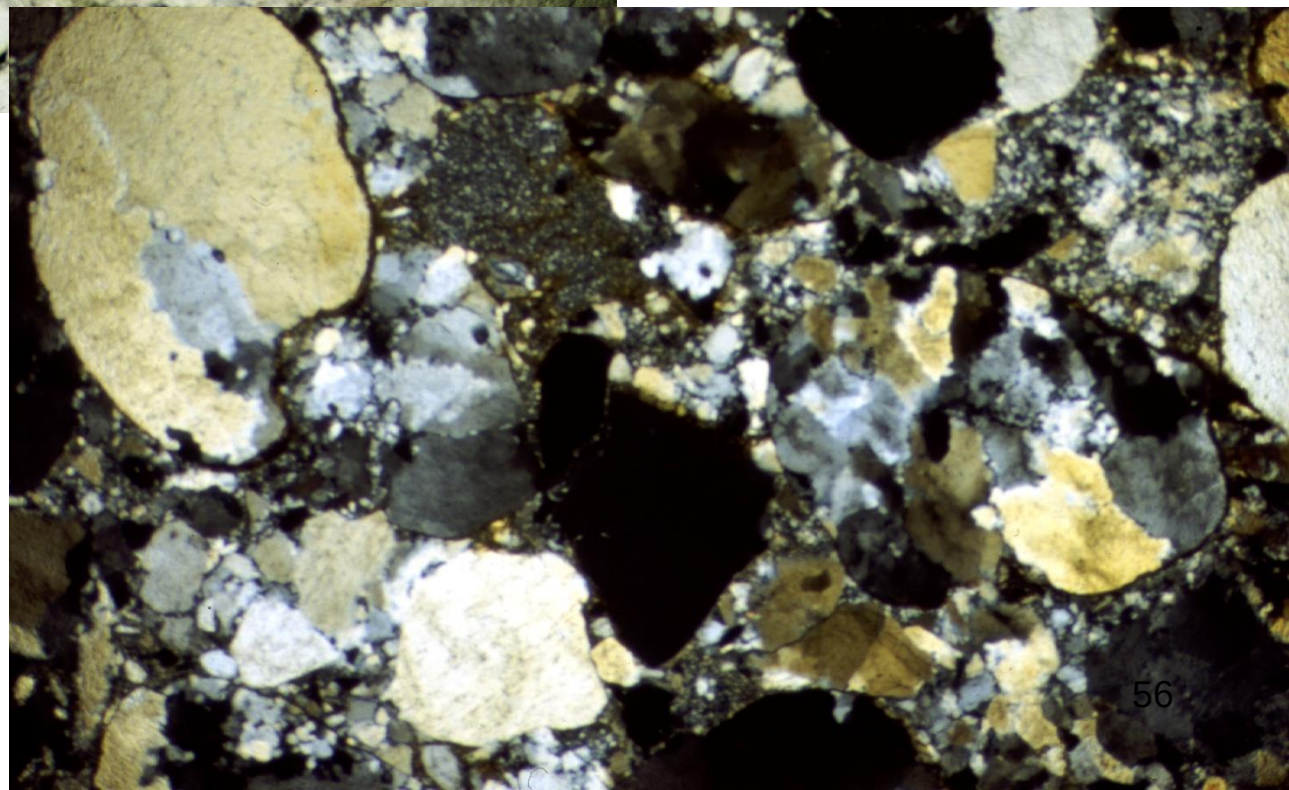

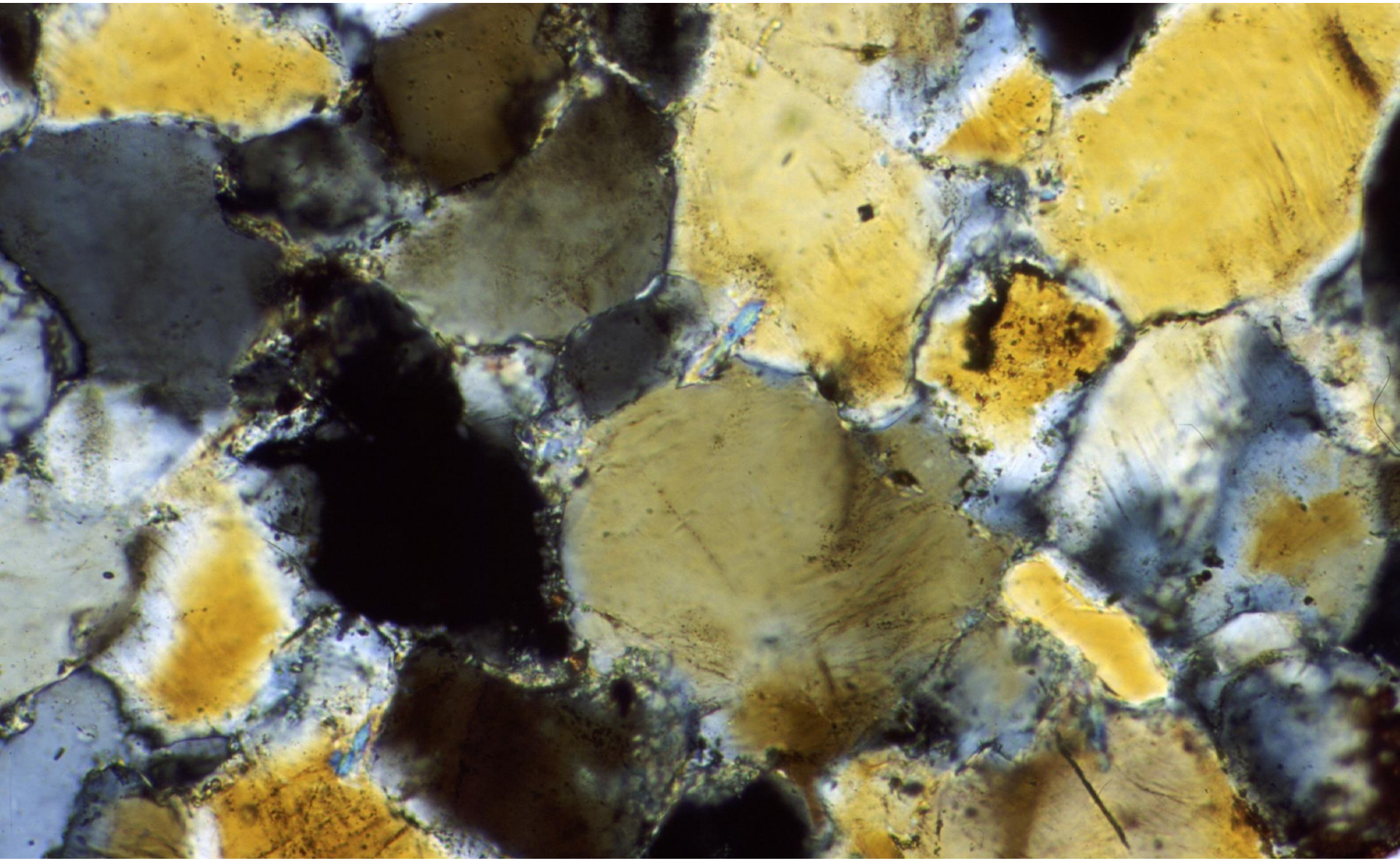

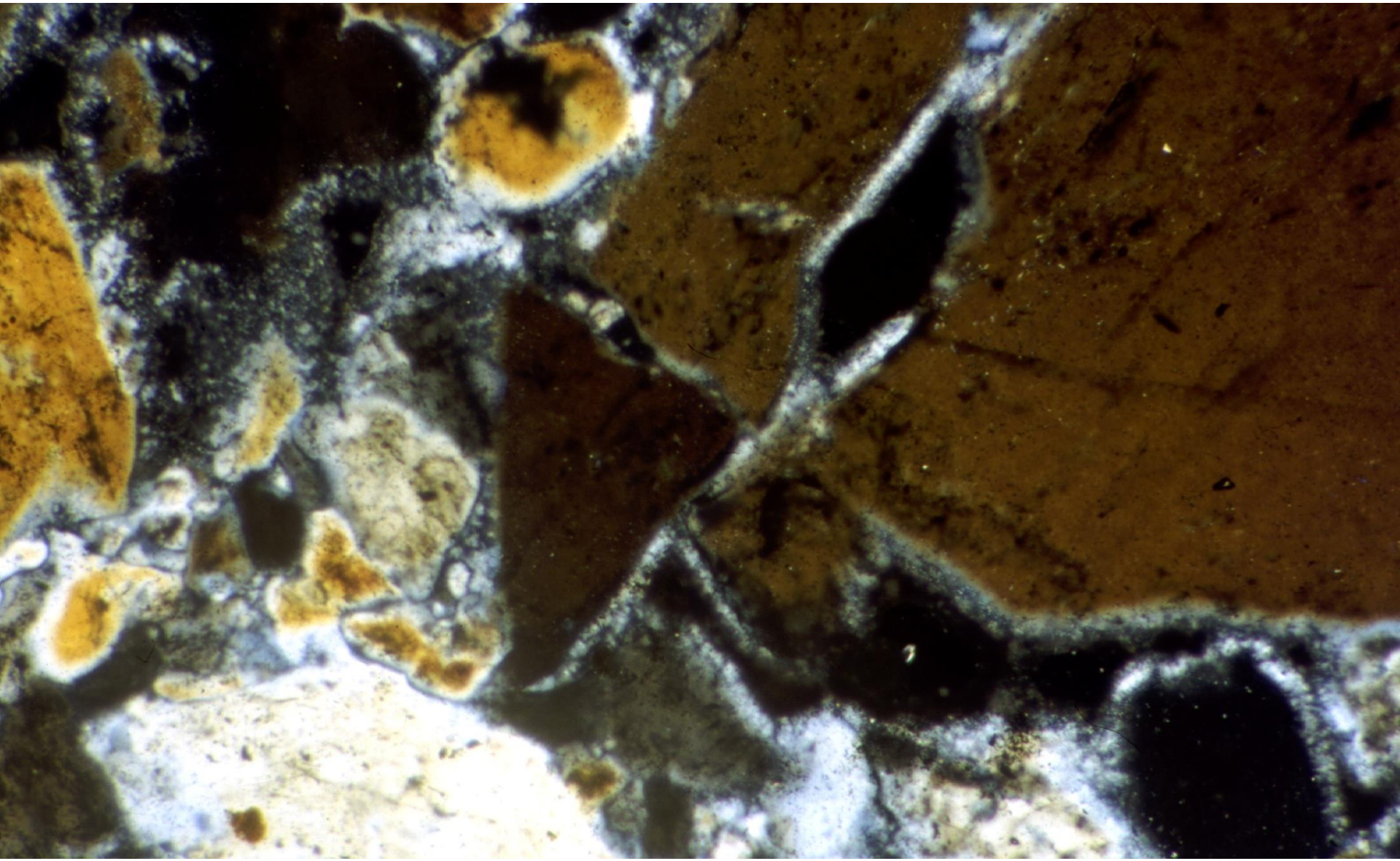

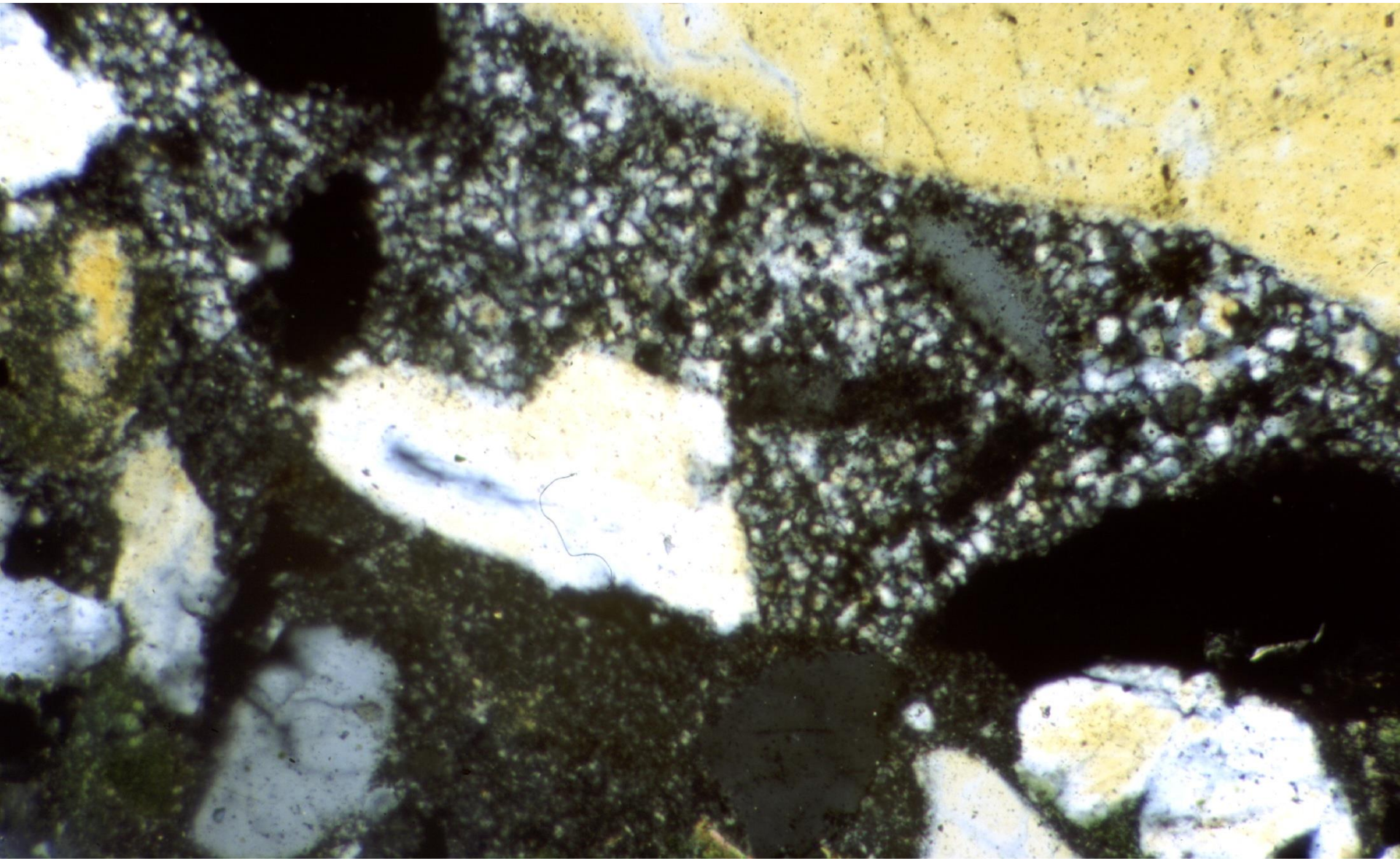

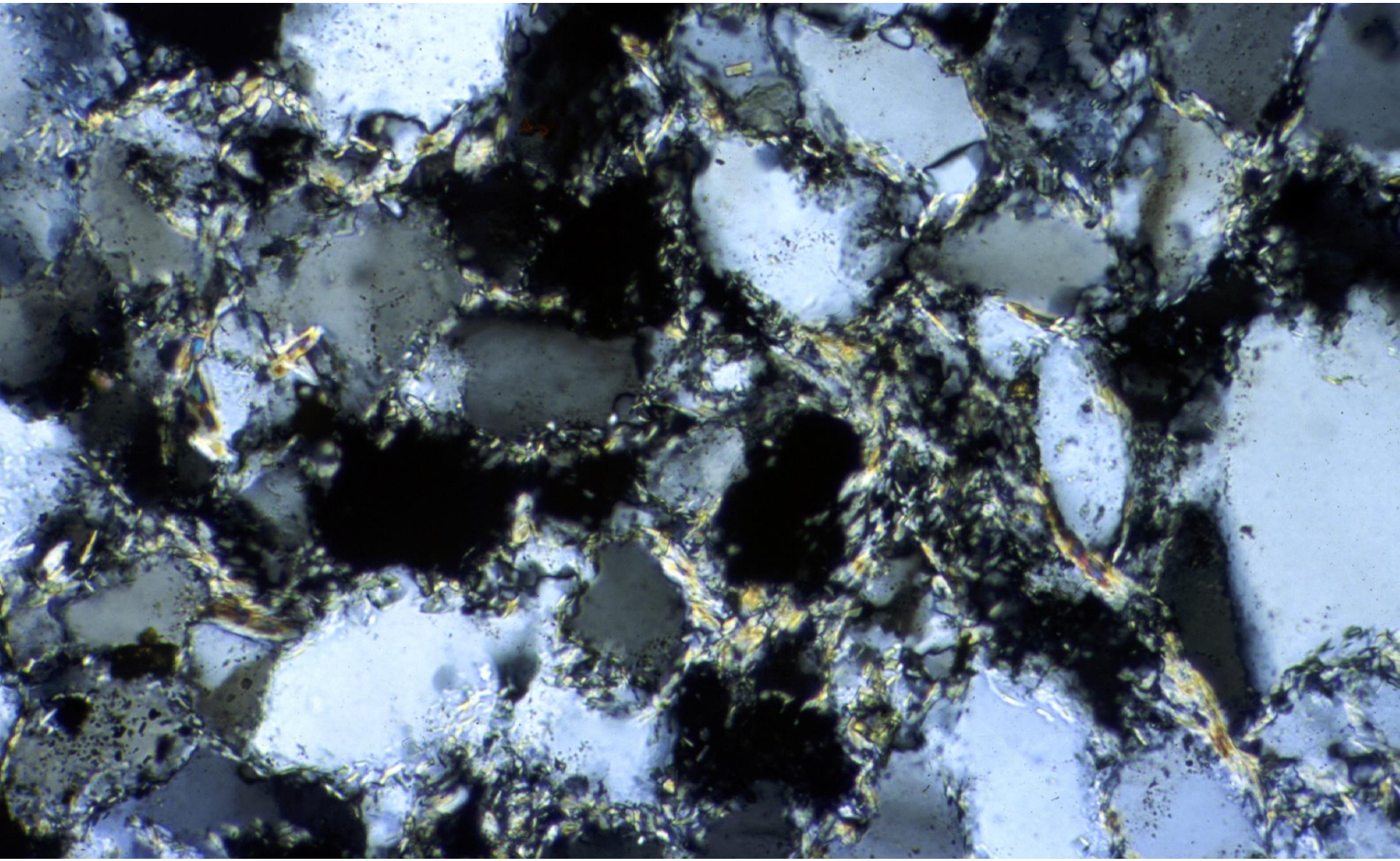

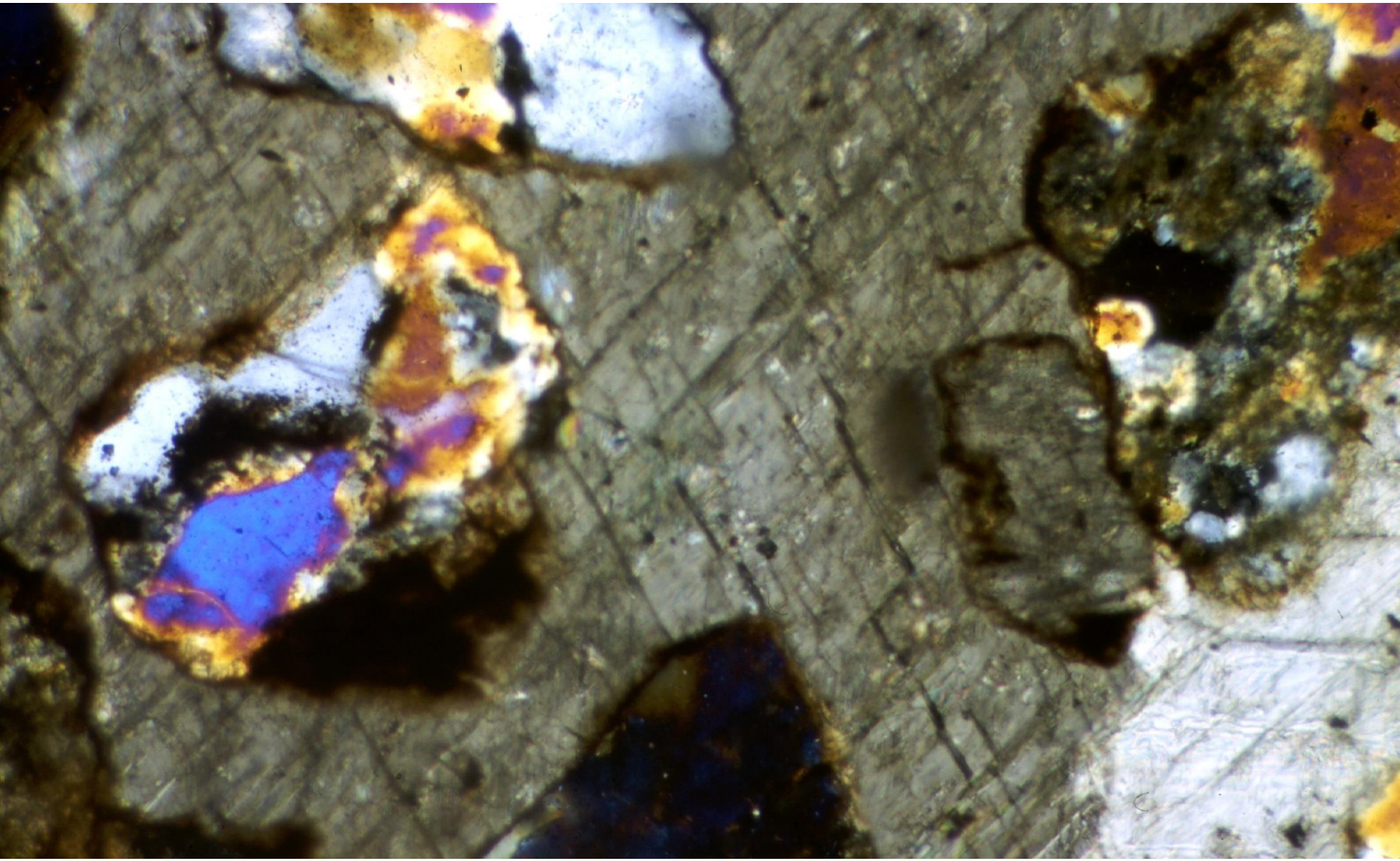

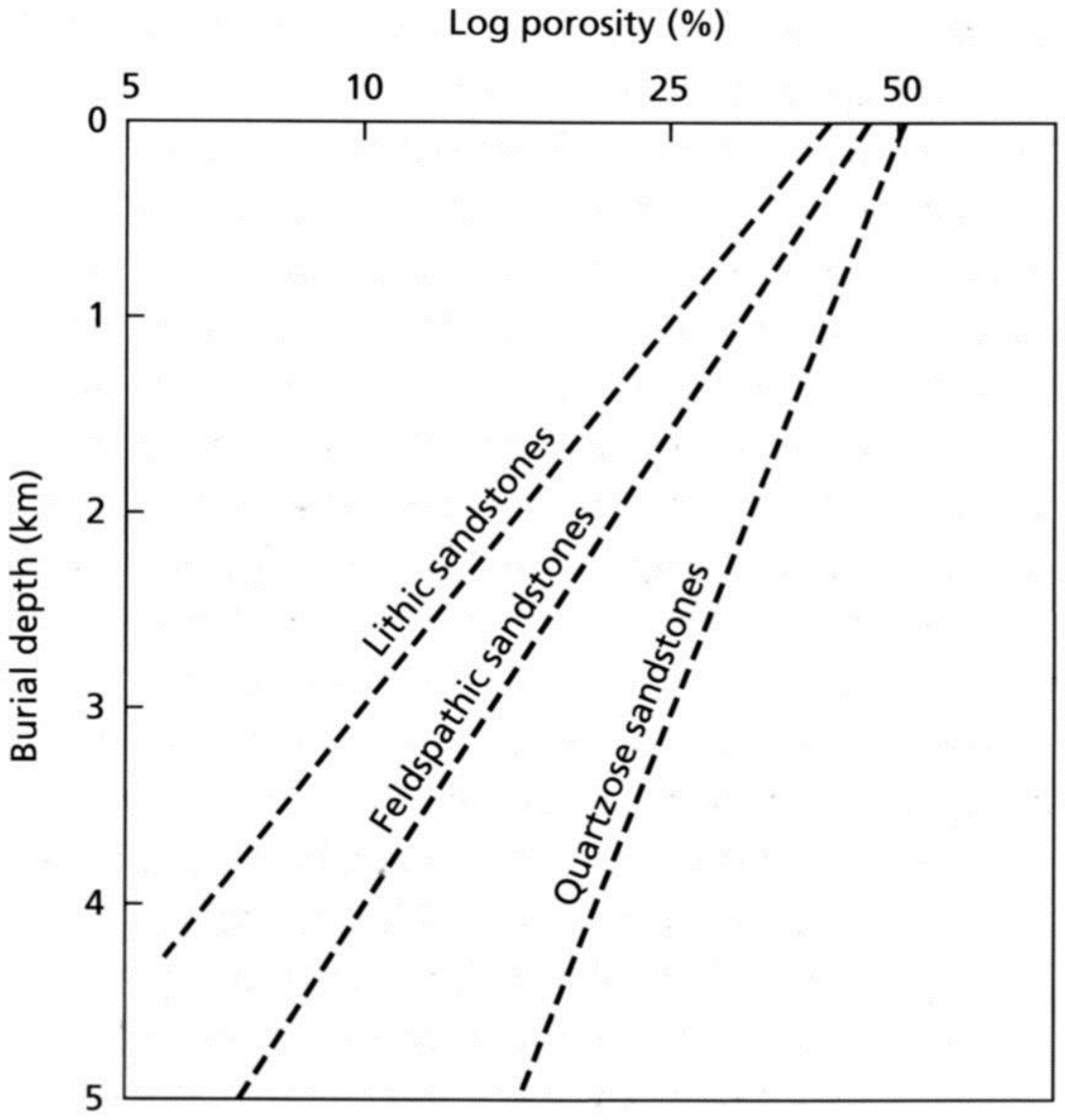

Fig. 2.60 Porosity–depth relationship for sandstones of different composition. After Dickinson (1985), based on several sources.

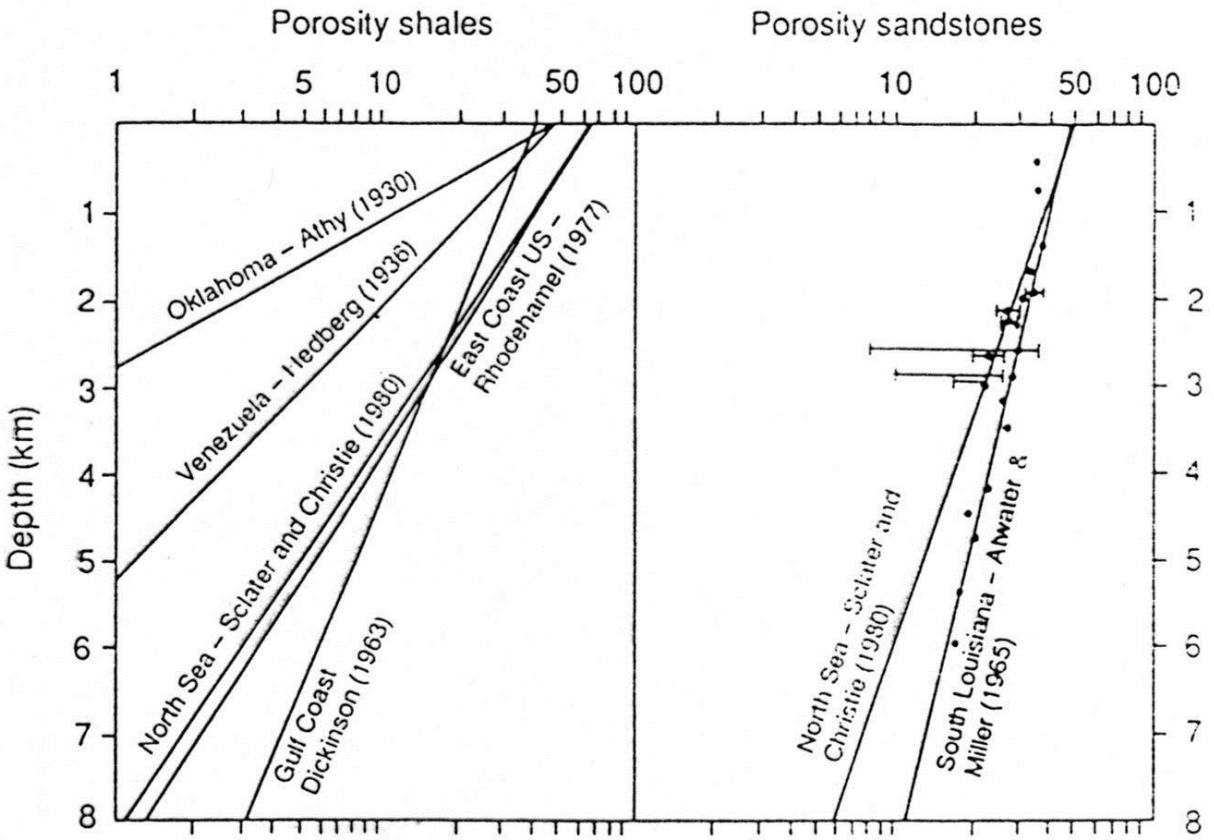

Fig. 8.2. Plots of log porosity against depth for shales and sandstones (after Sclater and Christie 1980). The North Sea shale data are from sonic log values in normally pressured sections, porosities being calculated from the sonic velocity/porosity relation proposed by Magara (1976). The North Sea sandstone data are from the data of Seeley (1978) supplemented by data from sonic logs. The best-fit lines for the North Sea data and for the south Louisiana data of Atwater and Miller (1965) are constrained to pass through the surface porosity values of Pryor (1973).

vliv diageneze
na modální složení

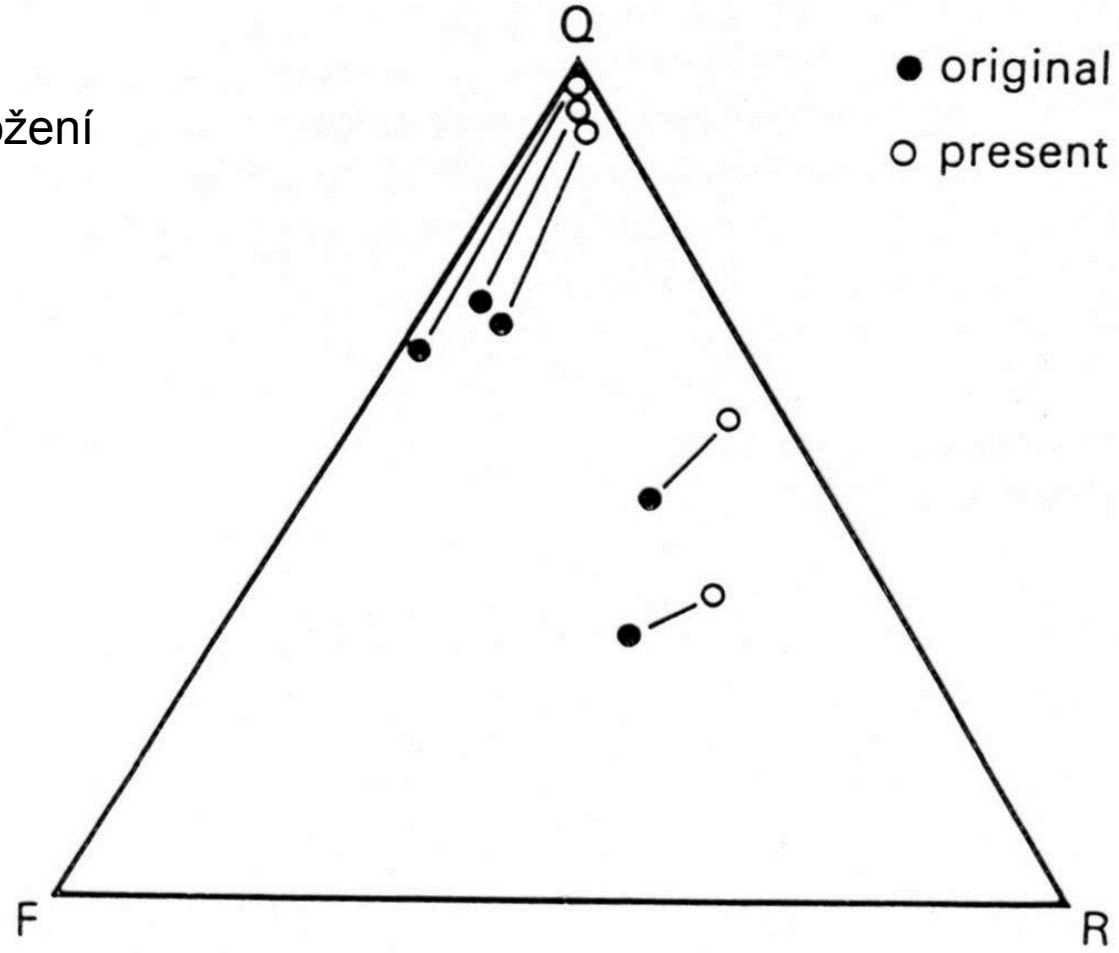

Fig. 5.37. Triangular diagram showing the present composition of five sandstones, after dissolution and alteration, and their reconstructed composition, assuming 15% of the grains which occupied oversized pores were rock fragments and 85% were feldspar (from McBride, 1985).

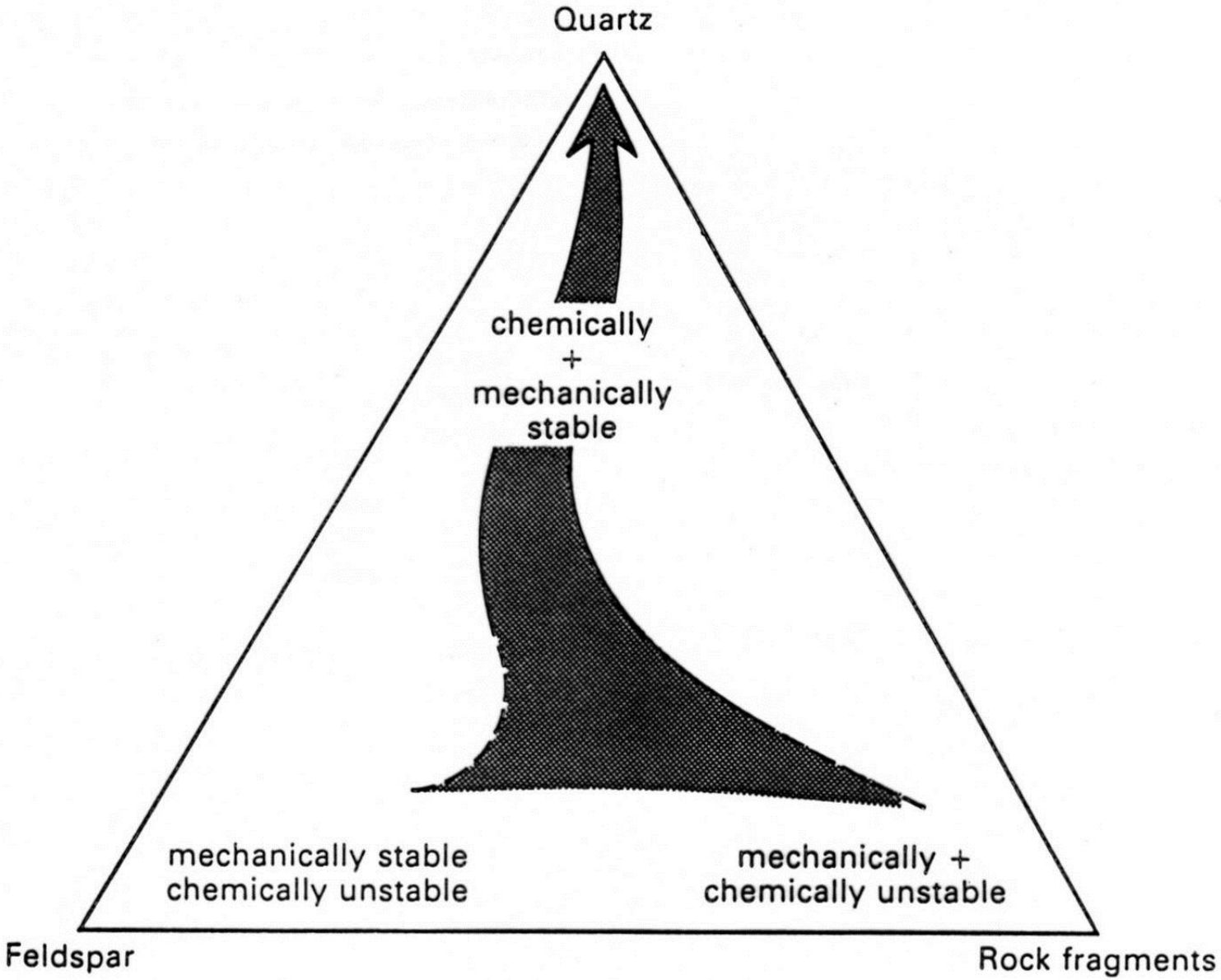
Quartz
chemically
+
mechanically
stable
mechanically stable
chemically unstable
mechanically +
chemically unstable
Feldspar
Rock fragments

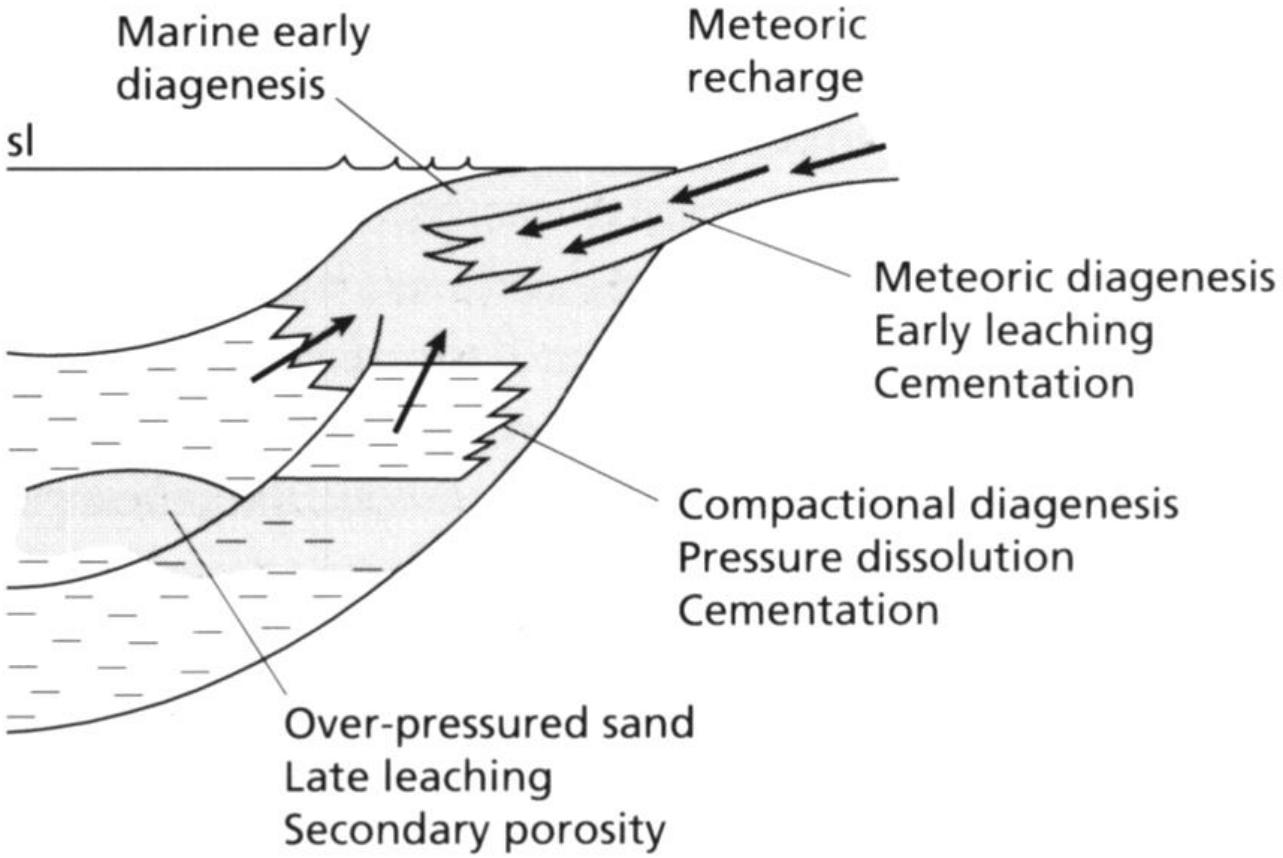

Fig. 2.57 Sketch illustrating main siliciclastic diagenetic environments. After Bjørlykke (1988).

vliv diagenetických procesů na jílové minerály

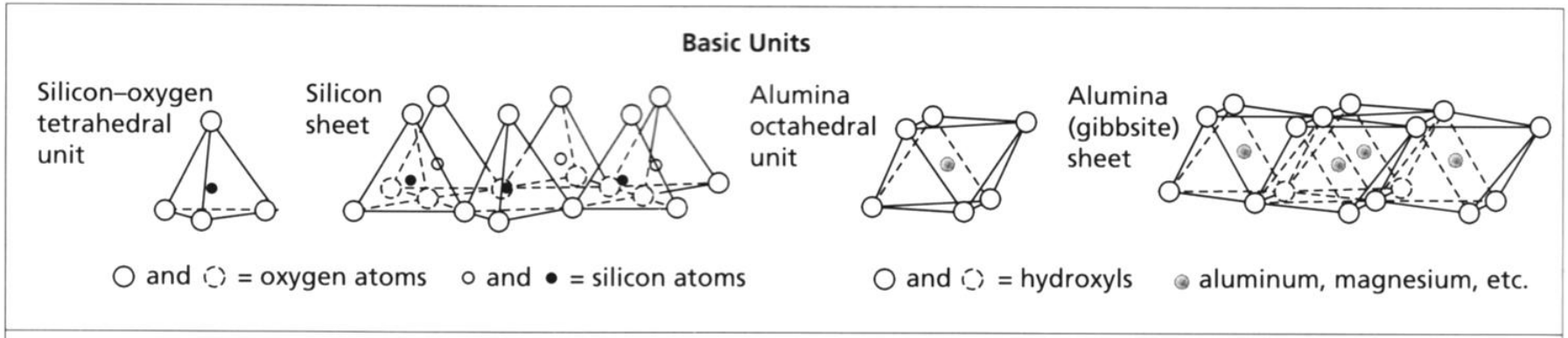

Kandite, e.g. kaolinite, $Al_2O_3.2SiO_2.2H_2O$

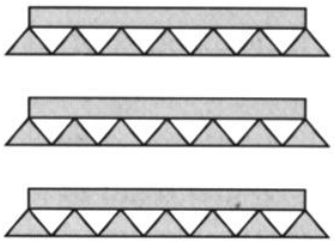

Alumina (gibbsite) layer
Silica layer

Basal spacing 7Å

Illite, $KAl_2(OH)_2.[AlSiO_3(O,OH)_{10}]$

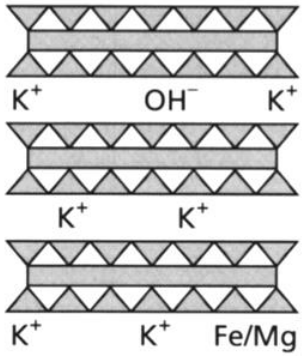

Substitution of Si by Al in silica layer

Interlayer K^+ together with some OH^-, Fe and Mg

Basal spacing 10 Å

Smectite basic formula, $2Al_2O_3.8SiO_2.2H_2O.nH_2O$
e.g. montmorillonite, $(Mg,Ca)O.Al_2O_3.5SiO_2.nH_2O$

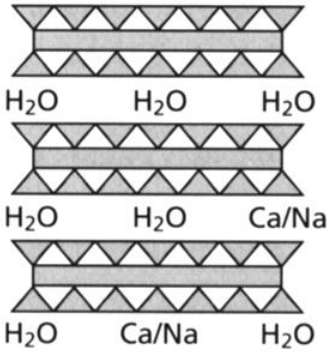

Much substitution of Al by Mg and Fe

Interlayer H_2O, and Ca and Na

Basal spacing 14 Å but expandable from 9.6 to 21.4 Å

Chlorite, $Mg_5(Al,Fe)(OH_8)(AlSi)_4O_{10}$

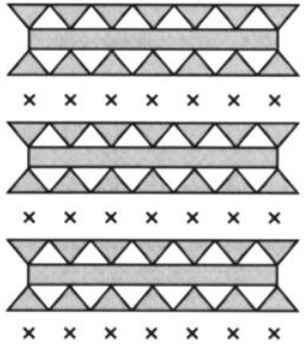

Substitution of Al by Fe

Brucite layers (Mg–OH) between Al–Si sheets

Basal spacing 14 Å

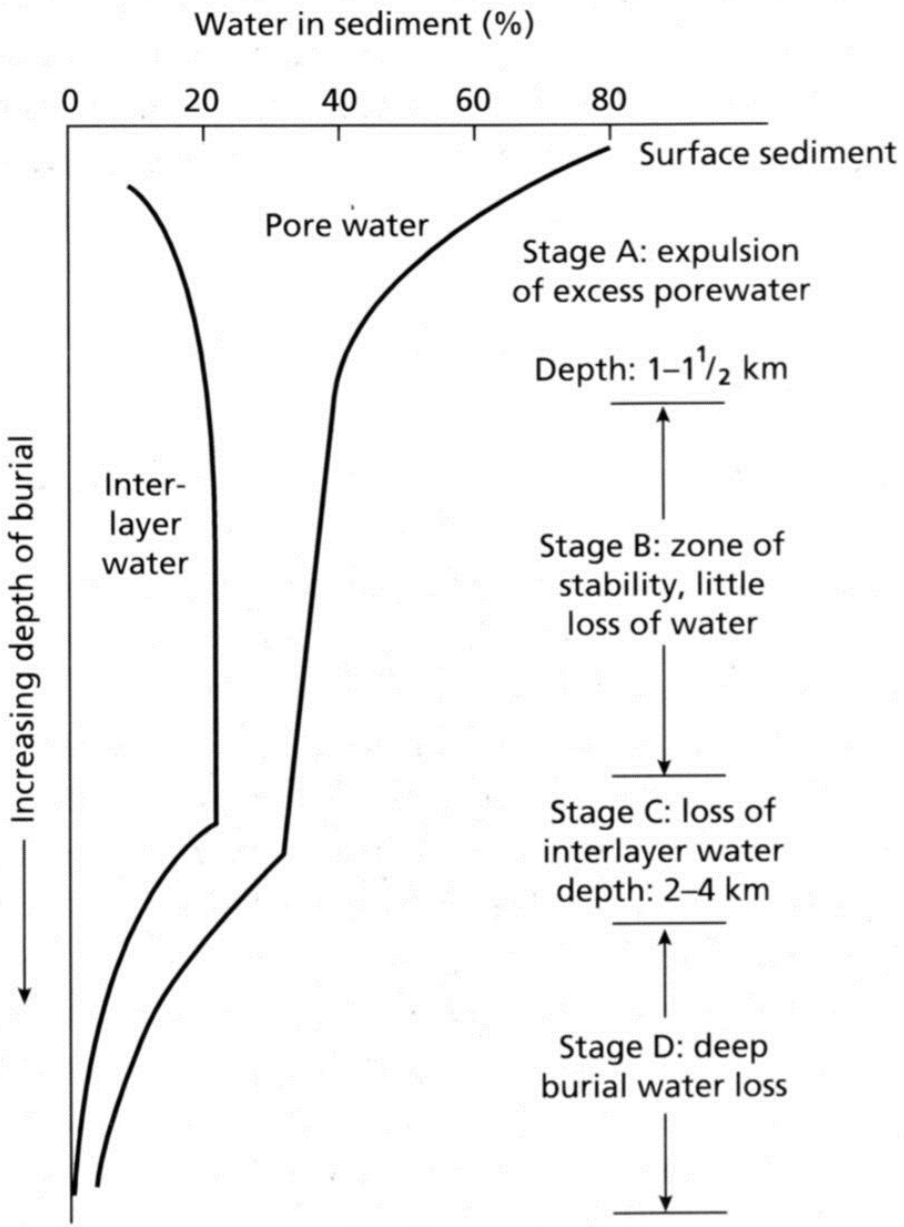

Fig. 3.8 Diagram illustrating the stages of water loss from muddy sediments with increasing depth of burial.

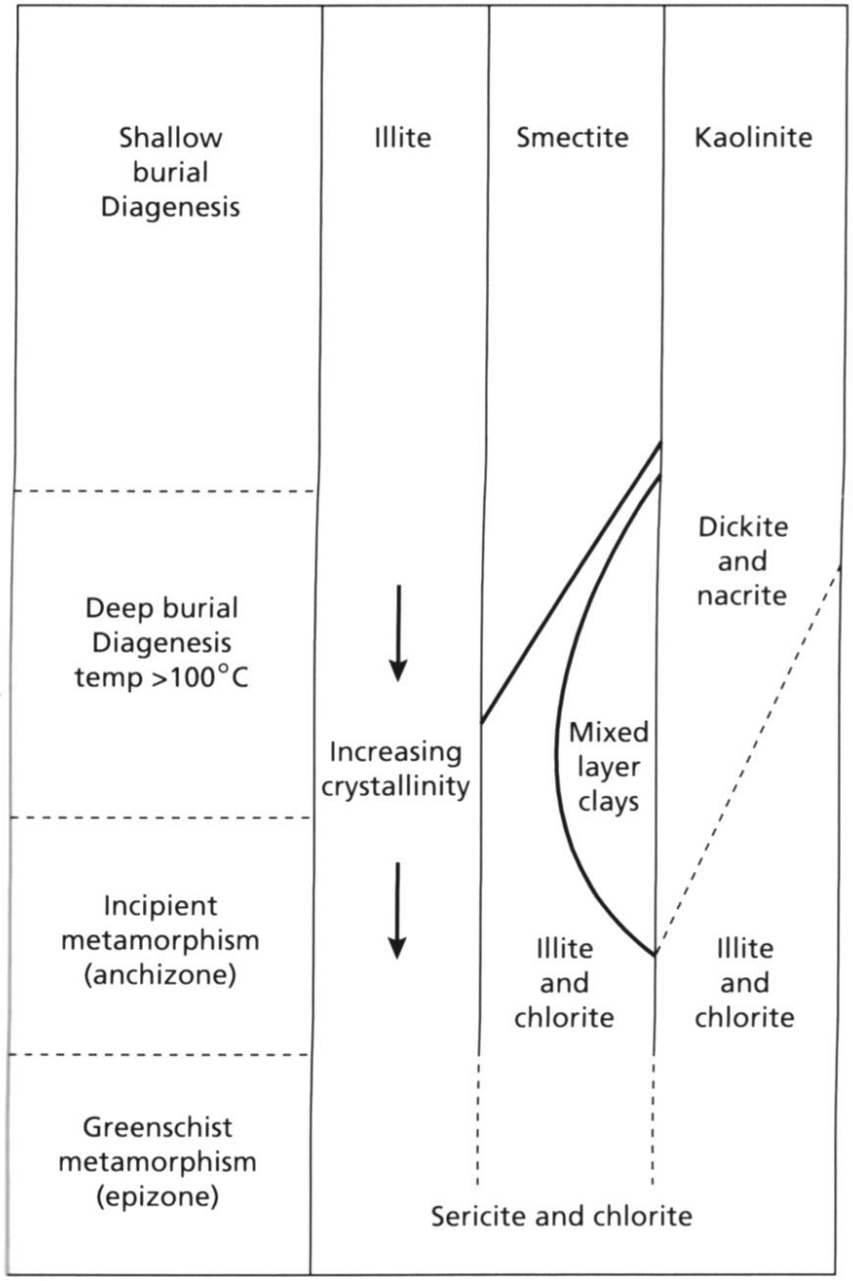

Fig. 3.9 Diagram illustrating the changes of clay minerals with increasing depth of burial and into metamorphism.

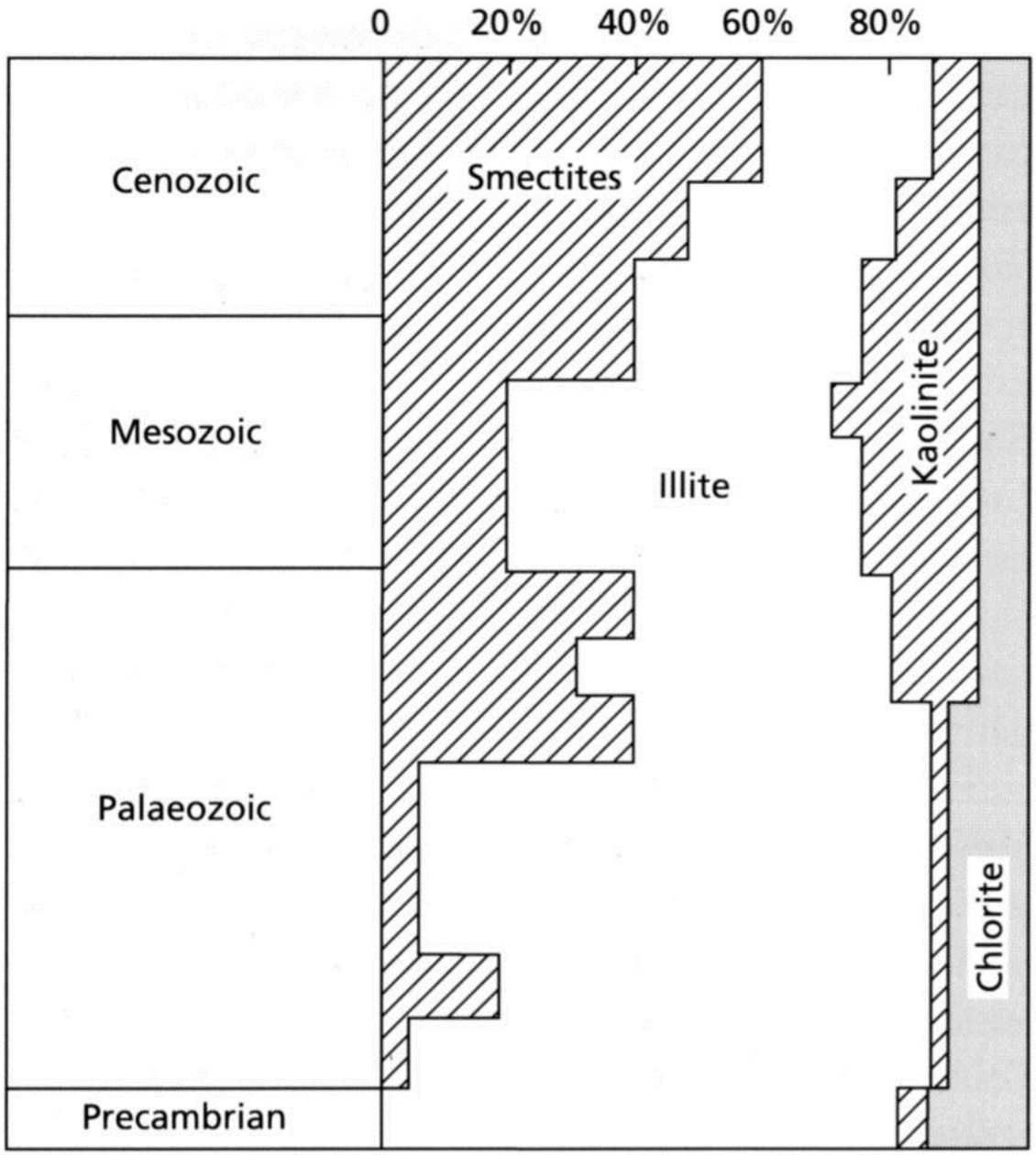

Fig. 3.10 The distribution of clay minerals through time.

a Zero intra plate stress

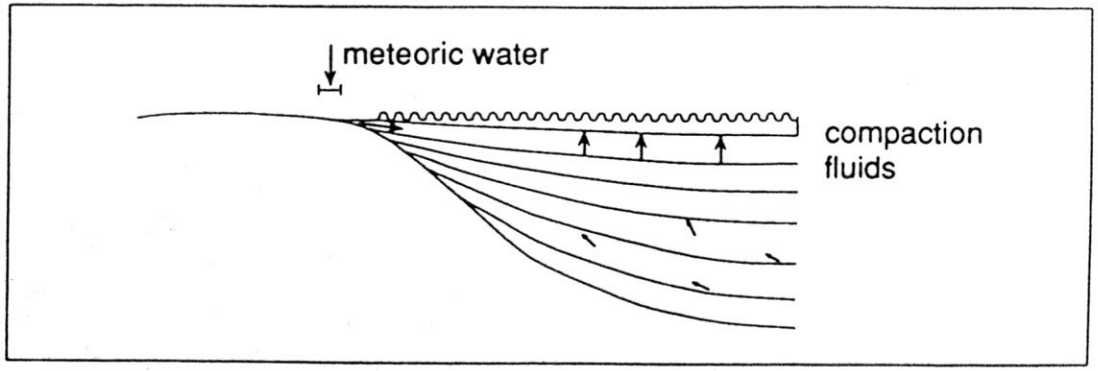

b Compressive intra-plate stress

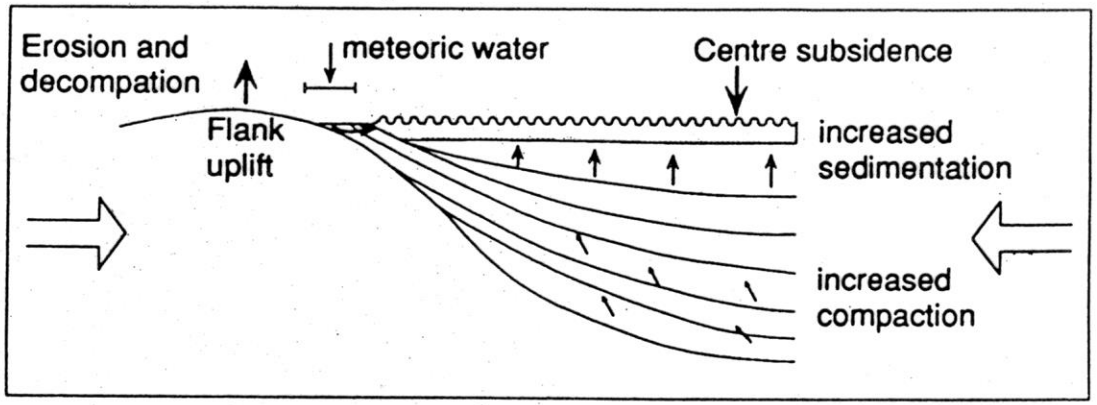

c Tensile intra-plate stress

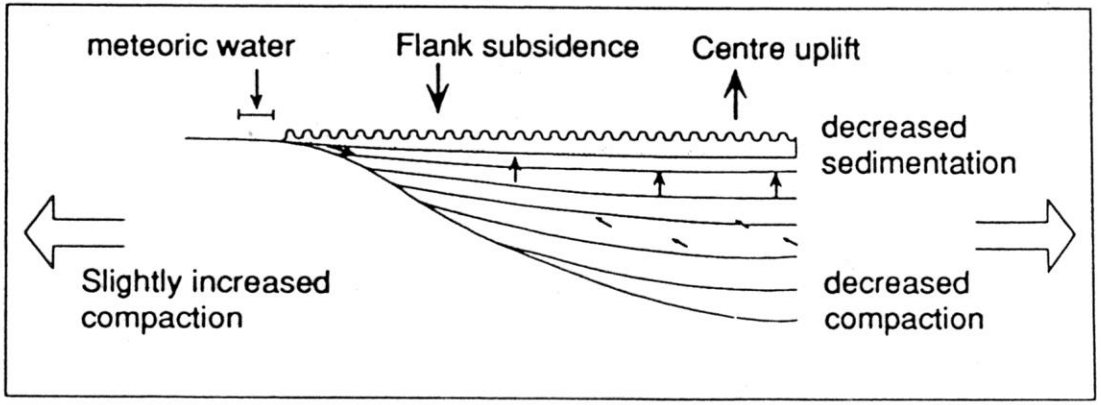

the effect of intra-plate stresses onfluid flow in sedimentary basins

van Baten&Cloeting 1994

čtení:

- **M.E.Tucker: Sedimentary petrology. 3rd ed. Blackwell, 2001, 2003.**
- Prothero: Interpreting stratigraphic record, 1990.
- Pettijohn F.J., Potter P.E. a Siever R. (1987): Sand and Sandstone. Springer-Verlag, New York, 553 pp.
- Chamley H. (1989): Clay Sedimentology. Springer-Verlag, Berlin, 623 pp.
- Potter P.E., Maynard J.B. a Pryor W.A. (1980): Sedimentology of Shale. Springer-Verlag, Berlin, 270 pp.